Diss. ETH No. 17260

HYGROSCOPIC PROPERTIES OF ORGANIC AND INORGANIC AEROSOLS

A dissertation submitted to
ETH ZURICH

for the degree of
Doctor of Sciences

presented by
NILS OLOF STAFFAN SJÖGREN

M. Sc. Chem. Eng., University of Lund, Sweden

born February 8th, 1976

nationality Swedish

accepted on the recommendation of
Prof. Dr. Thomas Peter, examiner
Prof. Dr. Hans-Christen Hansson, Prof. Dr. Urs Baltensperger and Dr. Ernest Weingartner,
co-examiners

2007

To the family

CONTENTS

Zusammenfassung

Unsere Atmosphäre besteht aus Gasen und Aerosolpartikeln. Eine wichtige Komponente sind organische Verbindungen, welche sowohl in der Gasphase als auch in der Aerosolphase vorhanden sind. Diese stammen einerseits aus biogenen Quellen (Vegetation) und andererseits aus anthropogenen Quellen, wie zum Beispiel der Biomassenverbrennung, der fossilen Brennstoffnutzung und der Industrie. Ein atmosphärisches Aerosolpartikel besteht häufig aus einem komplexen Gemisch aus organischen und anorganischen Verbindungen. Die Untersuchung von organischen Bestandteilen in Aerosolpartikeln ist von Interesse, da diese die Wasseraufnahme (Hygroskopizität) der anorganischen Aerosolkomponenten beeinflusst. Dies hat Auswirkungen auf den Strahlungshaushalt der Erde durch die so genannten direkten und indirekten Aerosoleffekte.

Die hygroskopischen Eigenschaften von Aerosolpartikeln, die aus einem Gemisch aus organischen und anorganischen Substanzen bestanden, wurden im Labor charakterisiert. Folgende Substanzen und Mischungen mit Ammoniumsulphat (AS) wurden untersucht: Adipin Säure (AA), Zitronensäure (CA), Glutarsäure (GA) und Huminsäure (NaHA). Die Messungen ergaben, dass die Mischungen aus festem AA und NaHA jeweils mit AS bis zu einer halben Minute benötigten, um das „Wassergleichgewicht“ zwischen Partikel und Gasphase zu erreichen. Die Wasseraufnahme kann aus diesem Grund unterschätzt werden, falls Messungen in zu kurzer Zeit durchgeführt werden. Der Fehler kann bis zu 10% im hygroskopischen Wachstumsfaktor (GF) betragen. Die beobachtete Wasseraufnahme wurde mit dem Zdanovskji-Stokes Robinson (ZSR) Mischungsgesetz modelliert. Für die Mischungen AS/GA und AS/CA wurde eine gute Übereinstimmung zwischen Modell und Theorie gefunden. Mit zunehmender CA Konzentration wurde eine Erniedrigung des Deliqueszenz- und Effloreszenzpunktes von AS beobachtet.

Des Weiteren wurde der Einfluss von Salpetersäure (HNO3) auf das hygroskopische Verhalten von Mineralstaub (Standard Arizona Teststaub) untersucht. Ein wichtiges Resultat ist dass unbehandelter Mineralstaub hydrophob ist. Dieser wird jedoch nach der Reaktion mit Salpetersäure leicht hygroskopisch. Dies ist von Relevanz für unsere Atmosphäre, da grosse (anthropogen verursachte) Mengen an Mineralstaub aus der Sahara und der Wüste Gobi durch Änderung der Landnutzung (Desertifikation, Abholzung) in die Atmosphäre emittiert werden. Mineralstaub ist ein wichtiger Eis-Kristallisationskeim und kann aufgrund seiner Grösse auch als Wolkenkondensationskeim wirken. Er beeinflusst massgeblich den Salpetersäurezyklus durch heterogene Chemie an seiner Oberfläche.

Die Messungen zu den hygroskopischen Eigenschaften von gealtertem atmosphärischem Aerosol wurden auf der hochalpinen Forschungsstation Jungfraujoch (JFJ) durchgeführt. Es zeigte sich, dass in der Regel das Aerosol an diesem Ort aus organischen und anorganischen Verbindungen besteht, welche weitgehend intern gemischt sind. Gelegentlich wurden jedoch Luftmassen aus der Sahara beobachtet, die Mineralstaub mitführten. Während solcher Ereignisse hatte ein Teil der Aerosolpartikel eine niedrigere Hygroskopizität (während dieser Ereignisse lag das Aerosol als externe Mischung vor). Es wurden keine eindeutigen Phasenübergänge im untersuchten Feuchtigkeitsbereich (rF = 10-90%) beobachtet. Das hygroskopische Wachstum der Aerosolpartikel als Funktion der relativen Feuchte konnte sehr gut mit einem einfachen empirischen Model beschrieben werden kann. Ausserdem konnte der hygroskopische Wachstumsfaktor mittels der ZSR Beziehung mit der gemessenen chemischen Zusammensetzung des Aerosols auf dem JFJ gut abgeschätzt werden.

Abstract

The atmosphere contains gases and particulate matter (aerosol). Organic material is present both in the gas phase and in the aerosol phase. Biogenic sources such as vegetation and anthropogenic sources such as biomass burning, fossil fuel use and various industries contribute to their emissions. The study of organic compounds in aerosol particles is of importance because they affect the water uptake (hygroscopicity) of inorganic aerosol, and hence the radiation budget of the earth through the direct and indirect aerosol effects.

The hygroscopicity of mixed organic/inorganic aerosol particles produced in the laboratory was characterized. This work reports on the following substances, and mixtures of them with ammonium sulfate (AS): adipic acid (AA), citric acid (CA), glutaric acid (GA) and humic acid sodium salt (NaHA). The AA and NaHA mixtures with AS were found to require up to tens of seconds for equilibrium water content to be reached. Therefore, measurements carried out on timescales shorter than a few seconds underestimate the hygroscopic growth factor (GF) with up to 10%, for samples containing a solid phase. Conversely, the GA and CA mixtures with AS were found to take up water readily and were well described by the Zdanovskii-Stokes-Robinson (ZSR) mixing rule. The distinct deliquescence and efflorescence points of AS could be seen to gradually disappear as the CA content was increased.

Furthermore mineral dust (standard Arizona test dust) was investigated, as well as the influence of nitric acid (HNO_3) uptake thereon. Mineral dust is hydrophobic, but after processing with HNO_3 turns slightly hygroscopic. Large amounts of dust are injected to the atmosphere (largely from the Sahara and the Gobi deserts, but also from human land-use). Mineral dust is important as ice nuclei, and due to its larger sizes it can also contribute as cloud condensation nuclei. Mineral dust also offers surface for heterogeneous chemistry, and can play an important role in the HNO_3 cycle in the atmosphere through scavenging of HNO_3 on the mineral dust surface.

Hygroscopicity measurements in the atmosphere at the high alpine site Jungfraujoch (JFJ) were performed. At the JFJ the aerosol consists most of the time of organic and inorganic salts, mostly as an internal homogeneous mixture. However, about 5% of the time (yearly average) air trajectories passing the Sahara are encountered which carry mineral dust from there. For these occasions a fraction of particles with lower hygroscopicity was observed. No distinct phase transitions were observed in the range of relative humidity (RH) studied (10-90% RH). It was shown that the hygroscopic growth of the aerosol as a function of RH can be well described with a single-parameter empirical model, and that the GF could be estimated with the ZSR relation by using the measured aerosol composition at the JFJ.

CHAPTER 1

1. Introduction

This thesis describes a part of the puzzle of how aerosol particles in the atmosphere interact with water vapor. It is thus a part of the description of how clouds are formed. Clouds have large influences on the earth's climate. The earth's climate has changed, and is still changing on geological timescales. But changes also occur on timescales relevant to us; during the last couple of thousand years, although relatively stable, there have been changes that have been large enough to cause shifts of eco-systems on earth, as well as forcing also the human civilization to adapt under stress. This has left remains such as shown in Fig. 1-1. It is highly probable that human (*anthropogenic*) influences today result in changes in our climate which will cause similar stress already during your and my lifetimes. Future generations will also have to adapt to further change originating from pollution of today.

Fig. 1-1. Mosaic from the roman ruins at Augusta Raurica, Switzerland. Several suggestions to the fall of the Roman Empire have been proposed, ranging from climate change, resource depletion (i.e. wood), increasing societal complexity and pollution, for example. These factors are reminiscent of our society of today. Courtesy department "Römerstadt Augusta Raurica", Canton Basel-Land, CH.

1.1. Motivation for this work

This thesis presents investigations on water uptake (hygroscopicity) of mixed organic/inorganic aerosol generated in the laboratory and of particles in the atmosphere. The inorganic substances in the atmosphere are well known. Further, it is known that organic material is present in the atmosphere both in the gaseous phase and as condensed matter. It is also known that it is involved in many fundamental atmospheric and geobiochemical processes, spanning from the microphysics of clouds to global climate and geochemical cycles. Moreover, the local monitoring of organic substances, some of which are harmful, is

crucial for human health and for air quality issues. However, the physico-chemical properties of organics are yet not well described, nor of more complex (several compounds or organic/inorganic) mixtures. Thus the Laboratory of Atmospheric Chemistry (LAC) at the Paul Scherrer Institute (PSI) and Institute for Atmospheric and Climate Science (IAC) at ETH Zurich started a joint project, with partial funding granted from the Swiss National Science Foundation, to investigate the hygroscopic properties of organic aerosol. How does the organics, which may or may not have a hysteresis behavior, influence the water uptake of ammonium sulfate at moderate relative humidities? How does the morphology of the particles influence the water uptake? How can hydrophobic particles be altered, aged, in the atmosphere to become more hygroscopic?

This dissertation has addressed some aspects of these questions. Several mixed inorganic/organic systems were studied with the help of two instrumental setups: an electrodynamic balance (EDB, at IAC ETH Zurich) and a hygroscopicity tandem differential mobility analyzer (HTDMA, at PSI). Furthermore mineral dust, and its interaction with nitric acid (HNO_3), was studied (at the Laboratory for Radiochemistry and Environmental Chemistry at PSI). Field campaigns at the high-alpine site Jungfraujoch (JFJ) were done to describe the hygroscopicity of atmospheric European background free tropospheric (FT) aerosol. The field campaigns had a continuous duration of one month per year during four years. This confirmed whether mixing rules used in the laboratory were also applicable to complex atmospherical aerosol.

1.2. Description of the atmosphere and its gases

The atmosphere is the layer of gases surrounding the planet and retained by gravity. It extends from the ground up to some hundreds of kilometers, slowly fading into empty space. The large part of the mass of the atmosphere is seen as the whitish line in Fig. 1-2, and it is a thin and sensitive layer of the Earth.

Fig. 1-2. Earth seen from space. The weak whitish line around the left side is most of the atmosphere (height about 100 km). Courtesy NASA Goddard Space Flight Center.

Why you see the atmosphere at all is due to scattering of light from the Sun (situated to the left). From the top of atmosphere downwards Rayleigh scattering on air molecules is dominant. Where aerosols are present Mie scattering takes place (or for micrometer range

aerosol non-selective scattering, such as hazes). The atmosphere is a dynamically and chemically active system which underwent continuous as well as abrupt changes from its formation together with the Earth, ~4.5 billion years ago, and it is still in evolution. The atmosphere we are familiar with has only existed a few hundred million years; since cyanobacteria and photosynthetic plants have been able to supply oxygen in large amounts.

Important functions of the atmosphere are to reduce the amount of ultraviolet (UV) radiation at the surface and, through the *greenhouse effect* (see Fig. 1-3), to increase the temperature to a balmy 14.5°C yearly global average, instead of –10°C which would be the case without our atmosphere. The global average temperature profile is shown in Fig. 1-4, where the different layers correspond to regions of the atmosphere with remarkably different properties. The daily weather (clouds and rain) is practically completely confined in the lowest region, the troposphere (from the Greek word "τρέπω" meaning to turn or mix), characterized by strong vertical convection, high level of water vapor and decreasing temperature with altitude. 90% of the atmospheric mass is in this layer, which also contains most of the aerosol particles. The pressure profile shown in Fig. 1-4 is instead representative of the weight of the overlying column of air and it has an exponential decay which is followed by the density of air as well.

Of the 92 natural chemical elements, the major constituents of atmospheric composition are only nitrogen (N_2, 78%), oxygen (O_2, 21%), argon (Ar, 0.9%), and water (H_2O). Other gases are present in the atmosphere at very low concentrations and are called trace gases, such as carbon dioxide, neon, ozone, helium, methane, krypton, hydrogen, nitrous oxide and many others. Despite their low concentrations, these trace gases can be of critical importance for the greenhouse effect, the ozone layer, smog formation, and other environmental issues. The total water content is highly variable and is about 1-4% of total mass (>99% of that water is present as clouds or rain, the remaining quantity of gaseous water vapor distribution is seen in Fig. 1-5). The water vapor and the hydrologic cycle (cloud formation) contribute to the greenhouse effect (water vapor alone about +⅓ and the indirect effect (clouds) with a cooling of very roughly 10%). It is crucial to understand the water cycle and its coupling to various components of the climate system. Under conditions of a naturally or anthropogenically forced climate, changes in rainfall may affect drinking water amounts and quality as well as availability of water for agricultural purposes (irrigation) and hydroelectric dams. Such changes may have a very large impact on our society in the near future.

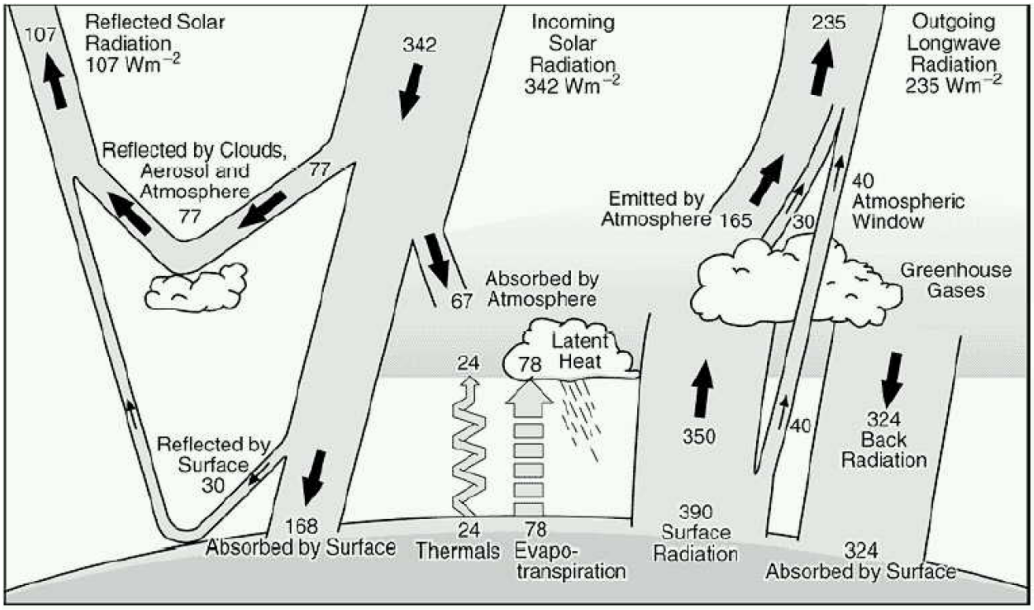

Fig. 1-3. Greenhouse gas effect and Earth's energy balance. Incoming solar energy is balanced by reflected solar energy and infrared heat loss (Kiehl & Trenberth, 1997).

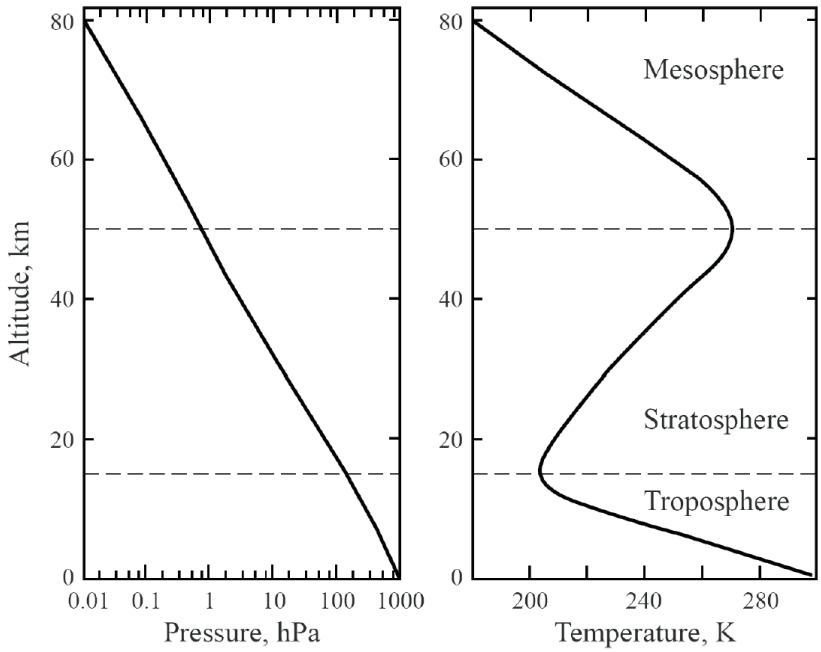

Fig. 1-4. Vertical profiles of pressure and temperature for the standard atmosphere up to 80 km. Distinct layers are identified according to the vertical temperature gradient. The lowermost layer, the troposphere, contains 90% of the weight of the atmosphere, and most of the particulate matter.

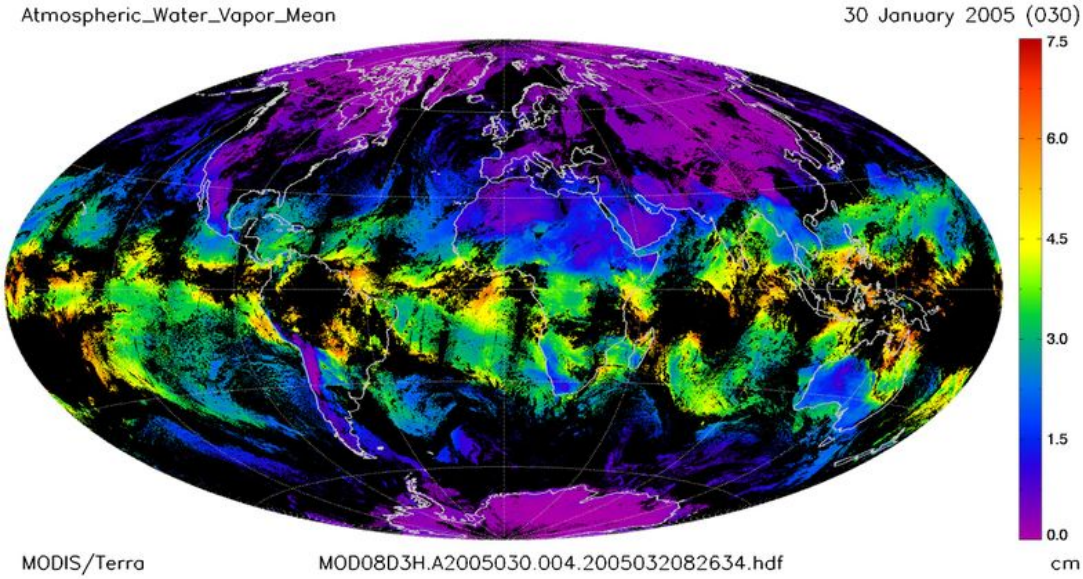

Fig. 1-5. Water vapor, from MODIS Atmosphere Discipline Group (http://modis - atmos.gsfc.nasa.gov/ index_intro.html) [in cm condensed water column].

Fig. 1-7 shows mixing ratio changes of the most important long-lived greenhouse gases (CO_2, methane (CH_4), nitrous oxide (N_2O) from the IPCC technical summary (Solomon et al., 2007). The direct net effect of warming, as indicated by the right hand axis in the graphs, from these three gases are well understood (for uncertainties see Fig. 1-8). The possibilities to reduce the CO_2 pollution appear low in the near-term (1-2 decades), today mostly originating from carbon usage for electricity production and liquid fossil fuels for transportation, as well as some from biomass burning. Recently the increase in CO_2 pollution has speeded up (Raupach et al., 2006, as well as the mentioned IPCC report), and is >2 ppm/year. Thus until we actually reduce our CO_2 emissions, and/or sequester large amounts from the atmosphere, the global average temperature of the earth, due to this factor, can be expected to rise further (see Fig. 1-6).

Furthermore Ozone (O_3) is also an important GHG and minor effects come from CFCs and hydrochlorofluorocarbons (HCFCs), hydrofluorocarbons (HFCs), perfluorocarbons (PFCs) and sulphur hexafluoride (SF_6), the latter two with increasing trends in radiative forcing.

CO_2: pollution or emission?
Today the most current term for CO_2 is *emission*. We might be going towards a framework where it will be labeled *pollutant* (defined as "undesirable contamination of a harmful substance as a consequence of human activities". Currently (April 2007) the Supreme Court of the U.S. has voted (5 to 4) for the EPA to regulate CO_2 emissions in the US. In this thesis CO_2 is mentioned, a bit modernly, as *pollutant*.

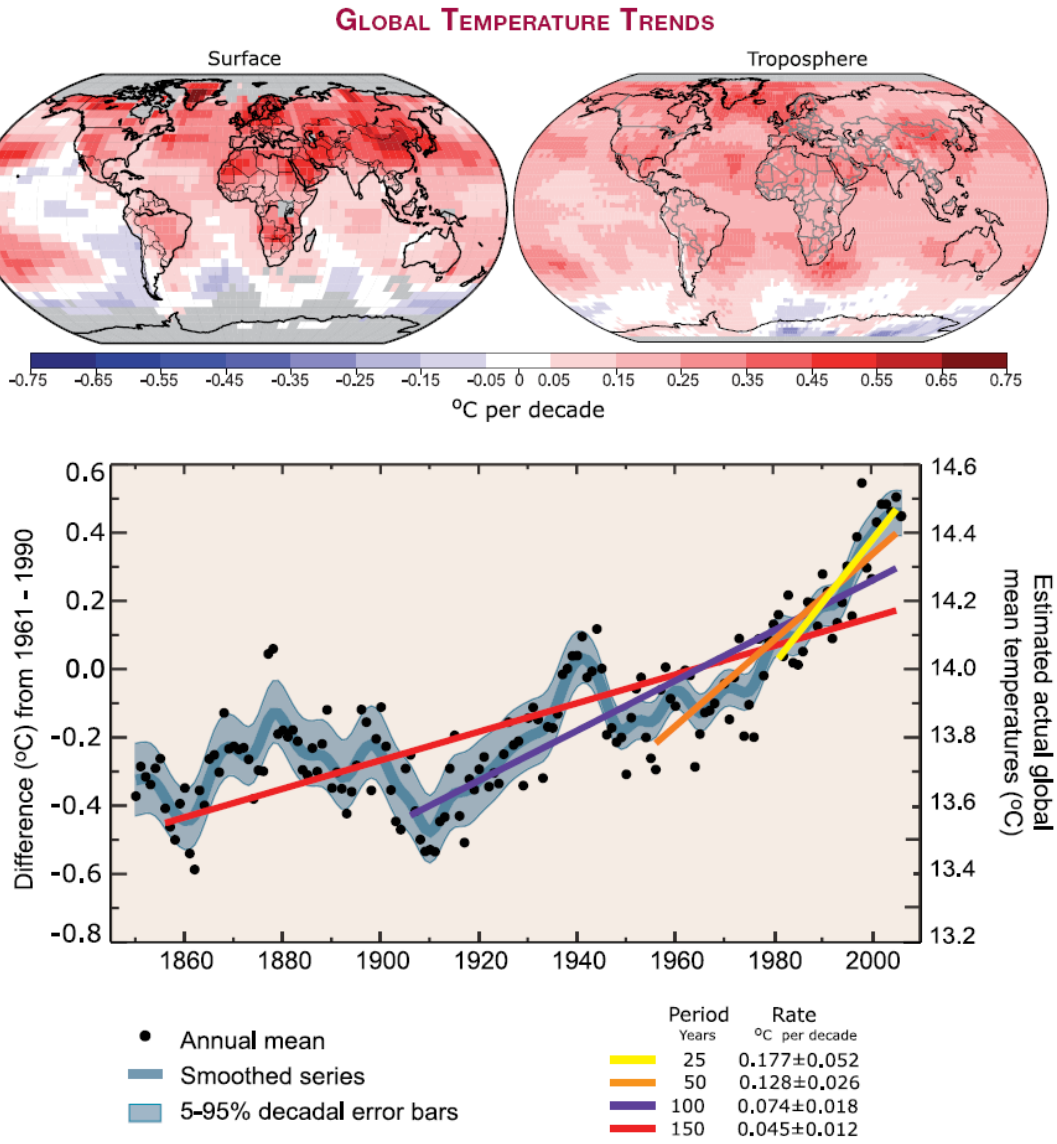

Fig. 1-6. (Top) Patterns of linear global temperature trends over the period 1979 to 2005 estimated at the surface (left), and for the troposphere from satellite records (right). Grey indicates areas with incomplete data. (Bottom) Annual global mean temperatures (black dots) with linear fits to the data. The left hand axis shows temperature anomalies relative to the 1961 to 1990 average and the right hand axis shows estimated actual temperatures, both in °C. Linear trends are shown for the last 25 (yellow), 50 (orange), 100 (magenta) and 150 years (red). From IPCC.

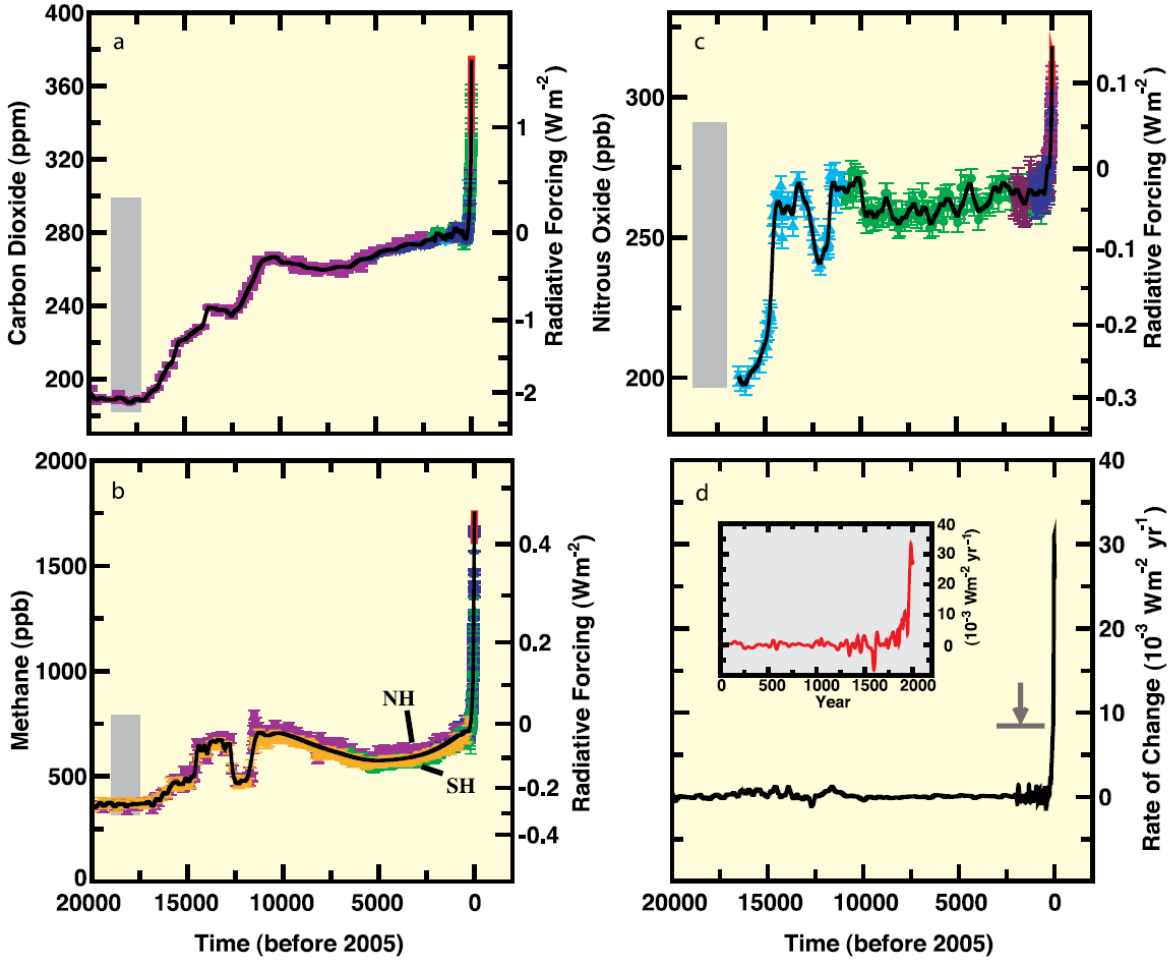

Fig. 1-7. The concentrations and radiative forcing by (a) carbon dioxide (CO_2), (b) methane (CH_4), (c) nitrous oxide (N_2O) and (d) the rate of change in their combined radiative forcing over the last 20,000 years reconstructed from Antarctic and Greenland ice and firn data (symbols) and direct atmospheric measurements (panels a,b,c, red lines). The grey bars show the reconstructed ranges of natural variability for the past 650,000 years. The rate of change in radiative forcing (panel d, black line) has been computed from spline fits to the concentration data. The width of the age spread in the ice data varies from about 20 years for sites with a high accumulation of snow such as Law Dome, Antarctica, to about 200 years for low-accumulation sites such as Dome C, Antarctica. The arrow shows the peak in the rate of change in radiative forcing that would result if the anthropogenic signals of CO_2, CH_4, and N_2O had been smoothed corresponding to conditions at the low-accumulation Dome C site. The negative rate of change in forcing around 1600 shown in the higher-resolution inset in panel d results from a CO_2 decrease of about 10 ppm in the Law Dome record. From IPCC.

1.3. Aerosol-climate interactions

The Earth's average temperature and climate result from the distribution and transformation of the incoming solar radiation. The aerosol radiative forcing is defined as the modification of the terrestrial radiative budget due to the presence of aerosols compared to the preindustrial situation (before ca. year 1750). Aerosols effect the radiation budget both directly following particle-radiation interactions (*direct aerosol effect*), and indirectly through cloud processes (*indirect aerosol effect*).

Aerosol particles are capable of scattering the short-wave radiation coming from the sun and the longwave radiation coming from the ground. They may also absorb light depending on their chemical composition. If the absorbance is very high, like in the case of black carbon aerosol particles, the local heat produced can then lead to an evaporation of the clouds and to a warming of the climate (this is called semi-direct effect).

Within the indirect effect aerosol particles play the role of cloud condensation nuclei (CCN). More CCN, for a given amount of condensable water vapor, induce the formation of smaller droplets which increase the cloud albedo (first indirect effect, in the 4th IPCC report now called cloud albedo effect) and possibly also decrease the precipitation and increase the cloud cover (second indirect effect, in the 4th IPCC report now called cloud lifetime effect). As can be seen in Fig. 1-8 aerosol particles have a negative forcing (cooling), in contrast to the greenhouse effect related to trace gases. Fig. 1-8 quantifies the different perturbations to Earth's radiative budget.

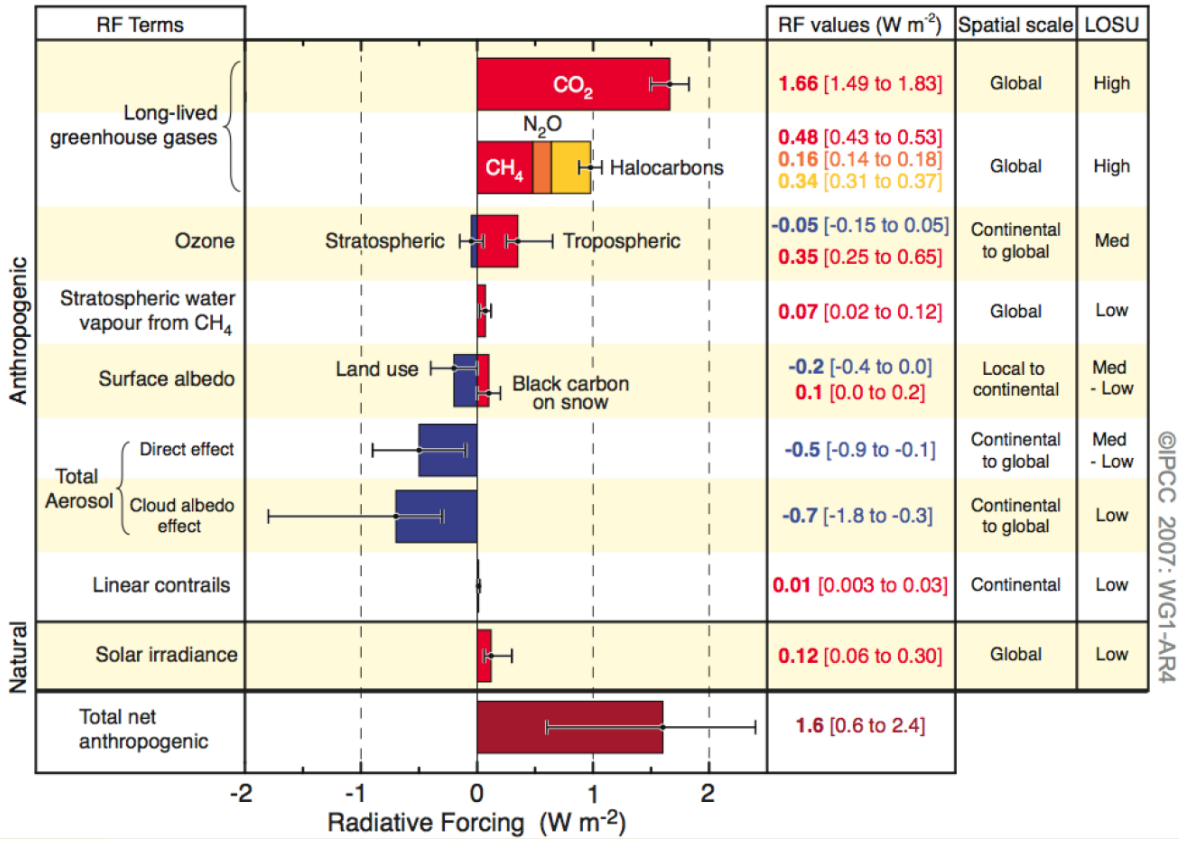

Fig. 1-8. The different contributions to the radiative forcing. Aerosol particles have a strong negative forcing through the indirect effect explained in the text. The uncertainty though, is of the same order as the forcing itself. Black carbon has instead a better assessment and a counteracting effect. LOSU stands for "Level of scientific understanding". From IPCC.

1.4. Particulate matter (PM)

The word "aerosol" defines a two-phase system made up of particles (which can be liquid, solid or amorphous) and the gas phase surrounding them. The term particle may be defined as a conglomerate of molecules on a size scale from nanometers to the centimeter. Particulate matter (PM) is the collective name for aerosol particles. Mineral dust, rain droplets, fog, smog, smoke, soot and haze consist of aerosol particles.

Aerosol particles can be classified according to the sources:

- primary particle are directly emitted by biogenic or anthropogenic sources
- secondary are formed in the atmosphere by chemical reactions

The main sources of atmospheric aerosol particles can be categorized into:

(i) widespread surface sources of primary aerosols like arid soils (mineral dust), ocean (sea salt), biosphere (pollen...), biomass (mostly OC) and fuel burning (OC and EC)

(ii) diffuse sources within atmospheric volume, such as air traffic, evaporation of clouds, secondary aerosols from chemical formation of volatile compounds (organics), extraterrestrial sources (vaporizing meteors)

(iii) intense point sources like volcanoes

Natural sources dominate the global aerosol emissions, but in urban areas the relative anthropogenic contribution becomes much more important. The lifetime of aerosol particles may vary from hours to many days, the latter enough to allow for long-range transport. As a result of multiple sources and relatively short lifetime compared with a number of trace gases, the major feature of aerosols is their variability and heterogeneity in time and space. The main sink is wet deposition. Dry and wet deposition are both important sinks for the coarse mode. In the stratosphere their lifetime may be close to the stratospheric residence time of an air parcel, i.e. several years, enabling global transport and distribution. Mineral dust is a general expression for the windblown particles of crustal origin that are generated mainly in the arid areas of the planet, in particular the great deserts.
In Table 1-1 burden and emissions of different aerosols are summarized.

Table 1-1. Global annual average aerosol burden and emissions (Textor et al., 2006).

	Burden, Tg	Emissions, Tg/a
Mineral dust	19.2	1840
Sea salt	7.5	16600
Sulfate	2	175
Particulate organic matter	1.7	96.6
EC	0.24	11.9

Fig. 1-9 shows electronic microscope pictures of quite spectacular organic debris: a pollen grain and brochosomas emitted by vegetation and insects, respectively. Fig. 1-10 shows a much more common particle, from diesel engine exhausts, in this case combined with ammonium sulfate. This was done in the laboratory, and in the atmosphere the particles will keep aging and take up further organic and inorganic material through processes such as condensation, chemical reactions and in-cloud droplet processing.

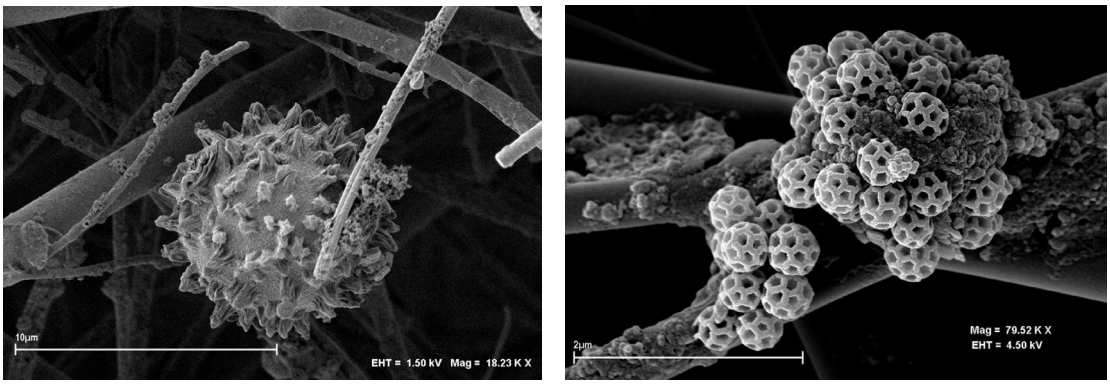

Fig. 1-9. Directly emitted organic particles: a pollen grain on the left and brochosomas on the right (secretory granules produced by some insects). The size bars in the left and right panel are 10 and 2 µm, respectively. Source: M. O. Andreae, MPI, Mainz.

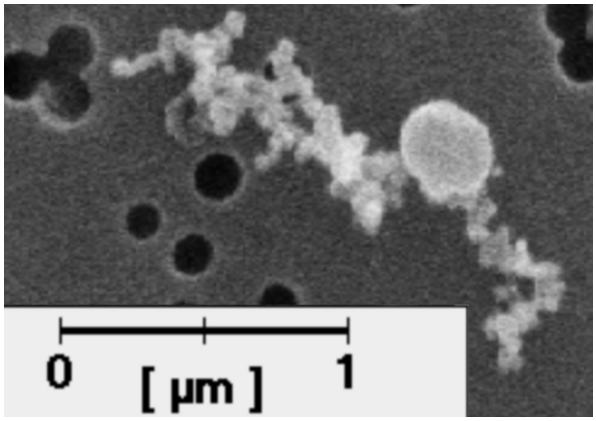

Fig. 1-10. Diesel soot (the "pearls", which are single diesel particles) with AS (the larger sphere). Source: H. Saathoff, Forschungszentrum Karlsruhe.

1.5. Human health

Particle size and chemical composition are the two main properties governing the behavior of particles in the respiratory tract. The depositions occur mainly via inertial impactation, sedimentation and Brownian diffusion. The inertial impactation, which is the most important process in the upper airways, is a flow dependent mechanism involving mainly large particles (>5 µm). The larger the particle's size and flow velocity the higher the probability for the particle to exit the flow lines and impact on the obstacles. Sedimentation occurs in the lower airways for medium particle size (1-5 µm), and is governed by gravity. Its efficiency depends on the size of the particle and the residence time. Brownian motion (random movements of the aerosol particles due to the kinetics of the gaseous medium in which they are suspended), which is well described (e.g. Hinds, 1999) is predominant for ultrafine particles (< 0.1 µm). A fraction of ultrafine particles can translocate directly into the blood.

There are numerous studies demonstrating the short-term and long-term effects of particulate air pollution like the famous one from Dockery and Pope (1993) or the book by Holgate et al. (1999). Summarizing the short-term damage, they show that a 10 µg/m^3 increase in PM_{10} (particle size less then 10 µm) is associated with a 0.8% increase in total daily mortality, and a 3% and a 1.5% in respiratory and cardiovascular mortality, respectively. About the long-term influences, a 6% and 9% for total and cardiopulmonary mortality are related to a 10 µg/m^3 increase in $PM_{2.5}$ respectively. Evidence that pollution reduction is

directly related to improved respiratory health can be found in a Swiss study by Bayer-Oglesby et al. (2005). The relevance of this health problem is better understood if instead of an individual relative risk of exposure to particulate air pollution an “attributable risk” is taken into account. This index includes the number of people exposed to the exposure distribution in the population. The problem was studied in an international project involving several European cities which has been published by Koistinen (1999).

1.6. Organic material

Organic material exist in the atmosphere in two phases: as gas phase and as particulate matter. The latter can originate from direct emissions (Primary Organic Aerosols, POA) or can be formed in the atmosphere as secondary organic aerosol (SOA) from organic reaction products undergoing phase transition processes. Both phases have biogenic and anthropogenic origin. Organics can be found in almost every kind of aerosol particle and gas phase sample, from urban megacities to remote locations atmosphere (Jacobson et al., 2000; Duce et al., 1983; Saxena and Hildemann; 1996; McMurry et al., 2004). In some cases they are the dominant component.

In literature, many acronyms defining the organic materials in the atmosphere can be found and their number is related to the complexity of organic chemistry. A first separation of the total carbon (TC) present in the atmosphere is between elemental carbon (EC, soot) and organic carbon (OC), which can be divided in volatile and particulate compounds (VOC and POC).

The work of Went (1960) was one of the earliest to suggest the potential importance of vegetation as a major source for atmospheric hydrocarbons. He also suggested that vapor phase terpenes emitted from certain types of vegetation rapidly undergo reactions to form condensed phase particles, the bluish haze often observed over and near forested areas. These blue hazes derived from organic species have potential important effects on the atmospheric radiation budget, but in general the relation between the organic content of atmospheric particles and their optical properties is poorly known (Penner et al., 1992). Some organics (mainly from anthropogenic origin, like polycyclic aromatic hydrocarbons (PAHs) or polychlorinated biphenyls (PCBs)) are hazardous and since year circa 1980 attention has been paid to their long distance transport, given the rather low but uniform concentrations found in soils and marine sediments. Finally, it is clear that organics impact upon many fundamental geochemical cycles, like the one of tropospheric ozone, or the halogens cycles (chlorine, bromine, iodide) (Saxena and Hildemann; 1996).

1.6.1. Vapor phase organic material

Volatile organic compounds (VOC), which include non-methane hydrocarbons (NMHC) and oxygenated NMHC (e.g., alcohols, aldehydes and organic acids), have short atmospheric lifetimes (fractions of a day to months), and small direct impact on radiative forcing. VOC influence climate through their production of organic aerosols and their involvement in photochemistry, i.e. production of O_3 in the presence of NO_x and light. The largest source, by far, is natural emission from vegetation. Isoprene, with the largest emission rate, is not stored in plants and is only emitted during photosynthesis. Isoprene emission is an important component in tropospheric photochemistry (Guenther et al., 1995).

Monoterpenes are stored in plant reservoirs, so they are emitted throughout the day and night. The monoterpenes play an important role in aerosol formation. Vegetation also releases other VOCs at relatively small rates, and small amounts of NMHC are emitted naturally by the oceans. Anthropogenic sources of VOC include fuel production, distribution, and combustion, with the largest source being emissions from motor vehicles due to either

evaporation or incomplete combustion of fuel, and from biomass burning. Thousands of different compounds with different lifetimes and chemical behavior have been observed in the atmosphere. Generally, fossil VOC sources have already been accounted for as release of fossil C in the CO_2 budgets, and thus VOC are not counted as a source of CO_2. Given their short lifetimes and geographically varying sources, it is not possible to derive a global atmospheric burden or mean abundance for most VOC from current measurements. VOC abundances are generally highest very near their sources. Natural emissions occur predominantly in the tropics (23°S to 23°N), with smaller amounts emitted in the northern mid-latitudes and boreal regions mainly in the warmer seasons. Anthropogenic emissions occur in heavily populated, industrialized regions (95% in the northern hemisphere peaking at 40°N to 50°N), where natural emissions are relatively low, so they have significant impacts on regional chemistry despite small global emissions. A few VOCs, such as ethane and acetone, have longer lifetimes and impact tropospheric chemistry on hemispheric scales. It is expected that anthropogenic emissions of most VOCs have risen since preindustrial times due to increased use of gasoline and other hydrocarbon products. Due to the importance of VOC abundance in determining tropospheric O_3 and OH, systematic measurements and analysis of their budgets will remain important in understanding the chemistry-climate coupling.

1.6.2. Organic aerosols

Organic compounds make up a large but highly variable fraction of the atmospheric aerosol. Organic aerosol particles are directly emitted, biogenically by vegetation and by the ocean, and anthropogenically by fossil fuel use, biomass burning and by industries. Together with these particulate emissions a gas phase emission is present and the degradation of these precursors through oxidation leads to SOA formation. The anthropogenic impact is evident in the major contribution, i.e. biomass burning. Organics are the largest single component of biomass burning aerosols (Andreae et al., 1988). The chemical composition of aerosol particles is highly variable depending on geographic location.

Measurements over the Atlantic in the haze plume from the United States indicated that organic aerosols scattered at least as much light as sulfate particles. Organics are also important constituents, perhaps even a majority, of upper-tropospheric aerosols and there are indications of their existence in the lower stratosphere (Immler et al., 2005). The presence of polar functional groups, particularly carboxylic and dicarboxylic acids, makes many of the organic compounds in aerosols water soluble. This affects the water uptake of aerosols particles (Saxena et al., 1995) and allows them to participate in cloud droplet nucleation (Choi et al., 2002). Recent field measurements have confirmed that organic aerosols may be efficient cloud nuclei and consequently play an important role for the indirect climate effect as well (Rivera et al., 1996).

1.7. The work presented in this thesis

The work presented here falls into two categories:

i) laboratory studies of water uptake

ii) hygroscopicity measurements of atmospheric aerosol particles

In order to characterize the hygroscopicity the author used an HTDMA (Weingartner et al., 2002). The functioning and methodology is described in more detail in chapter 2 below. Briefly; the instrument measures the change in diameter due to uptake of water by the aerosol (hygroscopic growth factor, GF). The hygroscopic growth of particles with diameters between 20 and 250 nm can be determined in the temperature range of -20°C to 30°C and the humidity range of 10% to 95% RH with an accuracy of 0.1°C and 1.6%, respectively. The aerosol particles (flow rate: 0.3 L min^{-1}) first enters a silica gel diffusion dryer in order to dry the sample to RH<10% at 25°C. The dry aerosol is then charged with a diffusion charger (^{85}Kr) and fed into a first differential mobility analyzer (DMA1), where a narrow size range of dry aerosol (often D_0=100 nm) is chosen. This selected dry diameter, D_0 was verified by measuring, while keeping the whole instrument dry at RH<10%. The monodisperse aerosol is then conditioned to a well-defined higher RH. The aerosol particle diameter is measured using the second DMA and a condensation particle counter (CPC).

To complement these studies for particles at larger sizes an EDB was used at IAC ETH Zurich. This instrument is described in more detail in chapter 2 and 3 below, and shortly, works as follows: an electrically charged particle (typically 2-10 µm in radius) is levitated in an electric field (Davis et al., 1990). The RH is set by adjusting the N_2/H_2O ratio of a constant gas flow, using automatic mass flow controllers. During an experiment, the temperature is kept constant while the RH is changed with a constant rate. The RH-sensor was calibrated directly in the trap using the deliquescence relative humidity of different salts. Its accuracy is ±1.5%RH between 10%RH and 80%RH and ±3%RH above 80%RH. To characterize the particle a HeNe laser (633 nm) illuminates the particle from below. The video image of the particle on a CCD detector and an automatic feedback loop are used to adjust the DC voltage for compensating the gravitational force. A change in DC voltage is therefore a direct measure of the mass change. If the voltage at dry conditions (RH<10%) corresponds to the dry mass of the particle (M_{dry}) we can deduce the mass growth factor.

Chapter 2 describes how two HTDMAs and the EDB were used in to investigate aerosols of prescribed composition with atmospheric relevance. In order to investigate the time needed to achieve equilibrium between the water vapor and the aerosol particles the exposure time at the preset RH was varied. For mixtures with at least one component remaining solid, equilibration times up to several tens of seconds were observed. At only a few seconds residence time the hygroscopic growth can, for these cases, be underestimated by up to 10% in D/D_0. Thus accurate measurements require that the residence time of the instrument should not be too low, a reasonable recommendation being about 10 s. Furthermore, it was suggested that the most plausible reason for the mass transfer limitation is related to solid enclosures, as the particle morphology can be quite complex. This was corroborated with an increased water uptake in the RH-range of interest, which could be explained with an inverse Kelvin effect at the surface, more precise at the opening of veins and cavities, of the solid part of the particle. The inverse Kelvin effect should be present as long as the surface is not completely covered with a liquid layer, i.e. as long as there are irregularities from the solid component's matrix still noticeable to produce inwards curved cavities. As the water uptake increases with increasing RH, one assumes that the inverse Kelvin effect vanishes. However, this has not been observed in detail in these studies, partly due to the high resolution that would be needed in the HTDMA for the mixtures studied. One case which indicate this behavior is the mixture of AS/AA 1:2 in chapter 2, where a slightly

increased water uptake is observed in the 80-90% RH range compared to theory, but at higher RHs the measured data again overlaps with theory.

If one considers atmospheric aerosol, the increased water uptake due to Kelvin effect has the potential to influence the radiation budget. For the single scattering albedo, assuming that the diameter change does not change the refractive index of the particle and only increases the particle size, an increase of the SSA of 3% can be estimated at 550 nm wavelength of incident light from Mie theory. However, this effect seem possible only for particles with a solid enclosure and at lower GFs. Furthermore, there is no indication that anthropogenic aerosol would be more prone to such a phenomenon than natural aerosol. It could actually be the inverse, with the anthropogenic aerosol containing more different compounds, resulting in an aerosol less prone to containing a solid crystal.

In Chapter 3 further measurements of mixtures generated in the laboratory are presented, now focusing on the different cases one could expect: liquid/liquid, liquid/solid and solid/solid (AS mixed with either a deliquescing organic, glutaric acid, or solid adipic acid). The measurements were done principally with the EDB, complemented with the HTDMA. Pure citric acid was always liquid, adipic was always solid, while glutaric acid showed a hysteresis during hygroscopicity cycles covering hydration and dehydration cases. We show that the hygroscopicity of mixtures of the above compounds is well described by the Zdanovskii-Stokes-Robinson (ZSR) relationship as long as the two-component particle is completely liquid. However, we observe discrepancies compared to what is expected from bulk thermodynamics when a solid component is present. The AS/AA mixture shows in detail in the EDB a pre-deliquescence water uptake, which indeed indicates a surface uptake of water, confirming an inverse Kelvin effect.

In the atmosphere one also encounters mineral dust. Chapter 4 describes a setup to generate a stable continuous output of different powders. As test substance Arizona test dust (ATD) was used. The equipment was verified with regards to particle size and number concentrations generated. It was also of interest to verify the hygroscopicity of ATD, and it was found to be hydrophobic. Electronmicrographs revealed the smallest single particles to be about 100 nm, and larger ones to be clusters of these. This was also noted during water uptake on the larger clusters, as the clusters compacted by a few percent in mobility diameter instead of growing. Further test on ATD in chapter 5, where the dust was exposed to various levels of HNO_3, showed that acidic processed mineral dust become more hygroscopic and an uptake takes place, which further is dependant on RH during the processing. This might be of atmospheric relevance. This is due to the fact that global climate models (GCMs) underpredict NO_x and overestimate HNO_3 (Gao et al., 1999), which could partly be caused by heterogeneous uptake of HNO_3 on mineral dust (Liao and Seinfeld, 2005). HNO_3 is a reservoir species for NO_x so incorporation of this process in models should improve accuracy.

In Chapter 6 hygroscopicity measurements from JFJ are presented. The aerosol at the JFJ shows a mix between inorganic and organic substances, as deduced from AMS composition measurements. The main inorganics are AS, ammonium bisulfate and ammonium nitrate, and the organics are a large range of individual components. There are also mineral dust events, shown by the single scattering albedo (Coen, 2004), and back trajectories indicates Sahara origin (Henning et al., 2003). Measurements campaigns at JFJ with the duration of about one month were carried out in 2000, 2002, 2004 and 2005. A winter campaign was again performed 2007, by a new PhD student, and is not included in this work, however it is worth noting that there are several investigations still to be done and questions to answer.

1.8. Outlook

In this work unknowns concerning the influence of organics on the atmospheric aerosol were investigated. The study of organic compounds in aerosol particles is of importance because they affect the water uptake (hygroscopicity) of inorganic aerosol, and hence the radiation budget of the earth through the direct and indirect aerosol effects. Aerosol mixtures were studied in the laboratory, ranging from known pure inorganic salts to more complex mixtures. The kinetics were investigated for the water uptake, and it was found that for mixtures with a solid phase, up to tens of seconds were required for equilibration. Mineral dust (standard Arizona test dust) was investigated, as well as the influence of nitric acid (HNO_3) uptake thereon. It was found that the RH during the uptake influences the uptake coefficient. Measurements from four field campaigns at the JFJ with a duration of one month each are presented. Results include description of the GF distribution and a hygroscopic closure, showing the connection of chemistry to hygroscopicity for atmospheric aerosol.

Thus at first the HTDMA was validated and precision and accuracy investigated through measurements with known salts. Then laboratory studies were done, with mixtures with increasing complexity. It is known that the aerosol at the JFJ is a mixture of inorganic and organic substances, but that mineral dust is also encountered at times, thus the opportunity to study mineral dust under controlled conditions in the laboratory was taken. These points studied in the laboratory helped increasing confidence in the hygroscopic closure for the atmospheric aerosol investigated. In this work the sulfate measured in the atmosphere was assumed to distribute into sulfuric acid, ammonium bisulfate or ammonium sulfate, depending on the amount of ammonium available for neutralization. This is one of the first works with such an approach, which improved the quality of the hygroscopic closure. However this approach has only been empirically deduced and further atmospheric and/or laboratory studies could be envisaged to verify the equilibria, especially with mixtures containing nitrate as well. Thus the data from a hygroscopic closure indicate that the water uptake can be modeled from the chemical compositions. As available measurements and data increase, such an approach can be incorporated in GCMs to describe the aerosol water uptake and thus scattering of the aerosol in sub-saturated environment. Questions that are currently being investigated are further how the hygroscopicity is connected to CCN activity. How useful are parameterizations of hygroscopicity for CCN activity? Field data for such comparisons, especially for higher altitudes (troposphere) are scarce and would be of large use for the aerosol-cloud interactions community. Thus further field measurements can be recommended.

Concerning especially the mineral dust studies one could recommend performing studies both in the laboratory and in the field. The reaction kinetics for HNO_3 processing in this study was measured on the 0.2-2 seconds time scale. It would be advantageous to increase this timescale, which is not easily solved experimentally due to aerosol residence times in air flows, in order to further approach atmospheric conditions. This would improve the studies with regards to diffusion into the particles and possible regeneration of active sites on the surface (Rudich et al., 2007). Additional questions aroused are: what are the reactive sites on mineral dust? And why is the reactivity increasing with RH? There exist other examples of uptake dependant on RH, with ambiguous results, depending on the mixture used: benzo[*a*]pyrene (BaP), on the surface of azelaic acid, reacts with O_3 increasingly with RH, but decreasingly for intermediate RHs, if condensed on soot particles. Another topic concerning the HNO_3 processing is how important photolysis of adsorbed HNO_3 on surface might be. Currently, the “state-of-the-art” atmospheric models treat mineral dust as a heterogeneous sink for gaseous HNO_3 in the upper troposphere. The uptake of nitric acid to dust is considered to prevent renoxification of HNO_3 by *in situ* photolysis in the atmosphere. The

models however do not consider the possibility of the reaction products (nitrates) photolysis on the surface of mineral dust. To improve the description of the role of mineral dust as a heterogeneous sink for nitric acid, photolysis of the nitrates on the surface of the dust aerosol should be investigated as no data are available so far.

Thus there remain questions concerning the transformation of aerosol in the atmosphere, and several laboratories work with these questions of ageing of the aerosol from the source point to the removal of the particles. The approach used today is to draw on results from laboratory studies, field campaigns and modeling results, and the proper combination of these techniques will probably be of even more importance in the future, as the complexity of the topic increases.

References

Andreae, M. O., Browell, E. V., Garstang, M., Gregory, G. L., Harriss, R. C., Hill, G. F., Jacob, D. J., Pereira, M. C., Sachse, G. W., Setzer, A. W., Dias, P. L. S., Talbot, R. W., Torres, A. L., & Wofsy, S. C. (1988). Biomass-Burning Emissions and Associated Haze Layers over Amazonia. Journal of Geophysical Research-Atmospheres, 93, (D2), 1509-1527.

Bayer-Oglesby, L., Grize, L., Gassner, M., Takken-Sahli, K., Sennhauser, F. H., Neu, U., Schindler, C., & Braun-Fahrlander, C. (2005). Decline of ambient air pollution levels and improved respiratory health in Swiss children. Environmental Health Perspectives, 113, (11), 1632-1637.

Choi, M. Y., & Chan, C. K. (2002). The effects of organic species on the hygroscopic behaviors of inorganic aerosols. Environmental Science & Technology, 36, (11), 2422-2428.

Coen, M. C., Weingartner, E., Schaub, D., Hueglin, C., Corrigan, C., Henning, S., Schwikowski, M., & Baltensperger, U. (2004). Saharan dust events at the Jungfraujoch: detection by wavelength dependence of the single scattering albedo and first climatology analysis. Atmospheric Chemistry and Physics, 4, 2465-2480.

Davis, E. J., Buehler, M. F., & Ward, T. L. (1990). The Double-Ring Electrodynamic Balance for Microparticle Characterization. Review of Scientific Instruments, 61, (4), 1281-1288.

Dockery, D. W., Pope, C. A., Xu, X. P., Spengler, J. D., Ware, J. H., Fay, M. E., Ferris, B. G., & Speizer, F. E. (1993). An Association between Air-Pollution and Mortality in 6 United- States Cities. New England Journal of Medicine, 329, (24), 1753-1759.

Duce, R. A., Mohnen, V. A., Zimmerman, P. R., Grosjean, D., Cautreels, W., Chatfield, R., Jaenicke, R., Ogren, J. A., Pellizzari, E. D., & Wallace, G. T. (1983). Organic Material in the Global Troposphere. Reviews of Geophysics, 21, (4), 921-952.

Gao, R. S., Fahey, D. W., Del Negro, L. A., Donnelly, S. G., Keim, E. R., Neuman, J. A., Teverovskaia, E., Wennberg, P. O., Hanisco, T. F., Lanzendorf, E. J., Proffitt, M. H., Margitan, J. J., Wilson, J. C., Elkins, J. W., Stimpfle, R. M., Cohen, R. C., McElroy, C. T., Bui, T. P., Salawitch, R. J., Brown, S. S., Ravishankara, A. R., Portmann, R. W., Ko, M. K. W., Weisenstein, D. K., & Newman, P. A. (1999). A comparison of observations and model simulations of NOx/NOy in the lower stratosphere. Geophysical Research Letters, 26, (8), 1153-1156.

Guenther, A., Hewitt, C. N., Erickson, D., Fall, R., Geron, C., Graedel, T., Harley, P., Klinger, L., Lerdau, M., McKay, W. A., Pierce, T., Scholes, B., Steinbrecher, R., Tallamraju, R., Taylor, J., & Zimmerman, P. (1995). A Global-Model of Natural Volatile Organic-Compound Emissions. Journal of Geophysical Research-Atmospheres, 100, (D5), 8873-8892.

Henning, S., Weingartner, E., Schwikowski, M., Gaggeler, H. W., Gehrig, R., Hinz, K. P., Trimborn, A., Spengler, B., & Baltensperger, U. (2003). Seasonal variation of water-soluble ions of the aerosol at the high-alpine site Jungfraujoch (3580 m asl). Journal of Geophysical Research-Atmospheres, 108, (D1).

Hinds, W. C. (1999). Aerosol Technology, 2nd edition, John Wiley & Sons Inc., New York.

Holgate, S. T., Samet, J. M., Koren, H. S., & Maynard, R. L. (1999). Air pollution and health, Academic Press.

Immler, F., Engelbart, D., & Schrems, O. (2005). Fluorescence from atmospheric aerosol detected by a lidar indicates biogenic particles in the lowermost stratosphere. Atmospheric Chemistry and Physics, 5, 345-355.

Jacobson, M. C., Hansson, H. C., Noone, K. J., & Charlson, R. J. (2000). Organic atmospheric aerosols: Review and state of the science. Reviews of Geophysics, 38, (2), 267-294.

Kiehl, & Trenberth (1997). Earth's annual global mean energy budget. Am. Met. Soc, 78, (197–208).

Koistinen, K. J., Kousa, A., Tenhola, V., Hanninen, O., Jantunen, M. J., Oglesby, L., Kuenzli, N., & Georgoulis, L. (1999). Fine particle (PM2.5) measurement methodology, quality assurance procedures, and pilot results of the EXPOLIS study. Journal of the Air & Waste Management Association, 49, (10), 1212-1220.

Liao, H., & Seinfeld, J. H. (2005). Global impacts of gas-phase chemistry-aerosol interactions on direct radiative forcing by anthropogenic aerosols and ozone. Journal of Geophysical Research-Atmospheres, 110, (D18).

McMurry, P., Shepherd, M., & Vickery, J. (2004). NARSTO. Particulate Matter Assessment for Policy Makers: A NARSTO Assessment. Cambridge University Press, Cambridge, England.

Penner, J. E., Dickinson, R. E., & Oneill, C. A. (1992). Effects of Aerosol from Biomass Burning on the Global Radiation Budget. Science, 256, (5062), 1432-1434.

Raupach, M. R., & Canadell, J. G. (2006). The global carbon cycle: drivers, dynamics and vulnerabilities. Abstracts: Cape Grim Baseline Air Pollution Station Annual Science Meeting 2006, Hobart ,Tasmania.

RiveraCarpio, C. A., Corrigan, C. E., Novakov, T., Penner, J. E., Rogers, C. F., & Chow, J. C. (1996). Derivation of contributions of sulfate and carbonaceous aerosols to cloud condensation nuclei from mass size distributions. Journal of Geophysical Research-Atmospheres, 101, (D14), 19483-19493.

Saxena, P., & Hildemann, L. M. (1996). Water-soluble organics in atmospheric particles: A critical review of the literature and application of thermodynamics to identify candidate compounds. Journal of Atmospheric Chemistry, 24, (1), 57-109.

Saxena, P., Hildemann, L. M., McMurry, P. H., & Seinfeld, J. H. (1995). Organics alter hygroscopic behavior of atmospheric particles. Journal of Geophysical Research, 100, (D9), 18755-18770.

Solomon, S., Qin, D., Manning, M., Alley, R. B., Berntsen, T., Bindoff, N. L., Chen, Z., Chidthaisong, A., Gregory, J. M., Hegerl, G. C., Heimann, M., Hewitson, B., Hoskins, B. J., Joos, F., Jouzel, J., Kattsov, V., Lohmann, U., Matsuno, T., Molina, M., Nicholls, N., Overpeck, J., Raga, G., Ramaswamy, V., Ren, J., Rusticucci, M., Somerville, R., Stocker, T. F., Whetton, P., Wood, R. A., & Wratt, D. (2007). Contribution of Working Group I to the Fourth Assessment Report of the Intergovernmental Panel on Climate Change - Technical Summary, Cambridge University Press, Cambridge, United Kingdom and New York.

Textor, C., Schulz, M., Guibert, S., Kinne, S., Balkanski, Y., Bauer, S., Berntsen, T., Berglen, T., Boucher, O., Chin, M., Dentener, F., Diehl, T., Easter, R., Feichter, H., Fillmore, D., Ghan, S., Ginoux, P., Gong, S., Kristjansson, J. E., Krol, M., Lauer, A., Lamarque, J. F., Liu, X., Montanaro, V., Myhre, G., Penner, J., Pitari, G., Reddy, S., Seland, O., Stier, P., Takemura, T., & Tie, X. (2006). Analysis and quantification of the diversities of aerosol life cycles within AeroCom. Atmospheric Chemistry and Physics, 6, 1777-1813.

Weingartner, E., Gysel, M., & Baltensperger, U. (2002). Hygroscopicity of aerosol particles at low temperatures. 1. New low-temperature H-TDMA instrument: Setup and first applications. Environmental Science & Technology, 36, (1), 55-62.

Went, F. W. (1960). Blue Hazes in the Atmosphere. Nature, 187, (4738), 641-643.

CHAPTER 2

2. Hygroscopic growth and water uptake kinetics of two-phase aerosol particles consisting of ammonium sulfate, adipic and humic acid mixtures

This chapter is a paper from the author of this dissertation and colleagues. Published in Journal of Aerosol Science, vol. 38, No. 2, p. 157-171, 2007.

S. Sjogren[a], M. Gysel[a], E. Weingartner[a], U. Baltensperger[a], M.J. Cubison[b,+], H. Coe[b], A. Zardini[c], C. Marcolli[c], U.K. Krieger[c] and T. Peter[c]

[a] *Laboratory of Atmospheric Chemistry, Paul Scherrer Institut, CH-5232 Villigen, Switzerland*
[b] *School of Earth, Atmospheric and Environmental Science, University of Manchester, UK*
[c] *Institute for Atmospheric and Climate Science, ETH, Zurich, Switzerland*
[+] *Now at: Cooperative Institute for Research in Environmental Science, University of Colorado, Boulder, USA*

2.1. Abstract

The hygroscopic growth of solid aerosol particles consisting of mixtures of ammonium sulfate and either adipic acid or Aldrich humic acid sodium salt was characterized with a hygroscopicity tandem differential mobility analyzer and an electrodynamic balance. In particular, the time required for the aerosol particle phase and the surrounding water vapor to reach equilibrium at high relative humidity (RH) was investigated. Depending on the chemical composition of the particles, residence times of >40 seconds were required to reach equilibrium at 85%RH, yielding a measured hygroscopic growth factor up to 7% too low from measurements at 4 s residence time compared to measurements at equilibrium. We suggest that the solid organic compound, when present as the dominant component, encloses the water-soluble inorganic salt in veins and cavities, resulting in the observed slow water uptake. Comparison with predictions from the Zdanovskii-Stokes-Robinson relation shows enhanced water up take of the mixed particles. This is explained with the presence of the salt solution in veins resulting in a negative curvature of the solution meniscus at the opening of the vein. In conclusion, it is important for studies of mixtures of water soluble compounds with insoluble material to allow for sufficient residence time at the specified humidity to reach equilibrium before the hygroscopicity measurements.

2.2. Introduction

Aerosol particles in the atmosphere affect the earth's radiation balance in various ways (IPCC, 2001). Firstly, aerosol particles absorb and scatter radiation. This *direct aerosol effect* is influenced by the hygroscopicity of the aerosol particles, which is determined mainly by their chemical composition. Secondly, the tendency for cloud formation and resulting cloud properties similarly depend on chemical composition as well as on size distribution of the aerosol particles (e.g. McFiggans et al., 2006). Thus the cloud albedo and the radiative properties of cloud droplets are influenced, coined the *indirect aerosol effect*.

Atmospheric aerosol components can be classified into inorganic and organic components (e.g. Kanakidou et al., 2005). The hygroscopic properties of most inorganic salts present in the atmosphere are well known (e.g. Ansari & Pandis, 1999; Colberg et al., 2003). Of the many organic species identified in the aerosol (e.g. Putaud et al., 2004), the hygroscopic properties of quite a few pure substances have been investigated. However, to date the hygroscopic properties of only a few mixtures have been investigated. Inorganic salts (for instance ammonium sulfate (AS) and sodium chloride) can show a hysteresis behavior during uptake and loss of water, i.e. by exhibiting a difference between the deliquescence and efflorescence relative humidities (DRH/ERH), and with a higher water content of the deliquesced than the effloresced particles in this relative humidity (RH) range. Conversely, organic constituents of the aerosol without hysteresis behavior can contribute to an uptake of water at lower RH than the DRH of inorganic salts. This has been reported by Dick et al. (2000) and is also theoretically expected, as such complex mixtures can remain in the liquid state and exchange water with the gas phase at lower RH's (Marcolli et al., 2004).

The response of aerosol particles to changes in RH can be measured by a variety of instruments. The particle levitation technique using an electrodynamic balance (EDB) has been demonstrated to be a valuable method for studying the hygroscopic properties of single aerosol particles (Davis et al., 1990). This technique has the advantage that the particle mass can be monitored continuously as a function of RH, thus providing unambiguous in situ characterization of the particle mass growth due to water uptake. It can be used for particles with diameters larger than a few micrometers. A different method for characterizing water uptake is the hygroscopicity tandem differential mobility analyzer (HTDMA, Rader & McMurry, 1986).

In this paper measurements performed by two HTDMAs are compared with each other and with results obtained with an EDB. One of the HTDMAs is from the University of Manchester (UMan), UK (Cubison et al., 2005), the other one from the Paul Scherrer Institute (PSI), Switzerland (Weingartner et al., 2002a), while the EDB is from ETH Zurich (Colberg et al., 2004). Hygroscopicity measurements for a variety of mixtures are presented. The growth of AS is compared with the theoretical prediction using the Aerosol Diameter-Dependent Equilibrium Model (ADDEM) (Topping et al., 2005a; Topping et al., 2005b) developed at the UMan. In the case of mixtures of different components (AS with organics), the hygroscopic growth was predicted using the Zdanovskii-Stokes-Robinson (ZSR) relation for water activities of mixed particles (Stokes & Robinson, 1966).

Mass transfer effects in hygroscopic measurements of aerosol particles have recently obtained more attention. It has been discussed whether organic/inorganic aerosol mixtures show mass transfer limitations of water (contrary to pure inorganic salts which equilibrate very fast, within timescales of <1 s). Kerminen (1997) considered the gas-phase transfer to particles before cloud activation, and reported calculated equilibration times < 1 s. However, a field study by Chuang (2003) found that a fraction of the particles exhibited a slower water uptake than the majority of particles sampled, which was explained by a low mass

accommodation coefficient in that study. Chan and Chan (2005) did a review of the different hygroscopicity studies with possible mass transfer effects for water uptake of aerosol particles, concluding the need for further investigation. Cubison (2005) described an experimental set-up and results for several systems. Our study further investigates and analyzes the results from measurements with varying residence times at elevated RH. In order to evaluate the water vapor equilibration time, the residence time of the particles at high relative humidity was varied from seconds to minutes. AS was chosen as the inorganic salt in this study, as its hygroscopicity is well known and it is a common constituent in the atmosphere. Adipic acid (AA) was chosen as an organic constituent. AA has a low vapor pressure and is only moderately soluble in water (high DRH). At the RH's studied here it is present in its crystalline form, which is assumed to contribute to a prolonged water uptake equilibration time. AA has also been identified in atmospheric samples (Ray & McDow, 2005). Furthermore tests were carried out with the commercially available Aldrich humic acid sodium salt (NaHA). This compound serves as a proxy for humic-like substances that were identified as a major component of the isolated organic matter in the atmospheric aerosol (Graber & Rudich, 2006; Kiss et al., 2003).

2.3. Experimental Methods

2.3.1. Hygroscopic growth and the ZSR relation

The hygroscopic growth (*GF*) indicates the relative increase in mobility diameter of particles due to water absorption at a certain RH, and is defined as

$$GF(RH) = \frac{D(RH)}{D_0} \quad , \qquad \textbf{(2-1)}$$

where *D(RH)* is the mobility diameter at a specific RH and D_0 is the dry particle mobility diameter measured for spherical particles (dynamic shape correction factor, χ, is 1). Near-sphericity (χ<1.01) was ensured by choosing D_0 either as the smallest diameter measured during hydration mode (see section 2.3.2 below), or, if the aerosol showed water uptake at low RH, by choosing the diameter extrapolated to 0%RH for the dehydration mode (droplets). Mobility growth factors obtained with an HTDMA are only equal to volume equivalent growth factors if the particles do not change the shape during water uptake. The *GF* is presented in humidograms (i.e. showing the response in hygroscopic growth versus relative humidity, see Fig. 2-2).

The hygroscopic growth factor of a mixture (GF_{mixed}) can be estimated from the growth factors of the pure components and their respective volume fractions, ε, with the ZSR relation (Gysel et al., 2004; Stokes et al., 1966)

$$GF_{mixed} = \left(\sum_k \varepsilon_k GF_k^3 \right)^{1/3} , \qquad \textbf{(2-2)}$$

where the summation goes over all compounds present in the particles. The model assumes spherical particles, ideal mixing behavior (i.e. no volume change upon mixing) and independent water uptake of the organic and inorganic components. The volume fractions for the two components in the dry particles were calculated as

$$\varepsilon_i = \frac{(w_i / \rho_i)}{\sum_k (w_k / \rho_k)} \quad , \qquad \textbf{(2-3)}$$

where w_i is the mass fraction and ρ_i the density of the pure substance *i*. Values of ρ used in the model were 1.77, 1.36 and 1.1 g/cm^3 for AS, AA and NaHA, respectively, obtained from the product suppliers. The hygroscopic growth of AS was parameterized for the deliquesced state from our measurements, between 35-93%RH, with:

$$GF = (1 - \%RH/100)^{\gamma} + c \quad \textbf{(2-4)}$$

where RH is given in percent, and the coefficients γ and c were fitted as -0.21821 and 0.070, respectively. The standard deviation of the residuals between this parameterization and the ADDEM model was 0.012 in *GF* (Topping et al., 2005a).

2.3.2. HTDMA

The two HTDMAs employed (from UMan and PSI) are operated in a similar manner. A differential mobility analyzer (DMA1) selects a monodisperse aerosol size, D_0, under dry conditions (RH<10%). The aerosol then passes through a humidifier with a controlled higher RH, and the diameter *D* is measured with a second DMA (DMA2). A scheme can be seen in Fig. 2-1. The two DMAs are similar to the TSI 3071 type. The instrument from PSI with a closed-loop sheath air uses only the aerosol flow entering the DMA2 to regulate the RH in the DMA2. The RH of the sheath air thus follows the RH of the aerosol flow. RH setpoint changes were kept small, in order to maintain similar RH in the aerosol flow as in the sheath air. In this study data was used only if the variation in the sheath air was <1%RH during each scan.

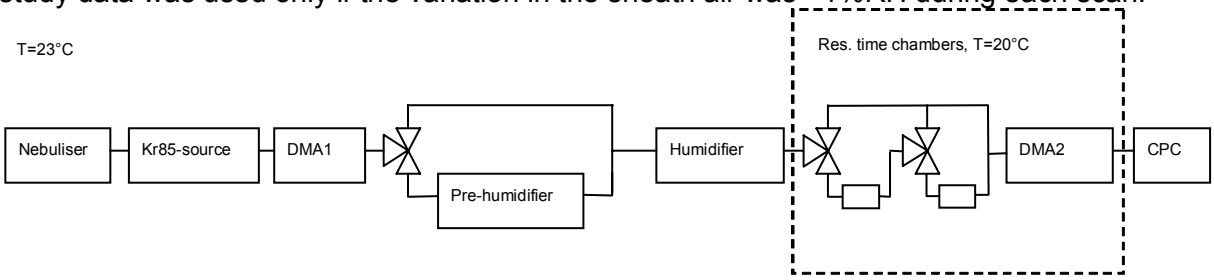

Fig. 2-1. Experimental set-up of the HTDMA.

The UMan instrument humidifies the aerosol flow and the sheath air flow with two independent humidifiers and controllers. The RH of the aerosol and the sheath air was kept identical. The two DMAs used were constructed in house and are of the Vienna design (Winklmayr et al., 1991). Both HTDMAs were kept at a constant temperature set in the range 18-23 °C (controlled by a water bath). A few degrees cooling of DMA2 with respect to the aerosol and sheath air conditioners (at constant laboratory temperature) was necessary to reach high RH's (>90%RH). The relevant RH in DMA2 was determined by measurement of the system temperature and the DMA2 excess sheath air dew point using a dew point mirror. The accuracy of the RH measurement at higher RH is for example 90±1.2%, assuming no temperature gradients in the DMA2. The hygroscopic growth factor (*GF*) can be determined with a precision (2x standard deviation) of $\Delta GF \approx \pm 0.01$ (at D_0) and $\Delta GF \approx \pm 0.03$ (at DRH). Measurements of solid inert material, such as mineral dust, performed with the same HTDMA set-up show a precision of $\Delta GF \approx \pm 0.005$ (see Vlasenko et al. (2006)).

Two different ways to operate the HTDMA were used; these are denoted hydration and dehydration mode. For the hydration mode, the mono-modal dry particles were exposed to a monotonically increasing RH until the size measurement in DMA2. For the dehydration mode the particles were first deliquesced at RH>80% in a pre-humidifier, and then the RH was monotonically lowered to the RH in DMA2, thus allowing the efflorescence relative humidity to be measured. For the ERH measurements the DMA2 was kept at a temperature similar to the

laboratory temperature in order to guarantee that the lowest RH behind the pre-humidifier occurs in DMA2, to avoid efflorescence before DMA2. The pre-humidifier switched on/off automatically. This setup allows a completely automated operation of the HTDMA.

2.3.3. Residence time chambers

In order to study the effect of residence time of the aerosol in the HTDMAs, chambers of different volumes were installed after the humidifier (before entry to DMA2), allowing the aerosol to equilibrate at the specified RH for a range of residence times. The chambers were kept at the same temperature as the DMA2 in order to ensure constant RH from the chambers to DMA2. The chambers were of different sizes yielding measured residence times (τ_{res}) ranging from 3 s to 2 min in total. The errors in τ_{res} were on the order of +/- 4 s for τ_{res}<30s and +/- 11 s for $\tau_{res} \geq$30 s. The geometries of the chambers were chosen as cylinders with a ratio of length to diameter of about 3 to 10, because of space availability and construction reasons. Several measurement scans, each with a duration varying between 1-3 min, were done after switching to the chamber with the longest τ_{res} to allow for a steady state to build up. Then, monotonically shorter τ_{res} were measured (by turning 3-way valves), until only connecting tubing was used for the shortest τ_{res}. If the pre-humidifier was used, the τ_{res} was increased by 10 s (time from the middle of the pre-humidifier to the main humidifier). The residence times stated below are thus from the middle of the first humidifier (pre-humidifier or main humidifier) through the tubing and residence chambers up to the entry point of the sheath air inside the DMA2. The time from the entry point of DMA2 to where the aerosol flow mixes with the sheath air is 3.5 s for the PSI HTDMA and 2 s for the UMan HTDMA.

2.3.4. Electrodynamic balance

An electrically charged particle (typically 2-10 µm in radius) is levitated in an electrodynamic balance (Davis et al., 1990). The RH is set by adjusting the N_2/H_2O ratio of constant gas flow, using automatic mass flow controllers. During an experiment, the temperature is kept constant while the RH is changed with a constant rate. The sensor was calibrated directly in the trap using the deliquescence relative humidity of different salts. Its accuracy is ±1.5%RH between 10%RH and 80%RH and ±3%RH above 80%RH.

To characterize the particle a HeNe laser (633 nm) illuminates the particle from below. The video image of the particle on a CCD detector and an automatic feedback loop are used to adjust the DC-voltage for compensating the gravitational force. A change in DC voltage is therefore a direct measure of the mass change. If the voltage at dry conditions (RH<10%) corresponds to the dry mass of the particle (M_{dry}) we can deduce the mass growth factor. In addition, we use a photomultiplier with a conical detection angle (approximately 0.2° half-angle) to measure the scattering intensity at 90° to the incident beam and feed this signal to an analog lock-in amplifier to measure the intensity fluctuations, that is, the root mean square deviation from the intensity mean (RMSD intensity). Because of its symmetry, a homogeneous spherical particle will show a constant scattering intensity and hence a very small fluctuation amplitude (corresponding to a value of 0.04, for our noise level). A nonspherical particle will scatter light with different intensity in the detection angle depending on its orientation relative to the incoming laser beam. All particles perform Brownian rotational motion in an EDB, which leads to an RMSD intensity between 0.5 and 5 depending on the deviation from spherical symmetry of the particle in its dry, solid state. We have used these intensity fluctuation amplitudes previously to characterize liquid microdroplets with a single solid inclusion (Krieger & Braun, 2001). In the following we will use this to identify the occurrence of phase transitions and to characterize the morphology of complex aerosol particles.

2.3.5. Aerosol generation / substances tested

Aerosol mixtures were generated using an atomizer (Type TSI 3076) operated with purified compressed air. Details on the substances investigated are found in Table 2-1. The substances were dissolved in MilliQ-water (18 MΩ·cm). All solutions appeared completely dissolved at visual inspection. It is assumed that the resulting aerosol was an internal mixture with the same mass ratio as in the solution (cf. Gysel et al., 2004). This seems plausible, as no broadening of the growth factor distributions from the HTDMA could be detected while switching from the pure AS to the mixtures. The solutions were diluted further with MilliQ-water in the case the original solution yielded too high particle concentrations for the HTDMA at the size studied. The nebulized aerosol produced was subsequently dried in a silica gel diffusion dryer (residence time 30 s). It was found that the mixed aerosol was irregular in shape and restructured up to 5% in mobility diameter after deliquescence. These shape effects have been minimized by introducing a subsequent hydration/dehydration cycle (RH>82%) to allow for deliquescence followed by efflorescence *before* the HTDMA. With this setup it was found that the particles did not restructure further in the HTDMA (within the instrument's precision), which indicates a more compact, spherical, shape. The dried particles were neutralized by means of a Kr-85 source and then fed into the HTDMA for the hygroscopicity measurement.

Table 2-1. Substances used during the experiments.

Substance	Purity	Producer	Product n°
Ammonium sulfate, MicroSelect	99.5	Fluka	09978
Adipic acid, Puriss	99.6	Riedel-deHaen	27635
Humic acid, sodium salt, tech. isolated from crude lignite	N.a.	Aldrich (purchased 2003)	H16752

2.4. Results

2.4.1. Comparison of the two HTDMAs with pure AS

The sizing of the DMAs in both instruments was verified with polystyrene latex spheres in the size range from 90-400 nm. Thereafter instrument performance was verified by measurements of hygroscopicity of the ammonium sulfate (AS). AS is a well investigated substance and the two HTDMA instruments measured reproducible results (GF_{PSI} = 1.48 and GF_{UMan} = 1.46 at 80%RH and for D_0=100 nm) which correspond well with literature (Gysel et al., 2002; Hennig et al., 2005). The modeled curve is calculated as in Topping et al. (2005a). The calculated DRH of AS is 79.9%RH for large particles (Tang & Munkelwitz, 1993). As the particle diameter decreases, the DRH is theoretically predicted to increase. Deliquescence occurs when the free energy of the effloresced particle surface equals the free energy of the deliquesced particle. The surface energy increases due to the Kelvin effect (Russell & Ming, 2002). A negligible increase is predicted for D_0=100 nm particles. Moreover, a recent experimental study showed no significant increase of DRH for AS nanoparticles down to 6 nm (contrary to NaCl), within the range of RH uncertainty (±2.5%RH in that study) (Biskos et al., 2006). The PSI HTDMA measured a DRH of 80.5%RH (average of 6 measurements, standard deviation 0.75%, D_0=100 nm), which is in the range of literature values reported. The τ_{res} at the conditioned RH for different runs was varied between 4 and 40 s, and no influence of varying the τ_{res} was detected. This confirms that equilibration of inorganic salts is fast, << 1s. Measurements of AS were done at the beginning of the intercomparison period and after regular intervals (about every 2 weeks) thereafter.

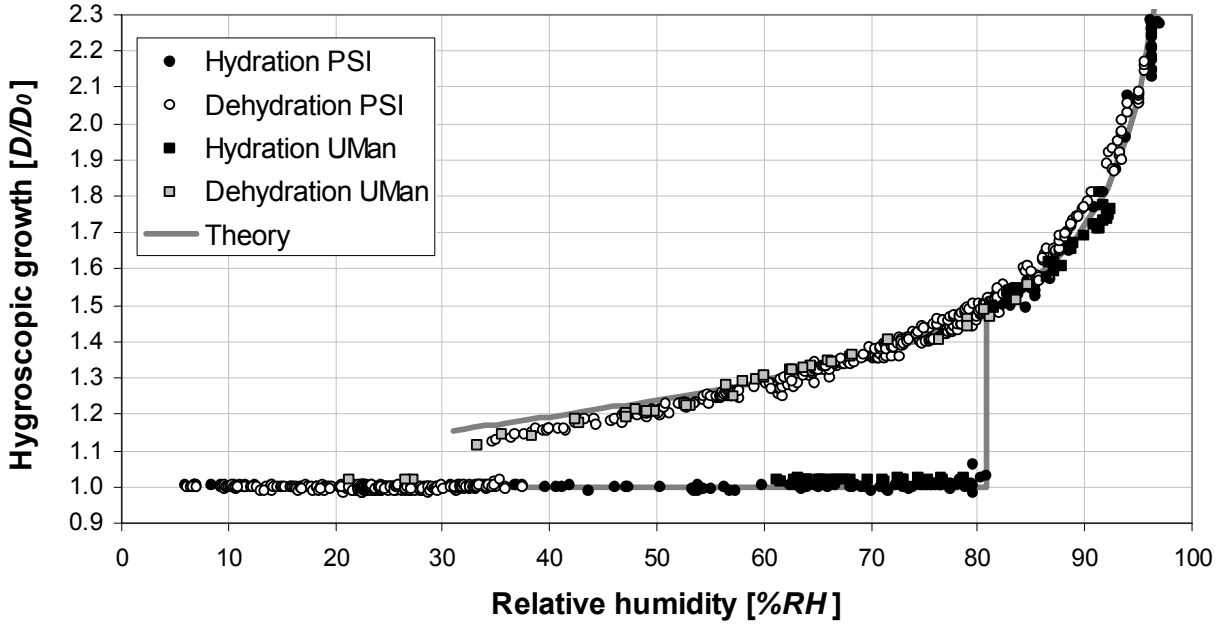

Fig. 2-2. Humidogram of laboratory-generated D_0=100 nm ammonium sulfate aerosol from the two HTDMAs (T ~20°C). The two instruments show a good agreement.

2.4.2. Hygroscopicity of pure adipic acid and pure humic acid

Pure adipic acid (AA) does not show any uptake of water (e.g. *GF* = 1.00 ± 0.02 up to 96%RH) (Joutsensaari et al., 2001), which was confirmed up to RH 92% with both HTDMAs and the EDB in this study. AA is considered to be present as a crystalline solid in this study. This was confirmed with the two-dimensional angular scattering pattern from the EDB.

The hygroscopicity of pure NaHA has also been measured in two former studies (Badger et al., 2006; Gysel et al., 2004). Within experimental error, our results on the growth measured with the dehydration mode are comparable with these studies. However, measurements with the hydration mode differ at lower RH just outside the experimental error. This could be due to different morphology of the particles caused by differences in nebuliser conditions and/or drying conditions after the nebuliser. Particles composed of only NaHA showed no difference in *GF* as the residence time was varied at high RH. However, as the hygroscopicity of the NaHA is relatively low, the resolution of the HTDMA might not be sufficient to discern an effect for pure NaHA.

2.4.3. Hygroscopicity of AS/AA mixtures

The hygroscopic growth of 4 mixtures, with mass ratios of 1:1, 1:2, 1:3 and 1:4 AS/AA, were measured. In order to evaluate the equilibration time of the water uptake, the hygroscopic growth factor was measured with the HTDMAs at various residence times. The hygroscopic growth factors of deliquesced particles measured in the RH range 70-95% (for the hydration mode data only above DRH was used) were interpolated with an empirical fit to 85%RH for each mixture and residence time. Most points were measured in the vicinity of 85%RH. Fig. 2-3 shows box plots of the determined growth factors at 85%RH as a function of residence time for the 1:1, 1:2, 1:3 and 1:4 mixtures. The box plots consist of the mean growth factor (star), as well as 75/25 percentile (box) and 95/5 percentile (whiskers) of the residuals between the measurements and the fit line. Experimental uncertainties for the *GF* precision and τ_{res} accuracy are as stated in section 2.3.2 and 2.3.3.

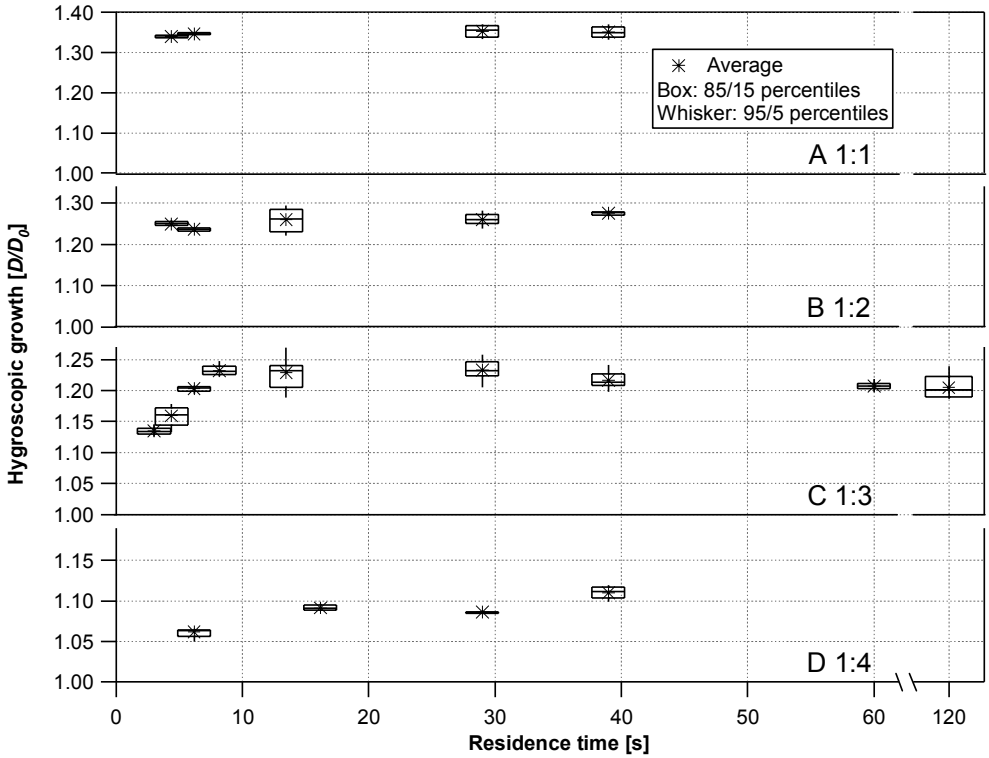

Fig. 2-3. Hygroscopic growth for AS/AA mass ratios 1:1, 1:2, 1:3 and 1:4 (top to bottom panel), measured with different residence times. D_0=100 nm and *GF* relates to 85%RH. The 3s and 60s residence time data for the AS/AA 1:3 mixture was measured with the UMan HTDMA, rest of data was measured with the PSI HTDMA. Each box represents on average 44 data points.

Fig. 2-4 (EDB) and Fig. 2-5 (HTDMA) show the humidograms of the AS/AA mixtures for residence times sufficiently long such that the equilibrium size is reached. In the ZSR relation AA was assumed solid, thus not contributing to the growth at all (*GF*=1.0 at any RH). The presence of AA as a solid was confirmed by intensity fluctuation data from EDB measurements shown in Fig. 2-4: all mixtures over the whole relative humidity range show RMSD of scattered light intensity significantly above what is observed for completely liquid particles. Hence there was always a solid phase present in the particle. Note, however, that at RH substantially lower than the DRH of ammonium sulfate the intensity fluctuations decrease as a consequence of water uptake, leading to an optically more homogeneous spherical particle. The water uptake below ammonium sulfate DRH is clearly detected by the hygroscopic mass growth. At DRH of AS the intensity fluctuations stay constant or increase again (1:1 and 1:2 mixtures) because the water content is now large enough for Brownian motion of the solid adipic acid inclusion in the aqueous solution particle to occur.

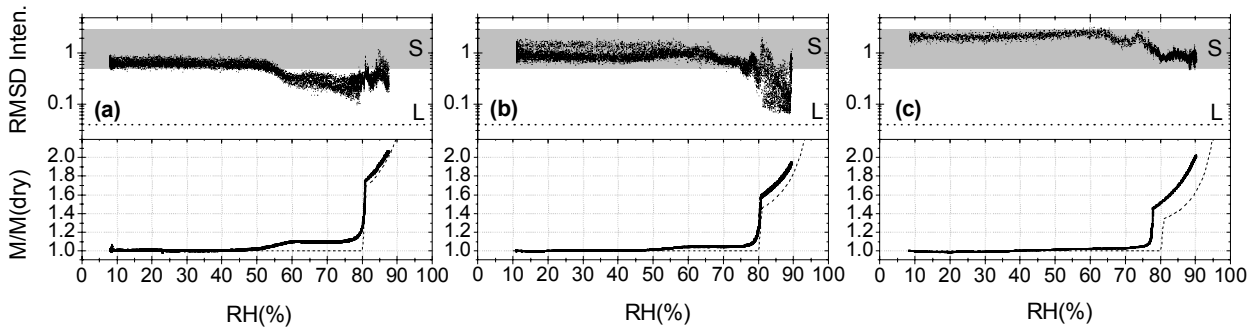

Fig. 2-4. Experimental hygroscopic mass growth (M/M_0, solid lines in lower panels) and ZSR model (dashed lines in lower panels) and intensity fluctuation data (RMSD intensity, upper panels) from EDB measurements for three mixtures of AS/AA: (a) 1:1 in mass ratio, (b) 1:2, (c) 1:3. The shaded area labeled (S) marks the RMSD intensities typical for a solid non-spherical particle, the line labeled (L) marks the RMSD intensity for a completely liquid and hence spherical particle. See text for details.

There is a substantial deviation of hygroscopic growth factors from ZSR prediction at RH above the DRH of ammonium sulfate for 1:2 and 1:3 mixtures, and a shift in DRH to lower RH. In 25 experiments with different particles of the 1:3 composition in the EDB we observed a scatter of values ranging from 1.16 to 1.45 in *GF* at DRH and a scatter ranging from 78 to 83%RH in DRH, which is significantly more scatter than instrument precision. This complex behavior of water uptake is most likely due to the morphology of the solid adipic acid (water uptake in confined spaces, e.g. grain boundaries), and it will be discussed to some extent in section 2.5.2 and in more detail in a separate paper.

For the 1:1 and 1:2 AS/AA mixture, no increase in growth with longer residence time at high RH was noted for the interval studied here (4.4-40s), as can be seen from the top two panels of Fig. 2-3. The hygroscopic growth of the 1:1 mixture is in good agreement with the ZSR approach (Fig. 2-4a and 2-5a) and with previous measurements (Hämeri et al., 2002; Prenni et al., 2003).

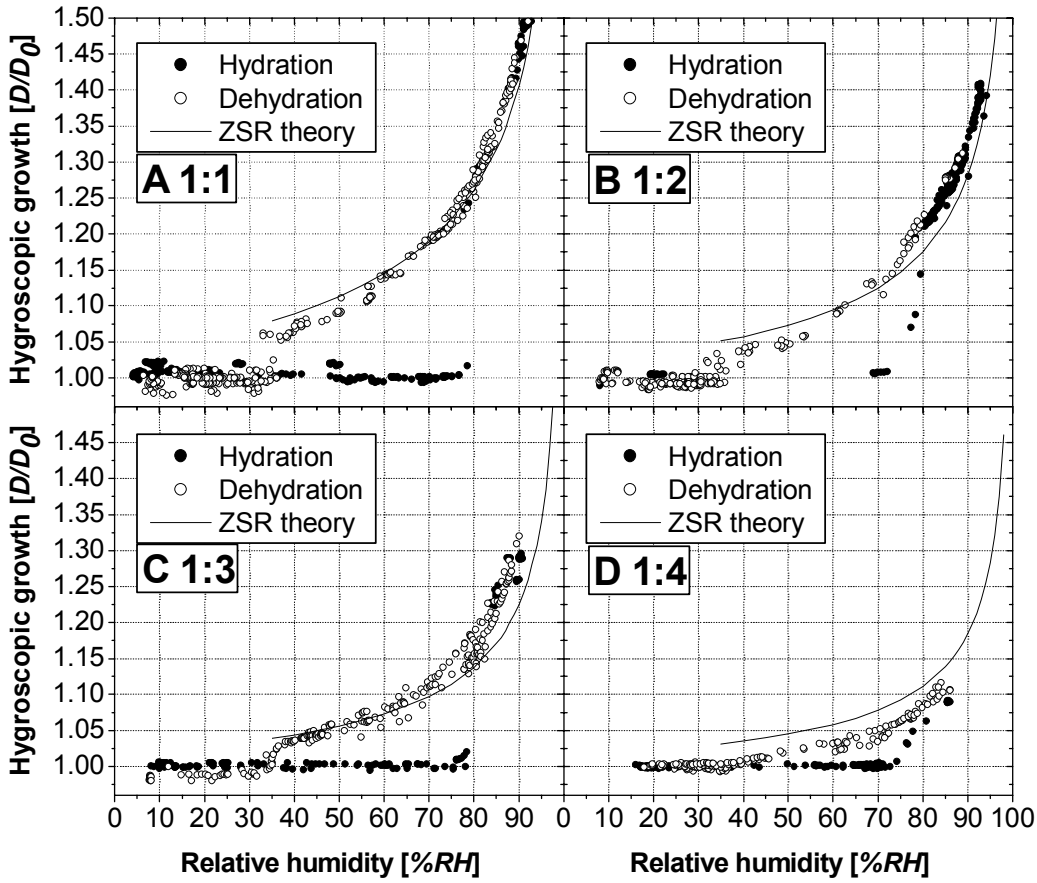

Fig. 2-5. Humidograms of ammonium sulfate-adipic acid mixtures AS/AA. Mass ratios are indicated by the labels A-D, D_0=100 nm and data points were measured at equilibrium (data for AS/AA 1:4 at residence time >30 s, see text).

In the HTDMA measurements of the 1:3 mixture, a dependence on residence time of the measured *GF* was observed, which was larger than the experimental precision (estimated as 2x standard deviation), irrespective of the HTDMA instrument used (UMan or PSI). During the observable residence times (3 – 120 s) the *GF* increased from 1.15 to 1.24, reaching its equilibrium value after about 10 s. For this mixture, the equilibrium hygroscopic growth exceeds the one predicted by the ZSR model by 0.08. This deviation is larger than the precision of the measurements, and also slightly larger than the typical deviations stated for instance in (Prenni et al., 2003), where the difference between measurement and prediction was on average 0.05 for 1:1 mixtures of ammonium sulfate and dicarboxylic acids at 90%RH. The 1:3 AS/AA mixture was also measured by (Hämeri et al., 2002) who reported a hygroscopic growth in agreement with ZSR predictions up to about 85%RH, but at higher RH the measured growth was higher than ZSR (i.e. *GF* 1.3 at 90%RH).

For the 1:4 mixture the hygroscopic growth doubles when the residence time is increased from 6s to 40 s. A comparison with the ZSR model in Fig. 2-5d shows that the observed growth is below the predicted one, indicating that even 40 s may not be sufficient to reach equilibrium. Furthermore the irregularity of the particles increases with increasing AA content (see section 2.5.2), and we cannot exclude compaction of the particles as they take up water, potentially leading to mobility diameter growth factors smaller than volume equivalent diameter growth factors due to shape effects in this case.

2.4.4. Hygroscopicity of AS/NaHA mixture

The hygroscopicity and dependence of residence time on the water uptake was measured for an AS/NaHA mixture with mass ratio 1:3 with the HTDMA. For this mixture a small increase, 0.04 in *GF*, was seen as the τ_{res} increased from 10 s to above 30 s (Fig. 6). This is close to the limits of the experimental repeatability, but as the 95/5 percentiles for this mixture are quite small, we find it worth mentioning. This would imply that some mass transfer limitations can also be expected in the presence of NaHA, which is an amorphous solid. In section 2.5.2, possibilities for mechanisms are discussed, which are based on two-phase systems. We visually investigated a mixture with a 1:3 mass ratio in a vial (~1 g total dry products), with water added accordingly to the measured hygroscopicity at 85%RH, and found the resulting mixture to be a thick paste, with undissolved grains from the NaHA inside. Thus it seems probable that the less soluble fraction of the NaHA remains solid also at higher RH. In Fig. 2-7 humidograms of the mixture and of pure NaHA can be seen. The results correspond well with another study (Badger et al., 2006). For the ZSR model, full efflorescence of AS at 35%RH was assumed. The hygroscopicity of the mixture is low compared to the ZSR relation (panel A), which was explained by Badger et al. (2006) as interactions between AS and NaHA. They investigated a range of concentrations, and we refer to their publication for further information.

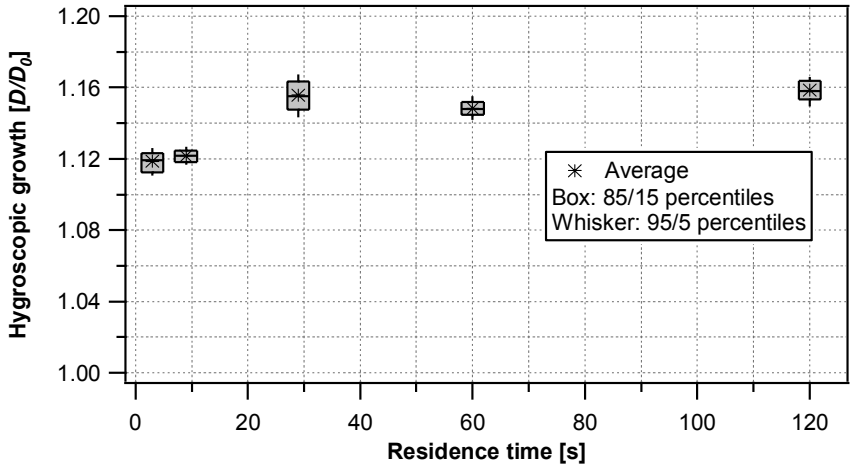

Fig. 2-6. Hygroscopic growth for AS/NaHA mass ratio 1:3, measured with different residence times. D_0=100 nm and *GF* relates to 85%RH. Data is from the UMan HTDMA, except the 29 s data which was measured by the PSI HTDMA.

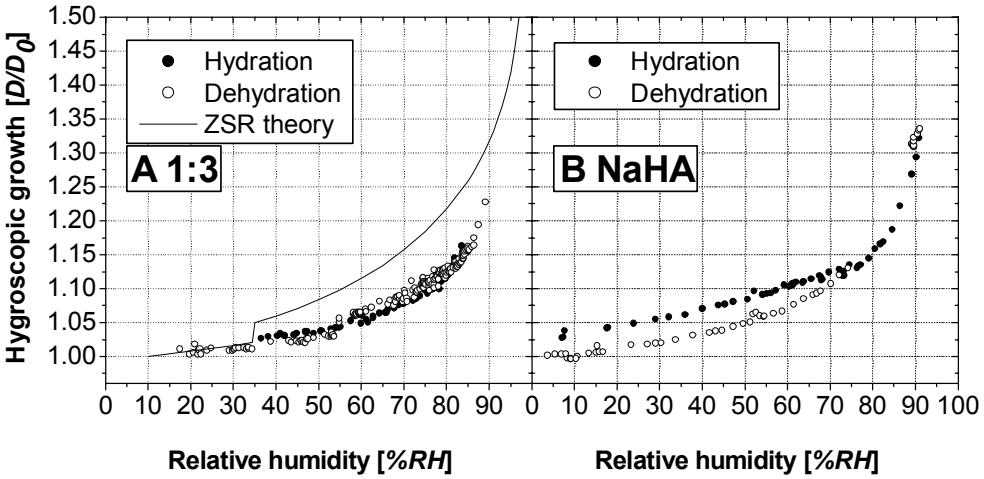

Fig. 2-7. Humidograms of ammonium sulfate-humic acid mixture (NaHA) from PSI HTDMA, mass ratio 1:3 (A), as well as of pure NaHA (B). D_0=100 nm, data points measured at equilibrium.

2.5. Discussion on mass transfer and hygroscopicity

There are several possible reasons for the observed effect of prolonged water vapor equilibration times. This will be addressed in the following.

2.5.1. Mass transfer limitations of water vapor transport to the particle

If we consider a particle and the surrounding water vapor, the first limiting step could be the *gas diffusion* of water molecules to the particle's surface (e.g. Kerminen, 1997). These studies show that gas diffusion is fast (i.e. <<1s), for the conditions used here. A subsequent step is the *transfer across the gas-particle interface*. This step is seen as a thin layer where water molecules are arriving from the gas, molecules are leaving the surface back to the gas, and molecules are diffusing into the particle. The rate governing these processes is described by the accommodation coefficient, α, defined as

$$\alpha = \frac{number\ of\ molecules\ entering\ the\ liquid\ phase}{number\ of\ molecular\ collisions\ with\ the\ surface} \qquad \textbf{(2-5)}$$

Under the assumptions of a spherical particle, a constant water vapor pressure, an equilibrium governed by Henry's law and a high water solubility, the accommodation coefficient, α, can be approximated with the following equation (Kumar, 1989):

$$\alpha \geq \frac{R_p H_A \sqrt{2\pi M_A RT}}{3\tau_p} \qquad \textbf{(2-6)}$$

where R_p is the particle radius, H_A the Henry's law constant for water in the concentrated solution, M_A the molecular weight of water and τ_p the time needed to obtain equilibrium. R and T are the universal gas constant and the temperature, respectively. If we consider the 1:3 mass ratio AS/AA mixture (measurements discussed in detail above), we obtain τ_p = 10 s for a particle with diameter 100 nm, for which α becomes >$3 \cdot 10^{-6}$ (for H_A =2.9 mol·g^{-1}·atm^{-1}). Such a low mass accommodation coefficient for a liquid in contact with the gas phase is not to be expected (Chuang, 2003), thus the mass transfer is consequently assumed

to be limited inside the particle. If the particle is completely liquid the *liquid diffusion* should be fast (<<1s for a submicrometer-sized particle consisting of a typical salt solution, if assuming a typical aqueous diffusion coefficient of 10^{-5} $cm^2 \cdot s^{-1}$). In the next section mass transfer limitations due to inhomogeneous morphology inside the particle will be discussed.

2.5.2. Influence of morphology on hygroscopic growth and transfer limitations

The hygroscopic growth of the AS/AA mixtures presented in section 2.3.4 shows deviations from the ZSR approach: for the HTDMA and the EDB measurements, the measured hygroscopic growths of the 1:3 and to a lesser extent the 1:2 mixtures are higher than predicted by the model with deviations that exceed the measurement uncertainties. Systematic changes of particle composition during the nebulizing process in the HTDMA or during the injection of a particle in the electrodynamic balance seem unlikely since such an effect was not found for other particle compositions. Moreover, we verified that no AA evaporated in the HTDMA by nebulizing pure AA particles for which no change in the mobility diameter was noted during the time in the HTDMA. This is consistent with the electrodynamic balance experiments which showed no weight loss of the particles over extended measurement periods.

The ZSR approach usually leads to accurate predictions of the water uptake of ammonium sulfate mixed with dicarboxylic acid mixtures (Choi & Chan, 2002; Marcolli et al., 2004). Since AA deliquesces only at 99.9%RH, we based the ZSR calculation for AS/AA mixtures on the assumption that there is no water uptake connected with the adipic acid fraction over the whole RH range. In addition to the results from the EDB as detailed above, we validated this assumption by determining the eutonic composition and the water activity of AS/AA mixtures by the methods described in Marcolli et al. (2004).

Table 2-2. Solubility measurements.

	Saturation solubility (moles/ kg water)		Water activity a_w
	Adipic acid	Ammonium sulfate	
Adipic acid	0.15 ± 0.01	-	0.999 ± 0.003
Ammonium sulfate	-	5.76 ± 0.02	0.802 ± 0.003
Eutonic composition	0.014 ± 0.003	5.74 ± 0.02	0.799 ± 0.003

The results in Table 2-2 show that the solubility of AA is reduced by about a factor of ten, while the one of ammonium sulfate remains unchanged within the error of the experiment. The water activity of the saturated AA solution is close to 1 while the eutonic composition deliquesces at a similar RH as AS. Moreover, we performed water activity measurements for 1:3 AS/AA aqueous suspensions in the range of a_w = 0.8 – 1 which showed good agreement with the ZSR model, indicating that the change of water activity due to the presence of dissolved or crystalline (particle sizes of a few micrometers) AA is below the detection limit. These bulk measurements confirm the findings from the electrodynamic balance that AA remains crystalline over the whole measured humidity range.

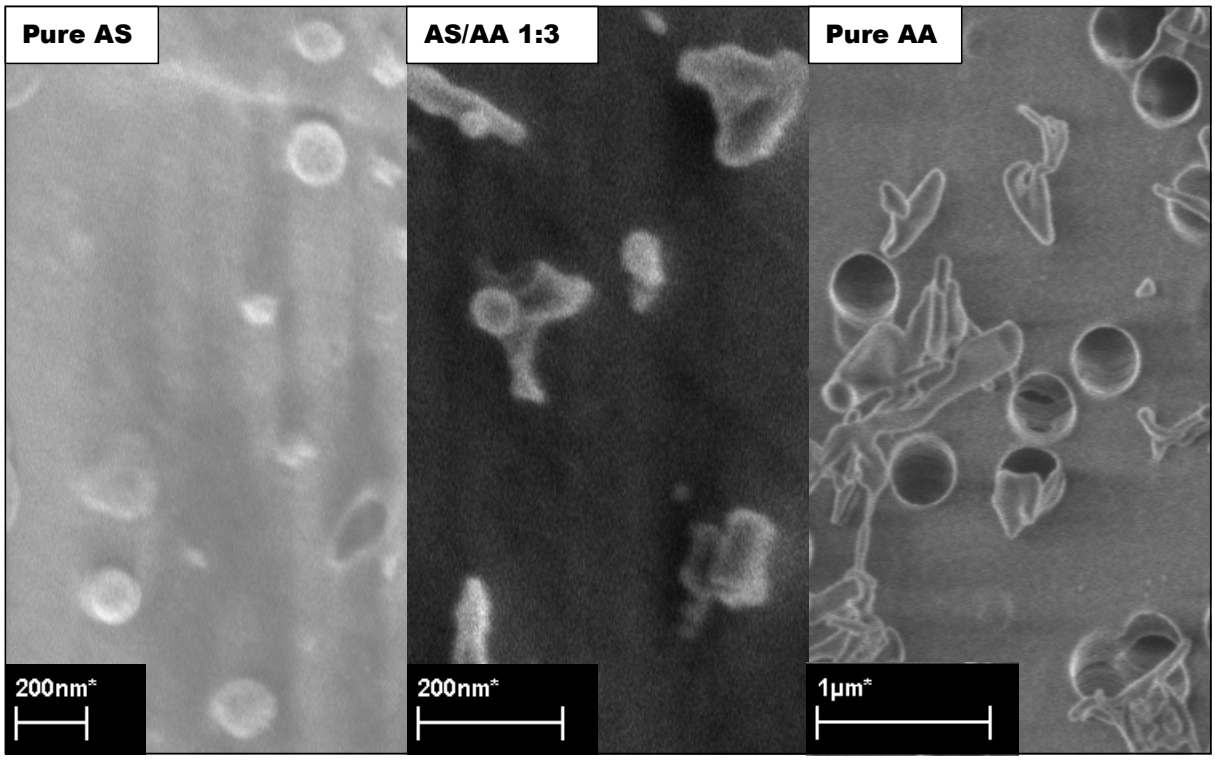

Fig. 2-8. SEM images of spherical pure ammonium sulfate particles, irregular particles of the 1:3 ammonium sulfate/adipic acid mixture and pure adipic acid (from left to right). The dark spherical features in the pure AA frame are the holes of the Nuclepore filter and not deposited particles.

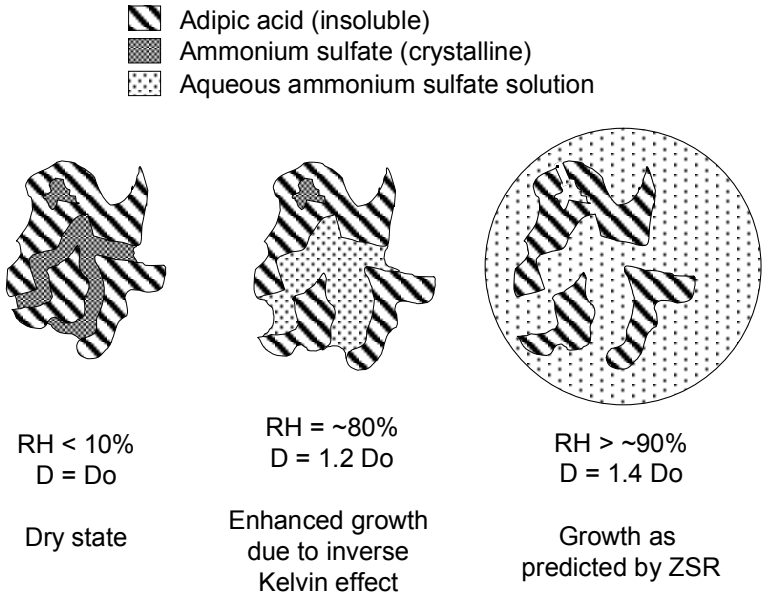

Fig. 2-9. Schematic drawing of the process resulting in an inverse Kelvin effect.

In the following, we explore the possibility that the high water uptake of the 1:2 and 1:3 and the low one of the 1:4 AS/AA mixtures are due to morphological effects. SEM images were taken (Fig. 2-8) showing that under dry conditions the AS/AA mixed particles consist of a

conglomerate of nanocrystals with irregular shapes, with cracks, pores and veins with diameters of 20 – 100 nm between them. When the DRH of ammonium sulfate is reached, it can be assumed that these pores and veins between the crystals fill with aqueous ammonium sulfate, because water molecules diffusing to the opening of a vein would more easily adsorb to the concave vein wall than the convex particle surface. The water uptake in such pores and veins is enhanced compared to the one of a flat surface or the convex particle surface. The enhancement depends on the vein diameter, determining the concavity of the liquid surface at the opening of the vein, and results in a Kelvin effect that is inverse compared to a convex liquid droplet. We denote this in the following with "*inverse Kelvin effect*" (Kärcher & Lohmann, 2003; Weingartner et al., 1997), as we describe the increased water uptake of the capillary due to the concave solution surface. The inverse Kelvin effect can be described by the standard Kelvin equation, with the difference that the water activity has to be divided by the Kelvin factor to obtain the equilibrium RH (Eq. 7). To explore the influence of this effect, we calculated the water uptake for a 1:3 AS/AA particle with vein systems of varying lengths. Assuming that the liquid portion of the particle is present totally in veins and keeping the length of the vein system constant with increasing RH, the veins have to increase in diameter to accommodate the increasing solution volume (for a schematic drawing, see Fig. 2-9). Thus, for a fixed length of the vein system and any given solution volume, the solution concentration (i.e. the Raoult effect) as well as the vein diameter assuming veins with circular cross sections (i.e. the Kelvin effect) is given and the equilibrium RH above the vein can be calculated by

$$RH = a_w \cdot e^{-4\sigma_{sol}\overline{V}_w \cos\phi / D_v RT} \qquad \textbf{(2-7)}$$

In this equation a_w is the water activity calculated from the growth factor of a pure AS particle as parameterized in Eq. 4, σ_{sol} is the surface tension of the solution, $\overline{V}_w$ the partial molar volume of water, D_v the vein diameter, ϕ the contact angle between the solution and the vein surface, R the ideal gas constant and T the absolute temperature. For simplicity, we calculated the vein diameter D_v assuming that AS is totally dissolved and AA totally insoluble and approximated the surface tension of the solution by the one of water. Moreover, we assumed that the solution is completely wetting the vein surface ($\phi = 0°$). This assumption is in accordance with Raymond and Pandis (2002).

In Fig. 2-10 the water uptake for a 100 nm diameter 1:3 AS/AA particle with a vein system of a total length of 400 nm is compared to the HTDMA measurement. This vein system length is compatible with a particle consisting of about eight AA crystallites with ~50 nm diameters. The inverse Kelvin effect leads to an enhanced water uptake above 50%RH. From 50 – 90%RH the vein diameter increases from 26 to 50 nm. These diameters have to be considered as upper limits, since in our model description, we assume that all the liquid is present in veins. In reality, it will be present in grain boundaries, triple junctions as well as veins, resulting in smaller vein diameters for the same water uptake. We assume that above a critical upper value of RH the solution volume can no longer be accommodated within the veins and the inverse Kelvin effect vanishes. This upper limit does not seem to be reached yet for the 1:3 mixture, while in the case of the 1:2 mixture the slightly increased water uptake around 80%RH might indicate an inverse Kelvin effect which vanishes again at higher RH.

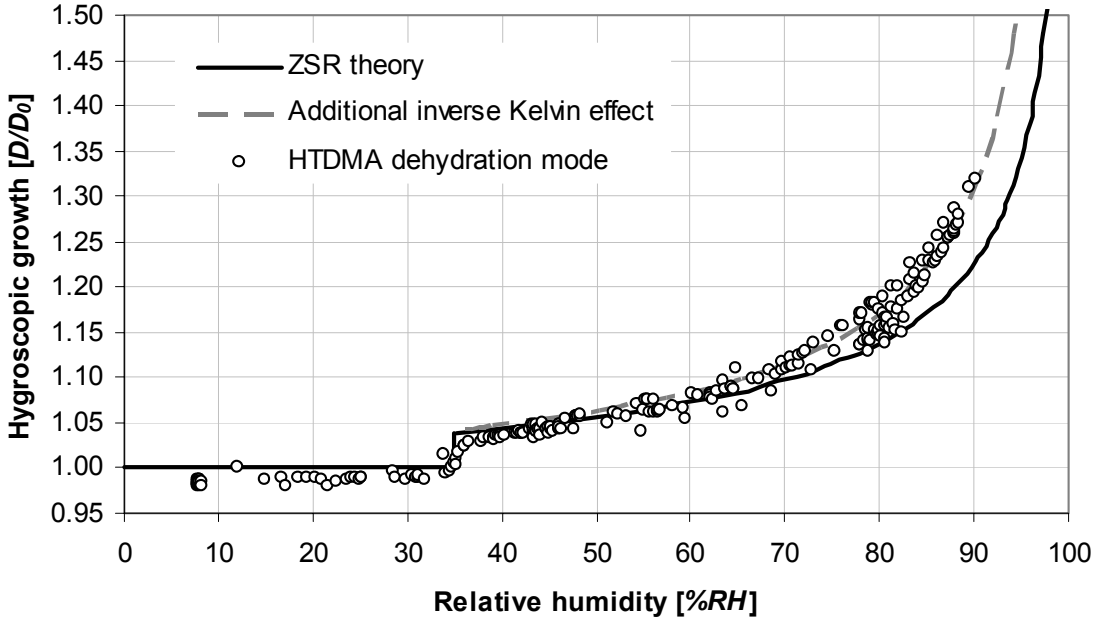

Fig. 2-10. HTDMA measurements of the 1:3 AS/AA mixture with the water uptake modeled with the ZSR relation, as well as modeled with the additional water uptake of an inverse Kelvin effect from a 400 nm length vein system.

The inverse Kelvin effect also leads to a decrease of the DRH. For the vein system of a total length of 400 nm, a decrease of the DRH from 80.8 to 76%RH is expected. A slight decrease of DRH was observed for the particle in the electrodynamic balance, and a DRH of 78.8%RH was measured with the HTDMA for the AS/AA 1:3 mixture. We assume that after efflorescence the AS crystals are present in the veins or even totally enclosed by AA (see Fig. 2-9). Due to capillary forces, water can enter the veins and dissolve AS partly before the deliquescence RH is reached, as can be seen from the mass increase of the particles in the electrodynamic balance starting at 50%RH. This partial dissolution is limited by the space available in the vein system and might be accompanied by a transport of AS out of the veins where it recrystallizes because the inverse Kelvin effect is no longer present. We assume that before the veins can start to grow in diameter, they have to be filled completely with solution because adhesion forces between crystals impede the expansion. Full deliquescence would therefore in this case only be reached at an RH closer to the one in the absence of a Kelvin effect.

We think that the long residence times needed in the HTDMA to reach full hygroscopic growth is due to the presence of AS in veins or even totally enclosed by AA. While the spreading of the solution in the veins should not be slowed down considerably as long as the solution is wetting the vein surface (Liu et al., 2005), the expansion of the veins in diameter might be the rate limiting step. Alternatively, in the case of a total enclosure, the AA forms a barrier that has to be overcome by the water molecules leading to a slow humidification. This effect seems to be stronger the higher the AA fraction is. The characteristic time for diffusion through the solid organic matrix can be described with:

$$\tau_p = \frac{R_p^2}{\pi^2 D_{Sol}} \qquad \textbf{(2-8)}$$

where R_p is the particle radius, D_{Sol} the solid diffusion coefficient and τ_p the characteristic time needed to reach equilibrium. If we calculate D_{Sol}, again for a 100-nm diameter particle and τ_p = 10 s, we obtain $8.0 \cdot 10^{-13}$ cm^2 s^{-1}. This is a value in the range for solids, but would in our case only be applicable to a part of the particle. If water must diffuse through this solid matrix to dissolve the AS into ions that participate in the hygroscopic growth, a fraction of the equilibration times measured can be explained.

2.6. Conclusions

Some of the inorganic/organic mixed-phase solutions studied with two HTDMAs in the present work required residence times of >40 seconds in order for the particles to reach equilibrium after water uptake. It is proposed that in these cases the organic compound, when present in major fractions, is solid (verified with an EDB) and encapsulates some of the inorganic species residing in between the solid organic grains in veins and pores. The water uptake rate of the mainly inorganic solution is possibly slowed down by solid phase diffusion. It is important for measurements of such mixtures to allow for a sufficient residence time at the specified humidity for the system to equilibrate. Otherwise, the resulting underestimation of the hygroscopicity may have implications for derived aerosol properties such as light scattering (direct aerosol effect in climate considerations) and cloud activation (indirect aerosol effect).

Acknowledgements

This work was supported by the National Science Foundation Switzerland (grant n° 200021-100280) as well as the EC project ACCENT. The UMan measurements were supported by the UK Natural Environment Research Council (grant n° NER/A/S/2001/01135). M.J. Cubison was supported during the period of this work through NERC studentship no. 06424. We gratefully acknowledge the Laboratory for Micro- and Nanotechnology and A. Weber for the SEM (Zeiss Supra55VP) micrographs (PSI, Switzerland). We appreciate the inspiring exchange of ideas with Marcia Baker (University of Washington, USA).

References

Adamson, A. W. (1982). *Physical Chemistry of Surfaces*, John Wiley & Sons, New York.

Al-Abadleh, H. A., & Grassian, V. H. (2003). FT-IR study of water adsorption on aluminum oxide surfaces. *Langmuir*, *19*, (2), 341-347.

Ansari, A. S., & Pandis, S. N. (1999). Prediction of multicomponent inorganic atmospheric aerosol behavior. *Atmospheric Environment*, *33*, (5), 745-757.

Arens, F., Gutzwiller, L., Baltensperger, U., Gaggeler, H. W., & Ammann, M. (2001). Heterogeneous reaction of NO2 on diesel soot particles. *Environmental Science and Technology*, *35*, (11), 2191-2199.

Badger, C. L., George, I., Griffiths, P. T., Braban, C. F., Cox, R. A., & Abbatt, J. P. D. (2006). Phase transitions and hygroscopic growth of aerosol particles containing humic acid and mixtures of humic acid and ammonium sulphate. *Atmospheric Chemistry and Physics*, *6*, 755-768.

Bian, H. S., & Zender, C. S. (2003). Mineral dust and global tropospheric chemistry: Relative roles of photolysis and heterogeneous uptake. *Journal of Geophysical Research-Atmospheres*, *108*, (D21), doi:10.1029/2002JD003143.

Biskos, G., Paulsen, D., Russell, L. M., Buseck, P. R., & Martin, S. T. (2006). Prompt deliquescence and efflorescence of aerosol nanoparticles. *Atmospheric Chemistry and Physics*, *6*, 4633-4642.

Chan, M. N., & Chan, C. K. (2005). Mass transfer effects in hygroscopic measurements of aerosol particles. *Atmospheric Chemistry and Physics*, *5*, 2703-2712.

Choi, M. Y., & Chan, C. K. (2002). Continuous measurements of the water activities of aqueous droplets of water-soluble organic compounds. *Journal of Physical Chemistry A*, *106*, (18), 4566-4572.

Choularton, T. W., Colvile, R. N., Bower, K. N., Gallagher, M. W., Wells, M., Beswick, K. M., Arends, B. G., Mols, J. J., Kos, G. P. A., Fuzzi, S., Lind, J. A., Orsi, G., Facchini, M. C., Laj, P., Gieray, R., Wieser, P., Engelhardt, T., Berner, A., Kruisz, C., Moller, D., Acker, K., Wieprecht, W., Luttke, J., Levsen, K., Bizjak, M., Hansson, H. C., Cederfelt, S. I., Frank, G., Mentes, B., Martinsson, B., Orsini, D., Svenningsson, B., Swietlicki, E., Wiedensohler, A., Noone, K. J., Pahl, S., Winkler, P., Seyffer, E., Helas, G., Jaeschke, W., Georgii, H. W., Wobrock, W., Preiss, M., Maser, R., Schell, D., Dollard, G., Jones, B., Davies, T., Sedlak, D. L., David, M. M., Wendisch, M., Cape, J. N., Hargreaves, K. J., Sutton, M. A., StoretonWest, R. L., Fowler, D., Hallberg, A., Harrison, R. M., & Peak, J. D. (1997). The Great Dun Fell Cloud Experiment 1993: An overview. *Atmospheric Environment*, *31*, (16), 2393-2405.

Chuang, P. Y. (2003). Measurement of the timescale of hygroscopic growth for atmospheric aerosols. *Journal of Geophysical Research-Atmospheres*, *108*, (D9), art. no.-4282.

Colberg, C. A., Krieger, U. K., & Peter, T. (2004). Morphological investigations of single levitated H2SO4/NH3/H2O aerosol particles during deliquescence/efflorescence experiments. *Journal of Physical Chemistry A*, *108*, (14), 2700-2709.

Colberg, C. A., Luo, B. P., Wernli, H., Koop, T., & Peter, T. (2003). A novel model to predict the physical state of atmospheric H2SO4/NH3/H2O aerosol particles. *Atmospheric Chemistry and Physics*, *3*, 909-924.

Cubison, M. J. (2005). Design, Construction and Use of a Hygroscopic Tandem Differential Mobility Analyser, PhD thesis, University of Manchester, Manchester.

Cubison, M. J., Coe, H., & Gysel, M. (2005). A modified hygroscopic tandem DMA and a data retrieval method based on optimal estimation. *Journal of Aerosol Science*, *36*, (7), 846-865.

Davis, E. J., Buehler, M. F., & Ward, T. L. (1990). The Double-Ring Electrodynamic Balance for Microparticle Characterization. *Review of Scientific Instruments*, *61*, (4), 1281-1288.

DeMott, P. J., Sassen, K., Poellot, M. R., Baumgardner, D., Rogers, D. C., Brooks, S. D., Prenni, A. J., & Kreidenweis, S. M. (2003). African dust aerosols as atmospheric ice nuclei. *Geophysical Research Letters*, *30*, (14), doi:10.1029/2003GL017410.

Dentener, F. J., Carmichael, G. R., Zhang, Y., Lelieveld, J., & Crutzen, P. J. (1996). Role of mineral aerosol as a reactive surface in the global troposphere. *Journal of Geophysical Research-Atmospheres*, *101*, (D17), 22869-22889.

Desboeufs, K. V., Losno, R., & Colin, J. L. (2003). Relationship between droplet pH and aerosol dissolution kinetics: Effect of incorporated aerosol particles on droplet pH during cloud processing. *Journal of Atmospheric Chemistry*, *46*, (2), 159-172.

Desboeufs, K. V., Losno, R., Vimeux, F., & Cholbi, S. (1999). The pH-dependent dissolution of wind-transported Saharan dust. *Journal of Geophysical Research-Atmospheres*, *104*, (D17), 21287-21299.

Dick, W. D., Saxena, P., & McMurry, P. H. (2000). Estimation of water uptake by organic compounds in submicron aerosols measured during the Southeastern Aerosol and Visibility Study. *Journal of Geophysical Research Atmospheres*, *105*, (D1), 1471-1479.

Dubowski, Y., Sumner, A. L., Menke, E. J., Gaspar, D. J., Newberg, J. T., Hoffman, R. C., Penner, R. M., Hemminger, J. C., & Finlayson-Pitts, B. J. (2004). Interactions of gaseous nitric acid with surfaces of environmental interest. *Physical Chemistry Chemical Physics*, *6*, (14), 3879-3888.

Durham, J. L., & Stockburger, L. (1986). Nitric-Acid Air Diffusion-Coefficient - Experimental-Determination. *Atmospheric Environment*, *20*, (3), 559-563.

Fenter, F. F., Caloz, F., & Rossi, M. J. (1995). Experimental-Evidence for the Efficient Dry Deposition of Nitric-Acid on Calcite. *Atmospheric Environment*, *29*, (22), 3365-3372.

Finlayson-Pitts, B. J., Wingen, L. M., Sumner, A. L., Syomin, D., & Ramazan, K. A. (2003). The heterogeneous hydrolysis of NO_2 in laboratory systems and in outdoor and indoor atmospheres: An integrated mechanism. *Physical Chemistry Chemical Physics*, *5*, (2), 223-242.

Fissan, H., Hummes, D., Stratmann, F., Buscher, P., Neumann, S., Pui, D. Y. H., & Chen, D. (1996). Experimental comparison of four differential mobility analyzers for nanometer aerosol measurements. *Aerosol Science and Technology*, *24*, (1), 1-13.

Goodman, A. L., Bernard, E. T., & Grassian, V. H. (2001). Spectroscopic study of nitric acid and water adsorption on oxide particles: Enhanced nitric acid uptake kinetics in the presence of adsorbed water. *Journal of Physical Chemistry A*, *105*, (26), 6443-6457.

Goodman, A. L., Underwood, G. M., & Grassian, V. H. (2000). A laboratory study of the heterogeneous reaction of nitric acid on calcium carbonate particles. *Journal of Geophysical Research Atmospheres*, *105*, (D23), 29053-29064.

Graber, E. R., & Rudich, Y. (2006). Atmospheric HULIS: How humic-like are they? A comprehensive and critical review. *Atmospheric Chemistry and Physics*, *6*, 729-753.

Guimbaud, C., Arens, F., Gutzwiller, L., Gaggeler, H. W., & Ammann, M. (2002). Uptake of HNO_3 to deliquescent sea-salt particles: a study using the short-lived radioactive isotope tracer N-13. *Atmospheric Chemistry and Physics*, *2*, 249-257.

Gysel, M., Weingartner, E., & Baltensperger, U. (2002). Hygroscopicity of aerosol particles at low temperatures. 2. Theoretical and experimental hygroscopic properties of laboratory generated aerosols. *Environmental Science & Technology*, *36*, (1), 63-68.

Gysel, M., Weingartner, E., Nyeki, S., Paulsen, D., Baltensperger, U., Galambos, I., & Kiss, G. (2004). Hygroscopic properties of water-soluble matter and humic-like organics in atmospheric fine aerosol. *Atmospheric Chemistry and Physics*, *4*, 35-50.

Hämeri, K., Charlson, R., & Hansson, H. C. (2002). Hygroscopic properties of mixed ammonium sulfate and carboxylic acids particles. *Aiche Journal*, *48*, (6), 1309-1316.

Hanisch, F., & Crowley, J. N. (2001). Heterogeneous reactivity of gaseous nitric acid on Al_2O_3, $CaCO_3$, and atmospheric dust samples: A Knudsen cell study. *Journal of Physical Chemistry A*, *105*, (13), 3096-3106.

Hendricks, J., Karcher, B., Dopelheuer, A., Feichter, J., Lohmann, U., & Baumgardner, D. (2004). Simulating the global atmospheric black carbon cycle: a revisit to the contribution of aircraft emissions. *Atmospheric Chemistry and Physics*, *4*, 2521-2541.

Hennig, T., Massling, A., Brechtel, F. J., & Wiedensohler, A. (2005). A tandem DMA for highly temperature-stabilized hygroscopic particle growth measurements between 90% and 98% relative humidity. *Journal of Aerosol Science*, *36*, (10), 1210-1223.

IPCC (2001). *Climate Change 2001: The Scientific Basis*, Cambridge Univ. Press, New York.

Joseph, D. W., & Spicer, C. W. (1978). Chemiluminescence Method for Atmospheric Monitoring of Nitric-Acid and Nitrogen-Oxides. *Analytical Chemistry*, *50*, (9), 1400-1403.

Joutsensaari, J., Vaattovaara, P., Vesterinen, M., Hämeri, K., & Laaksonen, A. (2001). A novel tandem differential mobility analyzer with organic vapor treatment of aerosol particles. *Atmospheric Chemistry and Physics*, *1*, 51-60.

Kalberer, M., Tabor, K., Ammann, M., Parrat, Y., Weingartner, E., Piguet, D., Rossler, E., Jost, D. T., Turler, A., Gaggeler, H. W., & Baltensperger, U. (1996). Heterogeneous chemical processing of (NO2)-N-13 by monodisperse carbon aerosols at very low concentrations. *Journal of Physical Chemistry*, *100*, (38), 15487-15493.

Kanakidou, M., Seinfeld, J. H., Pandis, S. N., Barnes, I., Dentener, F. J., Facchini, M. C., Van Dingenen, R., Ervens, B., Nenes, A., Nielsen, C. J., Swietlicki, E., Putaud, J. P., Balkanski, Y., Fuzzi, S., Horth, J., Moortgat, G. K., Winterhalter, R., Myhre, C. E. L., Tsigaridis, K., Vignati, E., Stephanou, E. G., & Wilson, J. (2005). Organic aerosol and global climate modelling: a review. *Atmospheric Chemistry and Physics*, *5*, 1053-1123.

Kärcher, B., & Lohmann, U. (2003). A parameterization of cirrus cloud formation: heterogeneous freezing. *Journal of Geophysical Research*, *108*, (D14), 4402-4416.

Kerminen, V. M. (1997). The effects of particle chemical character and atmospheric processes on particle hygroscopic properties. *Journal of Aerosol Science*, *28*, (1), 121-132.

Kiss, G., Tombacz, E., Varga, B., Alsberg, T., & Persson, L. (2003). Estimation of the average molecular weight of humic-like substances isolated from fine atmospheric aerosol. *Atmospheric Environment*, *37*, (27), 3783-3794.

Krieger, U. K., & Braun, C. (2001). Light-scattering intensity fluctuations in single aerosol particles during deliquescence. *Journal of Quantitative Spectroscopy & Radiative Transfer*, *70*, (4-6), 545-554.

Krueger, B. J., Grassian, V. H., Cowin, J. P., & Laskin, A. (2004). Heterogeneous chemistry of individual mineral dust particles from different dust source regions: the importance of particle mineralogy. *Atmospheric Environment*, *38*, (36), 6253-6261.

Kumar, S. (1989). The characteristic time to achieve interfacial phase equilibrium in cloud drops. *Atmospheric Environment*, *23*, 2299-2304.

Lavanchy, V. M. H., Gäggeler, H. W., Schotterer, U., Schwikowski, M., & Baltensperger, U. (1999). Historical record of carbonaceous particle concentrations from a European high-alpine glacier (Colle Gnifetti, Switzerland). *Journal of Geophysical Research Atmospheres*, *104*, (D17), 21227-21236.

Liu, B. Y. H., Pui, D. Y. H., Whitby, K. T., Kittelson, D. B., Kousaka, Y., & McKenzie, R. L. (1978). The Aerosol Mobility Chromatograph: a new detector for sulfuric acid aerosols. *Atmospheric Environment*, *12*, 99-104.

Liu, Y. C., Wang, Q., Wu, T., & Zhang, L. (2005). Fluid structure and transport properties of water inside carbon nanotubes. *Journal of Chemical Physics*, *123*, (23).

Marcolli, C., Luo, B. P., & Peter, T. (2004). Mixing of the organic aerosol fractions: Liquids as the thermodynamically stable phases. *Journal of Physical Chemistry A*, *108*, (12), 2216-2224.

Maxwell-Meier, K., Weber, R., Song, C., Orsini, D., Ma, Y., Carmichael, G. R., & Streets, D. G. (2004). Inorganic composition of fine particles in mixed mineral dust-pollution plumes observed from airborne measurements during ACE-Asia. *Journal of Geophysical Research-Atmospheres*, *109*, (D19).

McFiggans, G., Artaxo, P., Baltensperger, U., Coe, H., Facchini, M. C., Feingold, G., Fuzzi, S., Gysel, M., Laaksonen, A., Lohmann, U., Mentel, T. F., Murphy, D. M., O'Dowd, C. D., Snider, J. R., & Weingartner, E. (2006). The effect of physical and chemical aerosol properties on warm cloud droplet activation. *Atmospheric Chemistry and Physics*, *6*, 2593-2649.

Naumann, K. H. (2003). COSIMA - a computer program simulating the dynamics of fractal aerosols. *Journal of Aerosol Science*, *34*, (10), 1371-1397.

Neubauer, K. R., Johnston, M. V., & Wexler, A. S. (1998). Humidity effects on the mass spectra of single aerosol particles. *Atmospheric Environment*, *32*, (14-15), 2521-2529.

Pöschl, U., Rudich, Y., & Ammann, M. (2005). Kinetic model framework for aerosol and cloud surface chemistry and gas-particle interactions: Part 1 – general equations, parameters, and terminology. *Atmospheric Chemistry and Physics Discussions*, *5*, 2111–2191.

Prenni, A. J., De Mott, P. J., & Kreidenweis, S. M. (2003). Water uptake of internally mixed particles containing ammonium sulfate and dicarboxylic acids. *Atmospheric Environment*, *37*, (30), 4243-4251.

Putaud, J. P., Raes, F., Van Dingenen, R., Bruggemann, E., Facchini, M. C., Decesari, S., Fuzzi, S., Gehrig, R., Huglin, C., Laj, P., Lorbeer, G., Maenhaut, W., Mihalopoulos, N., Mullller, K., Querol, X., Rodriguez, S., Schneider, J., Spindler, G., ten Brink, H., Torseth, K., & Wiedensohler, A. (2004). European aerosol phenomenology-2: chemical characteristics of particulate matter at kerbside, urban, rural and background sites in Europe. *Atmospheric Environment*, *38*, (16), 2579-2595.

Rader, D. J., & McMurry, P. H. (1986). Application of the Tandem Differential Mobility Analyzer to Studies of Droplet Growth or Evaporation. *Journal of Aerosol Science*, *17*, (5), 771-787.

Ray, J., & McDow, S. R. (2005). Dicarboxylic acid concentration trends and sampling artifacts. *Atmospheric Environment*, *39*, (40), 7906-7919.

Raymond, T. M., & Pandis, S. N. (2002). Cloud activation of single-component organic aerosol particles. *Journal of Geophysical Research-Atmospheres*, *107*, (D24), art. no.-4787.

Rogak, S. N., Baltensperger, U., & Flagan, R. C. (1991). Measurement of mass transfer to agglomerate aerosols. *Aerosol Science and Technology*, *14*, 447-485.

Russell, L. M., & Ming, Y. (2002). Deliquescence of small particles. *Journal of Chemical Physics*, *116*, (1), 311-321.

Saathoff, H., Naumann, K. H., Schnaiter, M., Schock, W., Mohler, O., Schurath, U., Weingartner, E., Gysel, M., & Baltensperger, U. (2003). Coating of soot and $(NH_4)_2SO_4$ particles by ozonolysis products of alpha-pinene. *Journal of Aerosol Science*, *34*, (10), 1297-1321.

Sassen, K., DeMott, P. J., Prospero, J. M., & Poellot, M. R. (2003). Saharan dust storms and indirect aerosol effects on clouds: CRYSTAL-FACE results. *Geophysical Research Letters*, *30*, (12), doi:10.1029/2003GL017371.

Seinfeld, J. H., Carmichael, G. R., Arimoto, R., Conant, W. C., Brechtel, F. J., Bates, T. S., Cahill, T. A., Clarke, A. D., Doherty, S. J., Flatau, P. J., Huebert, B. J., Kim, J., Markowicz, K. M., Quinn, P. K., Russell, L. M., Russell, P. B., Shimizu, A., Shinozuka, Y., Song, C. H., Tang, Y. H., Uno, I.,

Vogelmann, A. M., Weber, R. J., Woo, J. H., & Zhang, X. Y. (2004). ACE-ASIA - Regional climatic and atmospheric chemical effects of Asian dust and pollution. *Bulletin of the American Meteorological Society*, *85*, (3), 367-380.

Stokes, R. H., & Robinson, R. A. (1966). Interactions in aqueous nonelectrolyte solutions. I. Solute-solvent equilibria. *J. Phys. Chem*, *70*, 2126-2130.

Sumner, A. L., Menke, E. J., Dubowski, Y., Newberg, J. T., Penner, R. M., Hemminger, J. C., Wingen, L. M., Brauers, T., & Finlayson-Pitts, B. J. (2004). The nature of water on surfaces of laboratory systems and implications for heterogeneous chemistry in the troposphere. *Physical Chemistry Chemical Physics*, *6*, (3), 604-613.

Tang, I. N., & Fung, K. H. (1997). Hydration and Raman scattering studies of levitated microparticles: Ba(NO3)2, Sr(NO3)2, and Ca(NO3)2. *Journal of Chemical Physics*, *106*, (5), 1653-1660.

Tang, I. N., & Munkelwitz, H. R. (1993). Composition and Temperature-Dependence of the Deliquescence Properties of Hygroscopic Aerosols. *Atmospheric Environment Part a-General Topics*, *27*, (4), 467-473.

Topping, D. O., McFiggans, G. B., & Coe, H. (2005a). A curved multi-component aerosol hygroscopicity model framework: Part 1 - Inorganic compounds. *Atmospheric Chemistry and Physics*, *5*, 1205-1222.

Topping, D. O., McFiggans, G. B., & Coe, H. (2005b). A curved multi-component aerosol hygroscopicity model framework: Part 2 - Including organic compounds. *Atmospheric Chemistry and Physics*, *5*, 1223-1242.

Underwood, G. M., Song, C. H., Phadnis, M., Carmichael, G. R., & Grassian, V. H. (2001). Heterogeneous reactions of NO_2 and HNO_3 on oxides and mineral dust: A combined laboratory and modeling study. *Journal of Geophysical Research-Atmospheres*, *106*, (D16), 18055-18066.

Usher, C. R., Michel, A. E., & Grassian, V. H. (2003). Reactions on Mineral Dust. *Chemical Reviews*, *103*, 4883-4939.

Vlasenko, A., Sjogren, S., Weingartner, E., Gaggeler, H. W., & Ammann, M. (2005). Generation of submicron Arizona test dust aerosol: Chemical and hygroscopic properties. *Aerosol Science and Technology*, *39*, (5), 452-460.

Vlasenko, A., Sjogren, S., Weingartner, E., Stemmler, K., Gaggeler, H. W., & Ammann, M. (2006). Effect of humidity on nitric acid uptake to mineral dust aerosol particles. *Atmospheric Chemistry and Physics*, *6*, 2147-2160.

Weingartner, E., Burtscher, H., & Baltensperger, U. (1997). Hygroscopic properties of carbon and diesel soot particles. *Atmospheric Environment*, *31*, (15), 2311-2327.

Weingartner, E., Gysel, M., & Baltensperger, U. (2002a). Hygroscopicity of aerosol particles at low temperatures. 1. New low-temperature H-TDMA instrument: Setup and first applications. *Environmental Science and Technology*, *36*, (1), 55-62.

Weingartner, E., Gysel, M., & Baltensperger, U. (2002b). Hygroscopicity of aerosol particles at low temperatures. 1. New low-temperature H-TDMA instrument: Setup and first applications. *Environmental Science & Technology*, *36*, (1), 55-62.

Winklmayr, W., Reischl, G. P., Lindner, A. O., & Berner, A. (1991). New electromobility apectrometer for the measuremnt of aerosol size distributions in the size range from 1 to 1000 nm. *Journal of Aerosol Science*, *22*, 289-296.

Xiong, J. Q., Zhong, M. H., Fang, C. P., Chen, L. C., & Lippmann, M. (1998). Influence of organic films on the hygroscopicity of ultrafine sulfuric acid aerosol. *Environmental Science and Technology*, *32*, (22), 3536-3541.

CHAPTER 3

3. A combined particle trap/HTDMA hygroscopicity study of mixed inorganic/organic aerosol particles

This chapter is a paper to be submitted by Alessandro Zardini, with joint measurements with the author of this dissertation. The author contributed with measurements of AS/CA and AS/AA mixtures with the HTDMA, and confirmed evaporation effects hampering the measurements of GA with the HTDMA, as well as considerations for the comparison of the two instruments and assistance during the manuscript writing process.

A.A. Zardini[1], S. Sjogren[2], C. Marcolli[1], U.K. Krieger[1], M. Gysel[2], E. Weingartner[2], U. Baltensperger[2], T. Peter[1]

[1]Institute for Atmospheric and Climate Science, ETH, CH-8092 Zurich, Switzerland
[2]Laboratory of Atmospheric Chemistry, Paul Scherrer Institute, CH-5232 Villigen, Switzerland

3.1. Abstract

Atmospheric aerosols are often mixtures of inorganic and organic material. Organics can represent a large fraction of the total aerosol mass and are comprised of water-soluble and insoluble compounds. Increasing attention was paid in the last decade to the capability of mixed inorganic/ organic aerosol particles to take up water (hygroscopicity). We performed hygroscopicity measurements of internally mixed ammonium sulfate and carboxylic acids (citric, glutaric, adipic acids) particles in parallel with an electrodynamic balance (EDB) and a hygroscopicity tandem differential mobility analyzer (HTDMA). The organic compounds were chosen to represent three distinct water uptake characteristics. Pure citric acid was always liquid, adipic acid was always solid, while glutaric acid can be both during hygroscopicity cycles covering hydration and dehydration measured by the EDB and the HTDMA. We show that the hygroscopicity of mixtures of the above compounds is well described by the Zdanovskii-Stokes-Robinson (ZSR) relationship as long as the two-component particle is completely liquid in the ammonium sulfate/citric acid and ammonium sulfate/glutaric acid cases. However, we observe discrepancies compared to what is expected from bulk thermodynamics when a solid component is present. We explain this by the complex morphology resulting from the crystallization process leading to pores, triple junctions and grain boundaries which allow for water sorption in excess of bulk thermodynamic predictions due to the Kelvin effect on concave surfaces.

3.2. Introduction

Atmospheric aerosols influence the climate directly through scattering and absorption of radiation, and indirectly through modification of clouds properties. The climate forcing resulting from these aerosol effects is still characterized by large uncertainties (IPCC, 2007). Organic material accounts for 20% to 50% in total fine aerosol mass at continental midlatitudes and for as much as 90% in tropical forested areas (Kanakidou et al., 2005). Organics in the condensed phase comprise a large variety of chemical compounds (Rogge et al., 1993). Although large uncertainty remains concerning the detailed composition, it is established that a considerable fraction of the organic aerosol is water-soluble, thus contributing to the aerosol hygroscopicity (Choi and Chan, 2002; Saxena et al., 1995). Moreover, organics are typically found to be internally mixed with inorganic compounds (Middlebrook et al., 1998; Murphy et al., 2006), and may therefore influence the water uptake and phase changes of the inorganic aerosol fraction (Saxena et al., 1995; Cruz and Pandis, 2000; Dick et al., 2000). Considering the complex composition of atmospheric aerosols with thousands of different compounds, Marcolli et al. (2004) suggested that the physical state of the organic aerosol fraction is typically liquid (or amorphous solid). The determination of the physical state (liquid or crystalline) and the amount of water present in the condensed matter is crucial to assess the aerosol impact on climate and atmospheric chemistry. Chemical interactions between the inorganic and organic species may lead to a decrease of the deliquescence relative humidity of the inorganic component, or even to a water uptake of the aerosol particle at every RH (Braban and Abbatt, 2004; Choi and Chan, 2002). Also, a liquid/liquid phase separation into a predominantly organic and an aqueous inorganic phase with no change of the inorganic salt deliquescence relative humidity may occur (Marcolli and Krieger, 2006). Moreover, mass transfer limitations between gas and particle phase play a role in water uptake kinetics, increasing the time needed for the particles to equilibrate with ambient relative humidity (Chan and Chan, 2005; Sjogren et al., 2007).

We observed slow water uptake for mixed inorganic/organic particles in HTDMA measurements (Sjogren et al., 2007) and we hypothesized that complex morphology of mixed solid/liquid aerosol particles is responsible for this behavior. The method of choice often used to predict the hygroscopic behavior of multicomponent particles is the Zdanovskii-Stokes-Robinson's approach (Zdanovskii, 1948; Stokes and Robinson, 1966). It assumes no mutual influences between components of the mixed solution particle, and therefore the total water uptake is simply the sum of the individual uptakes by the single components. While this method proved to be valid for many systems, discrepancies still remain for systems involving for instance pinonic acid (Cruz and Pandis, 2000), succinic acid (Svenningsson et al., 2006), and adipic acid (Sjogren et al., 2007, and this study). As pointed out by Fuzzi et al. (2006), despite the remarkable advances in recent years, physicochemical properties like the hygroscopicity of organic particles need further investigation and improvements of measurement techniques. This study aims at shedding more light on the problem by investigating the hygroscopicity (growth factor and phase changes) and morphologies of mixed inorganic/organic particles made of ammonium sulfate as inorganic and either citric, glutaric, or adipic acid as the organic components. These organic compounds are typically attributed to secondary or aged primary organic aerosols. Measurements are performed in parallel with an electrodynamic balance and an HTDMA instrument, and results are compared with literature data and/or bulk thermodynamics. A comparison of the measured growth factors with the Zdanovskii-Stokes-Robinson (ZSR) approach is also shown.

3.3. Experimental section

Electrodynamic Balance

The basic experimental setup has been described previously (Krieger et al., 2000). Briefly, an electrically charged particle (typically 5-25 µm in radius) is levitated in an electrodynamic balance (Davis et al., 1990), see a schematic of the setup in Fig. 3-1. The balance is hosted within a three wall glass chamber with a cooling agent flowing between the inner walls and an insulation vacuum between the outer walls. A constant flow (typically 30 sccm) of an N_2/H_2O mixture with a controlled H_2O partial pressure is pumped continuously through the chamber at a constant total pressure adjustable between 200 and 1000 mbar. The temperature can be varied between 330 K and 160 K with a stability better than 0.1 K and an accuracy of ±0.5 K. The relative humidity (RH) in the chamber is set by adjusting the N_2/H_2O ratio, using automatic mass flow controllers. The relative humidity is registered by a capacitive thin film sensor that is mounted in close vicinity of the levitated particle (<10 mm). The sensor was calibrated directly in the electrodynamic balance using the deliquescence relative humidity of different salts. Its accuracy is ±1.5% RH between 10% and 90% RH. A single-particle generator (Hewlett-Packard 51633A ink jet cartridge) is used to inject a liquid particle from solutions prepared by mass percent with MilliQ water using an analytical balance and analytical grade reagents with purities of 99% or higher. Two collinear laser beams illuminate the particle from below (HeNe @ 633 nm, Ar+ @ 488 nm).

To characterize the particle three different, independent methods are employed. First, we use the video image of the particle on CCD detector 1 and an automatic feedback loop to adjust the DC-voltage for compensating the gravitational force (Richardson, 1990). A change in DC voltage is therefore a direct measure of the mass change, allowing to calculate a radius change when the density of the particle is known or can be estimated. Second, the two-dimensional angular scattering pattern is recorded with CCD sensor 2 by measuring the elastically scattered light from both lasers over observation angles ranging from 78° to 101°. If the particle is liquid, and therefore of spherical shape, the scattering pattern is regular, with the mean distance between fringes being a good measure of the radius of the particle, almost independent of its refractive index (Davis and Periasamy, 1985). Third, we use a photomultiplier with a relatively small conical detection angle (approximately 0.2° half angle) to measure the scattering intensity at 90° to the incident beam, and feeding this signal to an analog lock-in amplifier (Stanford Research System model SR510) to measure the intensity fluctuations at the frequency of the AC field of the electrodynamic trap (with a 10 Hz ENBW). This yields the root mean squared deviation (RMSD) from the intensity mean of the scattered intensity, which can be associated with the particle morphology: low values for spherical homogeneous particle and high values for crystalline shape (see Videen (1997) and Krieger and Braun (2001) for details).

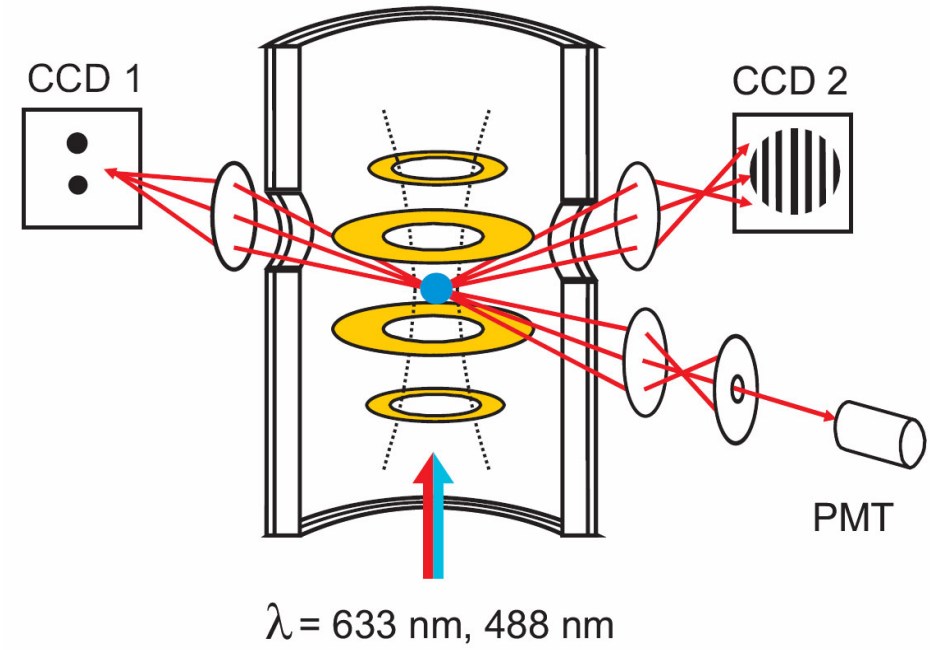

Fig. 3-1. Schematic of the electrodynamic balance. A three-wall glass chamber hosts four metal rings which supply the electric field needed for particle levitation. The particle is illuminated by two laser beams from below. The scattered light is collected in the near and far field view by two CCD cameras, and its intensity monitored by a photomultiplier (PMT).

Hygroscopicity Tandem Differential Mobility Analyzer

The HTDMA was used to determine the hygroscopic growth, i.e., the change of aerosol particles diameter due to the uptake of water. The experimental set up has been fully described before (Weingartner et al., 2002; Gysel et al., 2004; Sjogren et al., 2007). The compounds were dissolved in MilliQ water (typically 0.1-1 g/L) and all solute appeared completely dissolved at visual inspection. The particles were generated using an atomizer (TSI 3076) operated with purified compressed air. It is assumed that the resulting aerosol was internally mixed with the same mass ratio as in the solution as no broadening of the growth factor distributions from the HTDMA could be detected while switching from the pure ammonium sulfate to the mixtures. The particles first entered a silica gel diffusion dryer (flow rate: 300 sccm) in order to dry the sample to RH < 10% at 25°C. The dry aerosol is subsequently brought to charge equilibrium using a bipolar diffusion charger (^{85}Kr) and then fed into the first differential mobility analyzer (DMA), where a narrow size cut of the dry aerosol (D_0 = 100 nm) is selected. The particle diameter resulting after equilibration at a well defined higher RH (20 to 25 s residence time) is then measured using a second DMA and a condensation particle counter (CPC; TSI CPC 3022A). The exact D_0 is determined by keeping the particles exposed to dry conditions (RH ≤ 10%), in which case no size change occurs. With this apparatus, hygroscopic growth of particles with diameters between 20 and 250 nm can be determined in the temperature range of -20°C to 30°C and the humidity range of 10% to 95% RH with an accuracy of ΔT = ±0.1°C and ΔRH = ±1.6%. The hygroscopic growth factor is determined with a precision of ±0.01 (at D_0) and ±0.03 (at RH=80%) (Sjogren et al., 2007). Since the HTDMA D_0 is 100 nm, the Kelvin effect plays a role limiting the water uptake due to high curvature of smaller droplets. For solution droplets with surface tension of pure water the growth factors measured with the HTDMA are therefore expected to be 1-2% lower than those calculated with the EDB and bulk samples. No correction for this effect was applied.

During our measurement of hygroscopicity cycles, particles are exposed to RH increasing from RH 10% to RH 85% and again decreasing (at a typical rate dRH/dt ≈ 10%/hour for the EDB), while pressure and temperature are kept constant at T ≈ 290K and P ≈ 1atm. Particle mass (for the EDB) and mobility diameter (for the HTDMA) are monitored and the results are presented in so-called humidograms, where the mass growth factor *g* is plotted versus RH. In order to do so, the size change measured with the HTDMA is converted to a mass change via:

$$g(RH) = \frac{m(RH)}{m_o} = 1 + \left(G^3(RH) - 1\right)\frac{\rho_{H_2O}}{\rho_o}, \quad \textbf{(3-1)}$$

where $m(RH)$ is the mass of the particle depending on relative humidity, m_o and ρ_0 are the initial particle mass and density at dry conditions, and g and $G = D/D_o$ are the mass and size growth factors. This equation assumes that the density of the sample is linearly dependent on the volume mixing ratio of the solute and the absorbed water. It is further assumed that the measured mobility diameter is equal to the volume equivalent diameter, which is the case for a droplet with elevated water content, but might not be fulfilled for non-spherical dry particles due to dynamic shape factors being different from 1.0. As no significant deviations from sphericity at dry conditions were observed, the use of the above equation is justified. The EDB technique measures relative mass changes as explained in the experimental section. Therefore, it is necessary to identify a reference state to calculate the mass growth factor. One option can be the choice of the voltage at very dry conditions, typically RH=10%, as normalizing factor, in which case $g(10\%) = 1$. However, it is often difficult to assure that at a low RH the particle is completely free of water (Peng et al., 2001). In the present work, following previous hygroscopicity studies (Choi and Chan, 2002, for instance), we measured the water activity of the compounds listed in Table 3-1 and their mixtures at various concentrations using the AquaLab water activity meter. The EDB voltage was then normalized to match the bulk data at RH≈80%.

For two-component particles as the ones studied in this paper the Zdanovskii-Stokes-Robinson (ZSR) relation (Zdanovskii, 1948; Stokes and Robinson, 1966) can be simply written as:

$$g(RH) = g_1(RH)w_1 + g_2(RH)w_2 \quad \textbf{(3-2)}$$

where g is the total mass growth of the two-component particle as a function of relative humidity, g_1 is the ammonium sulfate's mass growth factor, calculated with the thermodynamic model proposed by Clegg et al. (1998) (available at http://mae.ucdavis.edu/wexler/aim.htm/), g_2 is the growth factor of pure organic particles measured with the EDB, and w_i are the mass fractions of the two components in the mixture. We assume therefore independent additive hygroscopic behavior of the different components in the mixed particles. The water activities of the compounds and their mixtures at different concentrations were measured using an AquaLab water activity meter (Model 3TE, Decagon Devices).

Table 3-1. Substances used during the experiments.

Substances	Purity	ρ (g/cm^{-3})	M (g/mol)	Producer	Product n°
Ammonium sulfate	99.99%	1.77	132.14	Aldrich	431540
Citric acid	≥ 99.5%	1.665	192.027	Fluka	27488
Glutaric acid	99%	1.424	132.12	Aldrich	U05447-124
Adipic acid	≥ 99.5%	1.362	146.14	Fluka	9582

3.4. Results and discussion

3.4.1. Ammonium sulfate and citric acid (AS/CA)

Hygroscopicity measurements of particles made of pure ammonium sulfate, pure citric acid, and mixtures of the two with different mixing ratios (AS:CA=4:1, 2:1, 1:1 molar ratios) are performed with the EDB and HTDMA. The results are compared with literature, bulk data and ZSR predictions in Fig. 3-2. The uppermost panel shows the humidogram of pure ammonium sulfate particles at ambient temperature. The hygroscopicity of a pure ammonium sulfate particle is well known: solid ammonium sulfate exposed to increasing RH initially does not take up water until it exhibits a distinct deliquescence point at RH≈80%, the deliquescence relative humidity (DRH), where the crystalline to liquid phase transition occurs. The particle then takes up or releases water gradually upon RH changes without undergoing a phase change at the DRH. Instead, it remains in a supersaturated metastable condition at intermediate RH until it crystallizes at RH≈40%, the efflorescence relative humidity (ERH), forming a solid particle again. The measured growth factors are in agreement with the thermodynamic model by Clegg et al. (1998) (see Fig. 3-2).

In contrast, pure citric acid particles are always in liquid state during our experiments as shown in the lowermost panel of Fig. 3-2: they take up or release water gradually without phase changes in the whole range of relative humidities studied here. EDB and HTDMA measurements of this study are in reasonable agreement with EDB and bulk measurements of previous studies (Levien, 1955; Apelblat et al., 1995; Peng et al., 2001). Note that citric acid retains some water even at low RH (g > 1 for RH≈10%). Our pure citric acid cycles measured with the EDB together with bulk points were fitted to obtain the following parametrization for the pure citric acid growth factor: $g_2(RH) = 1.27774 - 0.05705 \cdot RH + 0.00418 \cdot RH^2 - 1.43806 \cdot 10^{-4} \cdot RH^3 + 2.56938 \cdot 10^{-6} \cdot RH^4 - 2.27958 \cdot 10^{-8} \cdot RH^5 + 7.97803 \cdot 10^{-11} \cdot RH^6$) for RH between 10% and 90%.

This is used in Eq. 3-2 to calculate the ZSR predictions. In the AS:CA=4:1 case, panel b) of Fig. 3-2, the particles start to take up water well before the full deliquescence of AS at RH≈78%. Thereafter, the particles are in fully liquid state and adsorb or desorb water according to RH changes until AS effloresces at ERH between 35% (HTDMA) and 38% (EDB). The red line results from the ZSR calculations in Eq. 3-2, assuming full dissolution of the components for the dehydration branch, and no dissolution of AS up to its deliquescence point for the hydration branch. This underestimates the measured water uptake during hydration, indicating that in fact also AS takes up some water and start dissolving before full deliquescence. Results from both techniques, EDB and HTDMA, are in agreement with the ZSR prediction (within 10%) for the dehydration branch. Panel c) of Fig. 3-2 shows the hygroscopicity cycle of AS/CA particles, 2:1 mixture. Here the measurements from EDB and HTDMA differ: the single particle in the EDB exhibits clearly separated hydration/dehydration branches, while the HTDMA does not. After injection of the particle into the EDB, a solid inclusion forms and dissolves completely at RH≈76% during moistening. Upon subsequent drying the particle remains liquid and it cannot be forced to effloresce even at RH as low as 10%. The presence of a solid inclusion, its deliquescence and the absence of efflorescence are confirmed by the light fluctuation signal in the uppermost panel of Fig. 3-3: the RMSD datapoints decrease to values typical for a homogeneous, spherical particle (i.e. liquid) at t = 20 ks. Also, the algorithm for calculating the particle radius (uppermost panel) works properly after t = 20 ks, providing indirect evidence for spherical shape with a homogeneous particle phase.

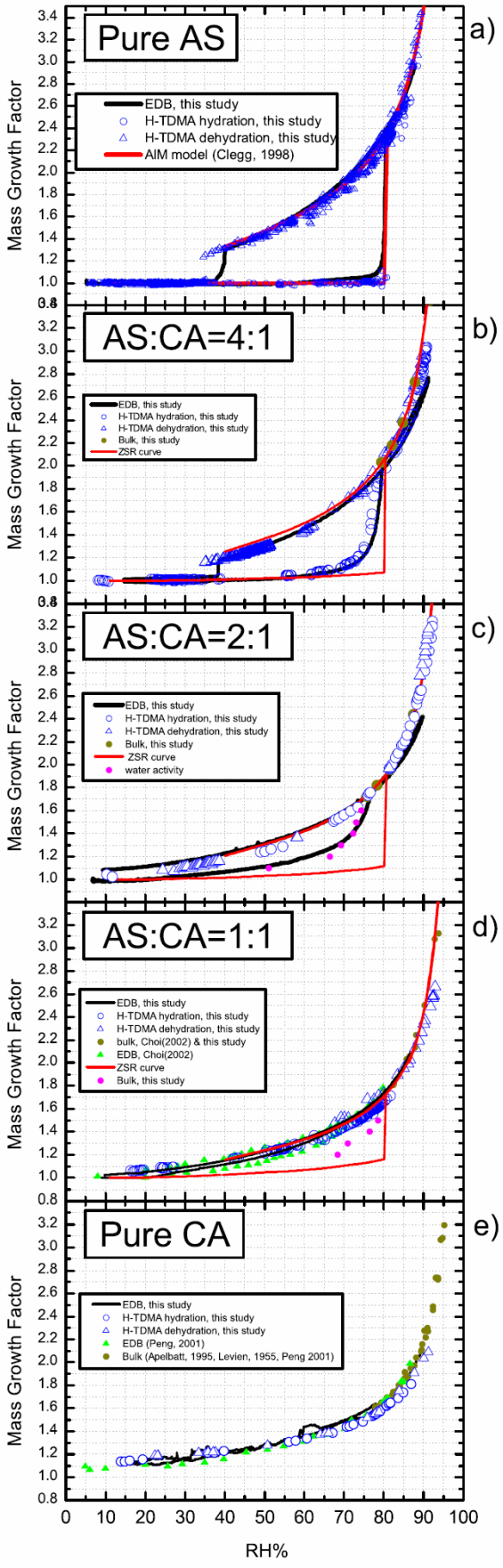

Fig. 3-2. Hygroscopicity cycles of pure ammonium sulfate (AS) and citric acid (CA) particles (panel a) and e)), and mixtures of AS and CA with different molar ratios (4:1, 2:1, 1:1, from panel (b) to panel (d)). Pure AS exhibits hysteresis with distinct deliquescence and efflorescence at RH≈80% and RH≈40%. Pure CA particles, instead, are always liquid and absorb and desorb water according to RH changes at any given RH. In the 4:1 case the water uptake starts at RH≈60%, the DRH and ERH are slightly decreased (2% and 3%, respectively) compared to the pure AS case. The 2:1 case exhibits different behavior for particles in HTDMA (always liquid) and the particle freshly injected at dry conditions in the EDB (solid AS present at dry conditions during hydration) with bulk points very close to the hydration branch of EDB measurements. The massive presence of CA in the 1:1 mixture suppresses the hysteresis of AS in both EDB and HTDMA cycles and particles are always in liquid state.

The physical reason for partial efflorescence only occurring at initial particle injection into the trap is not clear. The crystallization must be attributed to the ammonium sulfate fraction (since citric acid is always in liquid state in our experiments) and it could be a consequence of the fast evaporation experienced by the particle after injection in the EDB. In fact, a liquid droplet of about 50 μm size is produced by the injection device, and shrinks suddenly (few ms) to the particle size in thermodynamic equilibrium (radius≈5 μm) with ambient conditions. The fast evaporation induces a cooling of the particle which in turn could be responsible for the AS crystallization. The reproducibility of partial efflorescence of the particle upon injection but not in subsequent hygroscopicity cycles was tested and confirmed by several injections in the EDB. The particles in the HTDMA, instead, are always liquid and gradually absorb or desorb water at any given RH.

Panel d) of Fig. 3-2 shows the hygroscopicity cycle of AS/CA, 1:1 molar ratio. No efflorescence/deliquescence occurrence is detected with either technique, i.e. the particles remain liquid and gradually absorb/desorb water. EDB and HTDMA measurements agree with literature data and with the ZSR curve. Overall, the hygroscopicity of the two-component system ammonium sulfate/citric acid is characterized by a distinct, reduced, and completely absent hysteresis when decreasing the molar mixing ratio from 4:1 via 2:1 to 1:1, respectively. In the 2:1 case both DRH and ERH are reduced, the ERH potentially to such an extent that it does not occur at the lowest RH reached in the HTDMA and the EDB, but only occurs for initial particle injection into the EDB. For the dehydration branches of the fully liquid particles, EDB and HTDMA measurements are in good agreement and the ZSR approach provides a suitable description. For the hydration branches, the ZSR approach assuming no dissolution of AS before full deliquescence underestimates the observed water uptake, indicating that AS dissolves partially in aqueous citric acid at low RH.

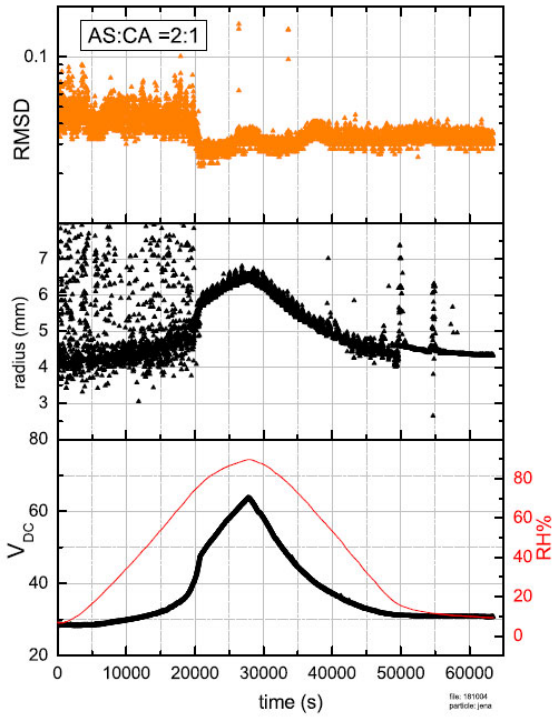

Fig. 3-3. Time evolution of the hygroscopicity cycle of one AS/CA particle, 2:1 molar ratio, in our EDB. The uppermost panel shows the RMSD of scattered light indicating AS deliquescence at *t*≈20 ks. Thereafter, the particle remains liquid without AS efflorescence reoccurring. The middle panel shows the radius calculated by means of the Mie phase functions (as explained in the experimental section). When the particle is not a homogeneous sphere (*t*≤20 ks), only an order of magnitude estimate for the radius can be inferred. The lowermost panel was used to construct the humidogram in Fig. 3-2, panel c).

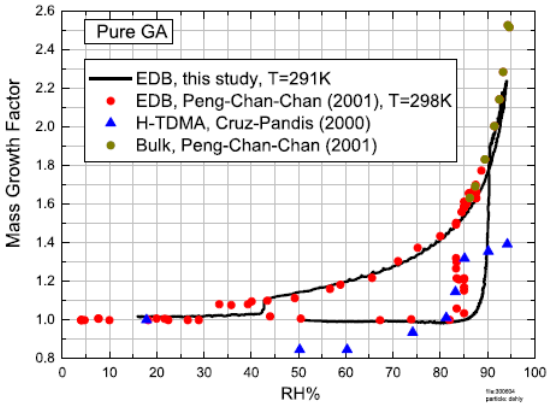

Fig. 3-4. Hygroscopicity cycles of pure GA particles. GA exhibits hysteresis with distinct DRH and ERH. The HTDMA cycle from literature do not fit the bulk data and shows a deviating hydration branch likely due to evaporation of the particle during measurements. The discrepancy in DRH measured with different techniques is due instead to different ambient temperatures.

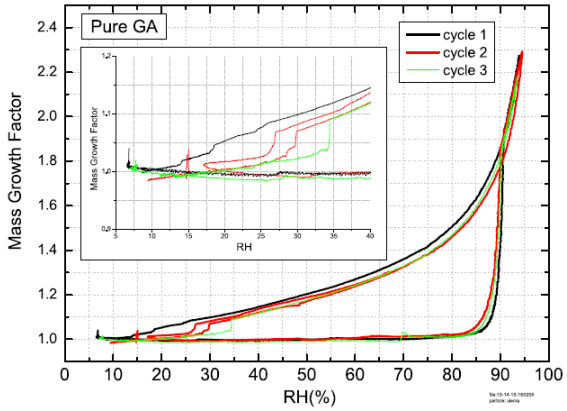

Fig. 3-5. Consecutive hygroscopicity cycles of a pure GA particle in our EDB. Insert: zoom on ERH showing that crystallization of GA has a low degree of reproducibility (in contrast to AS), ranging from gradual water release to a sharp efflorescence. This can lead to the presence of water also at very dry conditions.

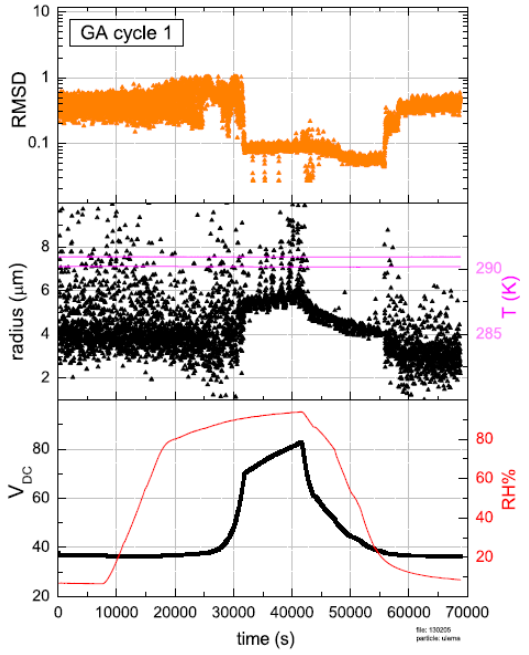

Fig. 3-6. Time evolution of one hygroscopicity cycle of a pure GA particle in our EDB. The light intensity fluctuations in the uppermost panel show a clear deliquescence (*t*≈32 ks, RH≈90.5%) and efflorescence (*t*≈55 ks, RH≈18%), proving that the particle changes its phase from liquid to crystalline with no detectable mass change. The optical radius evolution is plotted in the middle panel and it is an indirect indication of a liquid particle in the region 32≤*t*≤55 ks. The lowermost panel was used to construct the humidogram in Fig. 3-5, black curve, where no efflorescence was detected solely based on mass measurements.

3.4.2. Ammonium sulfate and glutaric acid (AS/GA)

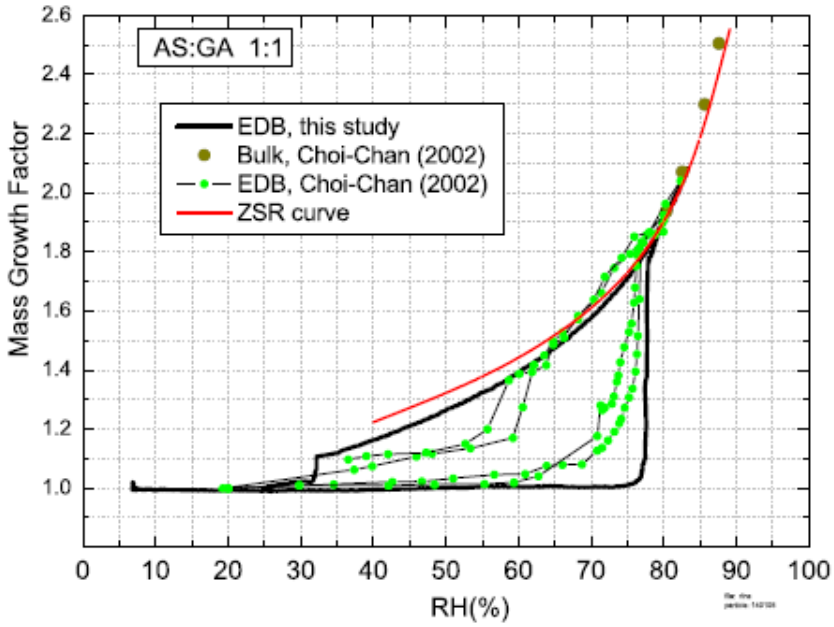

Fig. 3-7. Hygroscopicity cycle of AS/GA particles, 1:1 molar ratio. DRH and ERH points are lower compared to pure AS by 3% and 8%, respectively. DRH is lower than both deliquescence of pure AS and pure GA. ERH of GA is now triggered by the presence of AS.

Hygroscopicity cycles of pure glutaric acid and mixed ammonium sulfate/glutaric acid (AS:GA=1:1 molar ratio) particles were performed with the EDB. HTDMA cycles were also measured, but they are not shown because no reliable results could be achieved due to substantial evaporative shrinking of the particles within the instrument. Such evaporation artifacts in HTDMA instruments have previously been reported by Prenni et al. (2003), as well as Cruz and Pandis (2000) for submicrometer size glutaric acid particles. Pure glutaric acid exhibits hysteresis with distinct deliquescence and efflorescence as shown in Fig. 3-4. The DRH of glutaric acid has been determined by several groups: Brooks et al. (2002): DRH=87.5%; Wise et al. (2003): DRH=88.9%; Marcolli et al. (2004) DRH=88.2% (all bulk measurements at 25°). Pant et al. (2004) found DRH≈89% by using a reflected-light microscope technique. In this study we found DRH≈90%, a slightly higher value likely due to the temperature dependence of glutaric acid DRH: unlike ammonium sulfate, the solubility of glutaric acid is strongly temperature dependent. HTDMA data from Cruz and Pandis (2000) strongly underestimate the amount of water uptake at deliquescence (DRH≈85%). In addition, a size decrease at RH≈50% possibly caused by structural rearrangements inside the particle or shrinking due to evaporation was observed. The DRH determined with EDB at 25° by Peng et al. (2001) is 83.5%≤DRH≤85%. One reason for this lower value might be the presence of impurities in the glutaric acid used for the experiment. The efflorescence behavior, instead, is characterized by a low degree of reproducibility. EDB cycles in Fig. 3-4, suggests efflorescence at RH≈43% and between 28% and 32% for EDB measurements from this study and that by Peng et al. (2001). However, during consecutive cycles that we performed with another particle as shown in Fig. 3-5, efflorescence occurred at RH between 25% and 35% as a multi-step process, with a first mass decrease and a subsequent gradual water release (red and green curves), or as a gradual water release (black curve). In contrast, the analysis of scattered light fluctuations reveals that the phase change from liquid to solid is a well defined

efflorescence: during each cycle the particle solidifies at a well defined RH as indicated in Fig. 3-6, where the experimental raw data of the black curve in Fig. 3-5 are plotted. It is evident from the RMSD data (uppermost panel) that the particle undergoes two phase changes, one from solid to liquid at $t \approx 32$ ks (RH≈90.5%), and one from liquid to solid at t≈55 ks (RH≈18%). This confirms that the physicochemical behavior of glutaric acid is very complex and more than one experimental technique has to be invoked to fully characterize it. Figure 3-7 shows one hygroscopicity cycle of an ammonium sulfate/glutaric acid particle with 1:1 molar ratio of the mixture together with results from literature. The particle is completely crystalline and does not take up water until its full deliquescence at DRH≈77.5% while the efflorescence occurs at ERH≈32%. Both our cycle and the one from the literature (Choi and Chan, 2002) show a lower water uptake with respect to ZSR predictions in the metastable region at dry conditions, while the growth factor at DRH matches perfectly the ZSR curve. Pant et al. (2004) investigated in detail the DRH and ERH occurrence for the AS/GA system. For the AS:GA=1:1 mixture they found DRH≈78% and ERH≈28%. DRH=76.7% was observed in bulk measurements by Wise et al. (2003). All of these results are in agreement with ours.

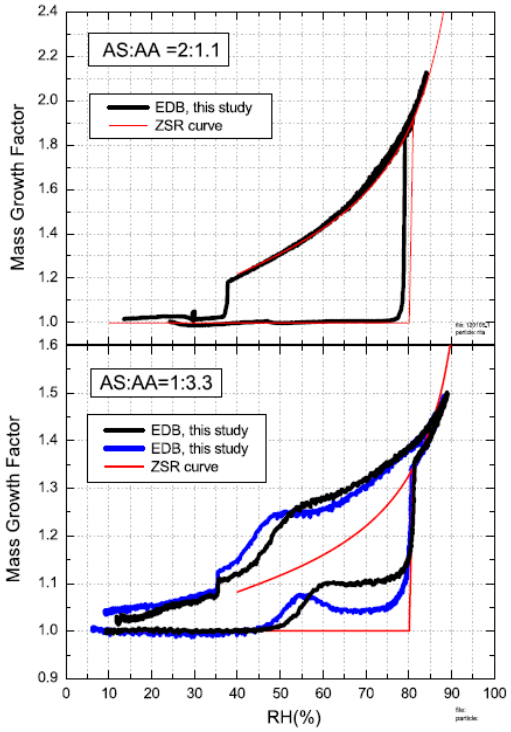

Fig. 3-8. Hygroscopicity cycles of AS/AA particles in our EDB; 2:1 molar ratio (upper panel) and 1:3 molar ratio (lower panel). The 2:1 case resembles the pure AS behavior, while there are modified hydration and dehydration branches in the 1:3 case which strongly differ from ZSR predictions. Non-monotonous mass changes must be due to structural changes (particle compaction) occurring during water uptake.

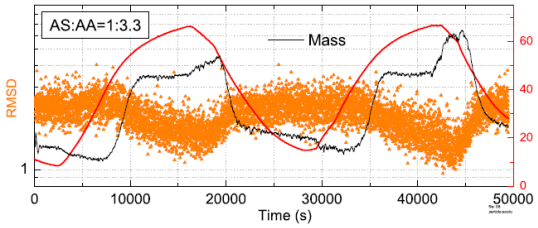

Fig. 3-9. Two incomplete consecutive cycles of an AS/AA particle, 1:3 molar ratio. Light intensity fluctuations (orange symbols) are in phase opposition with the mass and ambient RH (black and red curves, respectively). This indicates that the pre-deliquescence water uptake described in the lower panel of Fig. 3-8 is reversible.

3.4.3. Ammonium sulfate and adipic acid (AS/AA)

Pure adipic acid particles remain crystalline and do not deliquesce at relative humidities up to 99%, therefore adipic acid is generally regarded as an inert component of atmospheric aerosols (Sjogren et al., 2007; Hameri et al., 2002). We already presented hygroscopic measurements of mixed ammonium sulfate/adipic acid particles in Sjogren et al. (2007). In that study the kinetics and morphology of the system was investigated: it was proposed that adipic acid, when present in major fractions (and always in solid state, as verified with light fluctuation measurements in the EDB), can encapsulate some of the inorganic species residing in the crystalline organic veins and pores. The water uptake rate of the inorganic solution is probably limited by solid phase diffusion (water through solid adipic acid). The conclusion was that sufficient residence time in the HTDMA is required for such systems to equilibrate, or measurements will be misleading.

Here we present two cases where the particles consist mostly of ammonium sulfate (AS/AA 2:1 molar fraction) or adipic acid (AS/AA 1:3 molar fraction), see Fig. 3-8. The 2:1 case (upper panel) resembles the behavior of pure ammonium sulfate of Fig. 3-2, uppermost panel. But now the growth factors of the dehydration branch are lower due to the presence of the inert adipic acid, in agreement with ZSR predictions. However, in the 1:3 case (lower panel) the hygroscopic cycle strongly differs from the ZSR prediction in both hydration and dehydration branches of the EDB measurements. A pre-deliquescence water uptake starting at RH≈45% is followed by full deliquescence of ammonium sulfate. Upon dehydration, water is retained in the particle and released until the efflorescence of ammonium sulfate occurs. In particular, the blue curve in the lower panel indicates a pre-deliquescence water uptake which is followed by a water loss despite growing RH - presumably due to compaction and restructuring of the particle after partial dissolution of ammonium sulfate This morphology change would cause part of the water to be release by the particle (see the Discussion section for details). Consecutive cycles made on several particles show a similar pre-deliquescence behavior with water uptake of 5-15% in mass starting at RH between 45% and 61%.

We investigate whether the pre-deliquescence is a reversible process with respect to relative humidity changes. Figure 3-9 shows the temporal evolution of two consecutive incomplete cycles where RH, starting from less than 10%, is increased to 70% and then lowered again to reach very dry ambient conditions. The scattered light intensity fluctuations (RMSD, orange symbols) are in opposite phase with the mass changes, indicating that the shape of the particle is getting more spherical while its mass and the RH are increasing (black and red curves). RMSD values are typical for crystalline particles during the whole experiment. This is consistent with a water uptake which fills the pores of the solid particle because of the Kelvin effect on concave surfaces, conferring a more spherical shape and possibly a more homogeneous refractive index. By decreasing the relative humidity, the water evaporates, pores and cavities are depleted of water and the particle turns back to a more irregular crystalline shape. The process is hence reversible with respect to relative humidity changes.

3.5. Discussion

We have studied three two-component inorganic/organic systems representing three distinct hygroscopic growth characteristics that can be found in atmospheric aerosols:

- Liquid phases;
- Liquid/solid phases.
- Solid phases;

Liquid. When both components of the particle are in the liquid state, we believe that the hygroscopicity can be explained by the simple ZSR approach. The water uptake of the particle is the sum of the water uptakes of the single components (see AS:CA=4:1, 2:1, 1:1, and AS:GA=2:1, dehydration branches). Our EDB and HTDMA measurements agree with the ZSR predictions and with bulk measurements.

Solid/Liquid. For the solid/liquid case of AS:CA=4:1 and AS:CA=2:1 (AS being the solid phase) we do not know the detailed composition of the solution in the particle during the hydration before the deliquescence of AS. Unfortunately, it is often not possible to infer this composition from bulk measurements where needed because of the formation of a third phase. Hence, the ZSR approach can not be applied without further assumptions. Application of ZSR with the assumption that AS is present as an inert mass before deliquescence (CA being the only responsible for water uptake) underestimates the observed water uptake for AS/CA mixtures. We therefore conclude that AS is partially dissolved in aqueous citric acid. In a similar study, Marcolli and Krieger (2006) observed higher water uptake than the bulk measurements for the system AS/PEG400 (solid AS, liquid organic). The system AS/AA 1:3 can be regarded as an extreme case showing discrepancies from ZSR both in hydration and dehydration branches. In the dehydration branch (now the organic AA is the solid phase) more water is present than expected by the ZSR predictions. Thermodynamics alone cannot explain the higher water uptake; the complex morphology involved and the consequent Kelvin effect play a crucial role.

Solid. For the solid/solid case there is no water uptake before deliquescence for the AS/GA system. In contrast, the hydration branch of the AS:AA=1:3 mixture exhibits a pre-deliquescence water uptake where AS should not take up water before deliquescence and AA should not take up water at all. We attribute this process to morphology effects as explained below. It is known that the condensation of water in micropores can be important for materials with complex morphology (Camuffo, 1998), such as insoluble aerosol particles or soluble ones with an immersed solid component. The ambient relative humidity in equilibrium with a micropore of radius r has been calculated by Thomson, later Lord Kelvin (Thomson, 1871):

$$RH(r) = a_W \exp\left(\frac{2\sigma V_m}{rTR}\right), \qquad \textbf{(3-3)}$$

where a_w is the water activity (required when appling the equation to saline solutions), σ is the surface tension of water (σ = 72.2 Jm^{-2} at T=290 K), V_m is the molar volume of water and R the gas constant. The Kelvin equation will be applied in the following to illustrate the morphology effects on the AS/AA particle (1:3 molar ratio) in the hygroscopicity cycles of Fig. 3-8 (black curve). We assume that the internal cavities, pores and veins of the AS/AA particle can be described by cylindrical veins of radius r_v and total length l_v. For an average $RH \approx 53\%$ between the onset and the maximum of the pre-deliquescence Eq. 3-3 yields a vein radius of r = 2.6 nm calculated for equilibrium, when we assume that a_w = 0.8 for a solution inside the veins. The total vein length follows after quantifying the relative mass increase due to the water uptake (10% averaged on many cycles like the ones in Fig. 3-8, lower panel) simply from the formula for a cylindrical volume and from the density definition: $l_V = m_V / (\rho_V \pi r_V^2)$ where m_v is the mass of liquid in the vein and ρ_v its density, which we assumed to be that of water for simplicity. The optical radius of the particle in the EDB can not be exactly calculated for this particular system because the particle is always non spherical. Nevertheless, a rough

estimate of $r \approx 3\mu$m can be inferred from the spread radius datapoints like those shown in the middle panel of Fig. 3-3 before deliquescence. The particle density is ρ = 1.462 g/cm3, and thus the absolute mass of the particle, and hence of the water uptake, can be easily calculated considering the 10% relative mass increase estimate. This yields a vein length of l_v = 77 cm; this length, compared with a 3 μm particle size, has to be taken as evidence for the highly complex morphology of the particle required to accommodate the water.

Part of the water can be released by the particle in case of partial dissolution of AS after the pre-deliquescence water uptake. The internal structure may partially collapse with a consequent vein length decrease resulting in a less amount of water to be in equilibrium with the particle internal structure. This can explain the mass loss after pre-deliquescence at RH≈ 55%shown in Fig. 3-8 (blue curve). The same analysis can be repeated using more realistic geometries in order to describe the surface and internal morphology of the particle. For instance, a rugged surface made of semi-spherical pores with the same Kelvin radius r = 2.6 nm can be envisaged. This surface structure can be reproduced in a number of similar underlying layers necessary to accommodate the 10% water uptake. Repeating the calculation above for this geometry leads to a number of 105 layers with a width of 2.6 nm per layer. The high degree of complexity of the particle morphology is again confirmed. The highest degree of morphological complexity would be the one which describes the particle as a packing of spherical voids with a radius equal to the Kelvin radius calculated above. The AS/AA material would be in the lattice of this arrangement, with discontinuities which allows water to penetrate the particle and fill the voids. The problem of packing a sphere or a cube with small spheres (which in the present situation would represent the pores) is an old one in mathematics, starting with Kepler in the 17th Century and it is still a matter of discussion (Gensane, 2004). The percentage of filling ranges from 50% up to 77%, confirming that a high pre-deliquescence water uptake in pores structures is in principle possible, but not realized to such an extent for the AS/AA particles which take up water between 5% and 15% at low relative humidity.

3.6. Conclusions

This combined study aimed at shedding more light to the thermodynamic characterization of mixed inorganic/organic aerosol particles by means of two widely used techniques: the electrodynamic balance and the hygroscopicity tandem differential mobility analyzer. We focused on three organic acids of atmospheric relevance (citric, glutaric, adipic acids) in mixtures with ammonium sulfate. These are representative of three different types of water uptake characteristics. The results strongly indicate that as long as the two-component particles are fully liquid, the ZSR (Zdanovskii-Stokes-Robinson) relation adequately predicts the water uptake. Whereas with the presence of a solid phase, (being it inorganic, like in the AS:CA=2:1 particles, or organic like in the AS/AA 1:3 case), thermodynamics alone is not sufficient to fully characterize the system. In fact, morphology effects play an important role resulting in the presence of water in two-component particles even at dry ambient conditions. In addition, we showed that organic substances like glutaric acid need to be investigated by multiple independent techniques in order to assess the water uptake and the physical state of the particle at different ambient conditions.

Acknowledgements

This work was supported by the National Science Foundation Switzerland (grant n◦ 200021-100280).

References

Apelblat, A., Dov, M., Wisniak, J., and Zabicky, J.: Osmotic and Activity Coefficients of HO2CCH2C(OH)(CO2H)CH2CO2H (Citric Acid) in Concentrated Aqueous Solutions at Temperatures from 298.15K to 318.15K, J. Chem. Thermodynamics, 27, 347–353, 1995.

Braban C. F., and Abbatt, J. P. D.: A study of the phase transition behavior of internally mixed ammonium sulfate - malonic acid aerosols, Atmos. Chem. Phys., 4, 1451–1459, 2004.

Brooks, S., D.,Wise, M., E., Cushing, M., and Tolbert, M., A.: Deliquescence behavior of organic/ammonium sulfate aerosol, Geophys. Res. Lett., 29 (19), 1917, 2002.

Camuffo, D.: Microclimate for Cultural Heritage (Developments in Atmospheric Science), Elsevier, 1998. Chan, C.K., Flagan, R.C., Seinfeld, J.H.: Water activities of NH4NO3(NH4)2SO4 solutions. Atmospheric Environment, 26, 1661–1673, 1992.

Chan, C.K., Flagan, R.C., Seinfeld, J.H.: Water activities of NH4NO3(NH4)2SO4 solutions. Atmospheric Environment, 26, 1661–1673, 1992.

Chan, M. N. and Chan, C. K.: Mass transfer effects in hygroscopic measurements of aerosol particles, Atmos. Chem. Phys., 5, 2703–2712, 2005.

Choi, M. Y., and Chan, C. K.: The Effects of Organic Species on the Hygroscopic Behaviors of Inorganic Aerosols, Environ. Sci. Technol., 36, 11, 2422–2428, 2002.

Clegg, S. L., Brimblecombe, P., and Wexler, A. S.: A thermodynamic model of the system H+ - NH4+ - SO42- - NO3- - H2O at tropospheric temperatures, J. Phys. Chem. A, 102, 2137–2154, 1998.

Cruz, C. N., and Pandis, S. N.: Deliquescence and Hygroscopic Growth of Mixed Inorganic-Organic Atmospheric Aerosol, Environ. Sci. Technol., 34, 20, 4313–4319, 2000.

Davis, E. J., and Periasamy, R.: Light-scattering and aerodynamic size measurements for homogeneous and inhomogeneous microspheres, Langmuir, 1, 373–379, 1985.

Davis, E. J., Buehler, M. F., and Ward, T.L.: The double-ring electrodynamic balance for microparticle characterization, Rev. Sci. Instrum., 61, 1281–1288, 1990.

Dick, W. D., Saxena, P., and McMurry, P. H.: Estimation of water uptake by organic compounds in submicron aerosols measured during the Southeastern Aerosol and Visibility Study, J. Geophys. Res., 105(D1), 1471–1479, 2000.

Fuzzi, S., Andreae, M. O., Huebert, B. J., Kulmala, M., Bond, T., C., Boy, M., Doherty, S., J., Guenther, A., Kanakidou, M., Kawamura, K., Kerminen, V., M., Lohmann, U., Russell, L., M., and P¨oschl, U.: Critical assessment of the current state of scientific knowledge, terminology, and research needs concerning the role of organic aerosols in the atmosphere, climate, and global change, Atmos. Chem. Phys., 6, 2017–2038, 2006.

Gensane, T.: Dense packings of equal spheres in a cube, Electronic Journal Of Combinatorics, 11 (1), 2004. Gysel, M., Weingartner, E., Nyeki, S., Paulsen, D., Baltensperger, U., Galambos, I. et al.: Hygroscopic properties of water-soluble matter and humic-like organics in atmospheric fine aerosol, Atmos. Chem. Phys., 4, 35–50, 2004.

Gysel, M., Weingartner, E., Nyeki, S., Paulsen, D., Baltensperger, U., Galambos, I. et al.: Hygroscopic properties of water-soluble matter and humic-like organics in atmospheric fine aerosol, Atmos. Chem. Phys., 4, 35–50, 2004.

Hameri, K., Charlson, R., and Hansson, H. C.: Hygroscopic Properties of Mixed Ammonium Sulfate and Carboxylic Acids Particles, AIChE Journal, 48, 6, 1309–1316, 2002.

Intergovernmental Panel on Climate Change (IPCC): Fourth Assessment Report,Working Group I Report “The Physical Science Basis”, Chapter 2, http://www.ipcc.ch/. Jacobson, M. C., Hansson, H. C., Noone, K. J., and Charlson, R. J., Organic atmospheric aerosols: Review and state of science, Rev. Geophys., 38, 2, 267–294, 2000.

Jacobson, M. C., Hansson, H. C., Noone, K. J., and Charlson, R. J., Organic atmospheric aerosols: Review and state of science, Rev. Geophys., 38, 2, 267–294, 2000.

Kanakidou, M., Seinfeld, J H., Pandis, S. N. et al.: Organic aerosol and global climate modelling: a review, Atmos. Chem. Phys., 5, 1053–1123, 2005.

Krieger, U. K, Colberg, A. C., Weers, U., Koop, T., and Peter, Th.: Supercooling of single H_2SO_4/H_2O aerosols to 158 K: no evidence for the occurrence of the octahydrate, Geophys. Res. Lett., 27, 2097–2100, 2000.

Krieger, U., K., Braun, C.: Light-scattering intensity fluctuations in single aerosol particles during deliquescence, J. Quant. Spectrosc. Radiat. Transfer, 70, 545–554, 2001.

Levien, B. J.: A Physicochemical Study of Aqueous Citric Acid Solutions, J. Phys. Chem., 59, 640–644, 1955.
Marcolli, C., and Krieger, U. K.: Phase Changes during Hygroscopic Cycles of Mixed Organic/Inorganic Model Systems of Tropospheric Aerosols, J. Phys. Chem. A, 110, 1881–1893, 2006.
Marcolli, C., Luo, B., and Peter, T.: Mixing of the organic aerosol fractions: liquids as the thermodynamically stable phases, J. Phys. Chem. A, 108, 2216–2224, 2004.
Middlebrook, A. M., Murphy, D. M., and Thomson, D. S.: Observations of organic material in individual marine particles at Cape Grim during the First Aerosol Characterization Experiment (ACE 1), J. Geophys. Res., 103(D13), 16475–16483, 1998.
Murphy, D. M., Cziczo, D. J., Froyd, K. D., et al.: Single-particle mass spectrometry of tropospheric aerosol particles, J. Geophys. Res., 111, D23S32, 2006.
Pant, A., Fok, A., Parson, M. T., Mak J., and Bertram, A. K.: Deliquescence and crystallization of ammonium sulfate-glutaric acid and sodium chloride-glutaric acid particles, Geophys. Res. Lett, 31, L12111, 2004.
Peng, C.; Chan, M. N., and Chan, C. K.: The Hygroscopic Properties of Dicarboxylic and Multifunctional Acids: Measurements and UNIFAC Predictions, Environ. Sci. Technol., 35, 4495–4501, 2001.
Prenni, A. J., De Mott, P. J., and Kreidenweis, S. M.: Water uptake of internally mixed particles containing ammonium sulfate and dicarboxylic acids, Atmospheric Environment, 37 (30), 4243–4251, 2003.
Richardson, C. B.: A stabilizer for single microscopic particles in a quadrupole trap, Rev. Sci. Instrum., 61, 1334–1335, 1990.
Rogge, W. F., Mazurek, M. A., Hildemann, L. M., and Cass, G. R.: Quantification of urban organic aerosols at a molecular level: identification, abundance and seasonal variation, Atmos. Environ., 27A, 8, 1309–1330, 1993.
Saxena, P., Hildemann, L. M., McMurry, P. H., and Seinfeld, J. H. J.: Organics alter hygroscopic behaviour of atmospheric particles, J. Geophys. Res., 100(D9), 18755–18770, 1995.
Sjogren, S., Gysel, M.,Weingartner, E., Baltensperger, U., Cubison, M. J., Coe, H., Zardini, A. A., Marcolli, C., Krieger, U. K., and Peter, T.: Hygroscopic growth and water uptake kinetics of twophase aerosol particles consisting of ammonium sulfate, adipic and humic acid mixtures, J. Aerosol Sci., 38, 157–171, 2007.
Stokes, R. H., and Robinson, R. A.: Interactions in aqueous nonelectrolyte solutions, solute-solvent equilibria, J. Phys. Chem., 70, 7, 2126–2131, 1966.
Svenningsson, B., Rissler, J., Swietlicki, E., Mircea, M., Bilde, M., Facchini, M. C., Decesari, S., Fuzzi, S., Zhou, J., Mønster, J., and Rosenørn, T.: Hygroscopic growth and critical supersaturations for mixed aerosol particles of inorganic and organic compounds of atmospheric relevance, Atmos. Chem. Phys., 6, 1937–1952, 2006.
Thomson, W.: On the equilibrium of vapour at a curved surface of liquid, Phil. Mag. 42, 448–452, 1871.
Videen G., Pellegrino P., Ngo D., Videen, J., S., Pinnick, R., G.: Light-scattering intensity fluctuations in microdroplets containing inclusions. Appl. Opt., 36, 6115–6118, 1997.
Videen G., Pellegrino P., Ngo D., Videen, J., S., Pinnick, R., G.: Light-scattering intensity fluctuations in microdroplets containing inclusions. Appl. Opt., 36, 6115–6118, 1997.
Weingartner, E., Gysel, M., and Baltensperger, U.: Hygroscopicity of aerosol particles at low temperatures. 1. New low-temperature H-TDMA instrument: Setup and first applications, Env. Sci. Tech., 36, 1, 55–62, 2002.
Wise, M., E., Surratt, J., D., Curtis, D., B., Shilling, J., E., and Tolbert, M., A.: Hygroscopic growth of ammonium sulfate/ dicarboxylic acids, J. Geophys. Res., 108 (D20), 4638, 2003.
Zdanovskii, A. B., Zh. Fiz. Khim., 22, 1486–1495, 1478–1485, 1948.

CHAPTER 4

4. Generation of submicron Arizona Test Dust aerosol: chemical and hygroscopic properties

This chapter is a paper to which the author of this dissertation contributed and appears as a co–author. The author contributed with hygroscopicity measurements of the investigated mineral dust (Standard Arizona test dust) and interpretation of the mineral dust morphology from SEM images and the restructuring observed, as well as assistance during the manuscript writing process. Published in Journal of Aerosol Science and Technology, vol. 39, No. 5, p. 452-460, 2005.

A. Vlasenko[1,2], S. Sjogren[3], E. Weingartner[3], H.W. Gäggeler[1,2] and M. Ammann[1]

[1]Laboratory of Radio- and Environmental Chemistry, Paul Scherrer Institute, Villigen PSI CH-5232, Switzerland

[2]Department for Chemistry and Biochemistry, University of Berne, Bern CH-3008, Switzerland

[3]Laboratory of Atmospheric Chemistry, Paul Scherrer Institute, Villigen PSI CH-5232, Switzerland

4.1. Abstract

This paper describes a submicron dust aerosol generation system based on a commercially available dust disperser intended for use in laboratory studies of heterogeneous gas-aerosol interactions. Mineral dust particles are resuspended from Arizona Test Dust (ATD) powder as a case study. The system output in terms of number and surface area is adjustable and stable enough for aerosol flow reactor studies. Particles produced are in the 30-1000 nm size range with a log-normal shape of the number size distribution. The particles are characterized with respect to morphology, electrical properties, hygroscopic properties and chemical composition. Submicron particle elemental composition is found to be similar for the particle surface and bulk as revealed by X-ray photoelectron spectroscopy (XPS) and inductively coupled plasma optical emission spectroscopy (ICP-OES), respectively. A significant difference in chemical composition is found between the submicron aerosol and the ATD bulk powder, from which it was generated. The anionic composition of the water soluble fraction of this dust sample is dominated by sulfate. Resuspended dust particles show, as expected, non-hygroscopic behaviour in a humid environment. Small hygroscopic growth of about 1% (relative change in mobility diameter) was observed for 100 nm particles when the relative humidity (RH) was changed from 12% to 94%. Particles larger than 100-200 nm shrank about 1% once exposed to RH > 90%. This was interpreted as a restructuring of the larger agglomerates of dust to particles of smaller mobility diameter, under the influence of water vapor.

4.2. Introduction

Arid areas of our planet generate large amounts of dust, which is uplifted to the atmosphere. These natural sources are mainly deserts, which together with anthropogenic dust sources are considered to be responsible for one-third to one-half of annual aerosol emissions by mass [*Penner et al.*, 2001]. Through processes of saltation and sandblasting, dust particles are uplifted into the air and may travel over long distances. While larger particles sediment out due to gravity in the vicinity, smaller particles (<10μm) could reside in the atmosphere for more than a week. The strongest regional effect of so-called "dust events" is the considerable decrease of visibility due to light-scattering enhanced by dust particles. Mineral dust aerosol could also absorb incoming solar radiation and reflect back the infrared radiation coming from the ground. Due to the complexity of dust composition and the incomplete understanding of transport and removal processes, an assessment of the influence of dust on the global radiation balance is still uncertain [*Ramaswamy et al.*, 2001]. Recent field studies have shown dust particles acting as ice nuclei in clouds [*Cantrell and Heymsfield*, 2005; *DeMott et al.*, 2003; *Sassen et al.*, 2003]. Although large dust storms are episodic, dust particles are often present in the atmosphere and so could affect ice formation in clouds.

Heterogeneous interactions between atmospheric trace gases and mineral dust aerosol are important in several issues of atmospheric chemistry. This processing may affect the chemical and physical properties of the aerosol [*Putaud et al.*, 2004]. On the other hand, it may also impact the global budget of important trace gas compounds [*Bauer et al.*, 2004; *Bian and Zender*, 2003; *Liao and Seinfeld*, 2005]. Among the many potential reactions occurring, the reaction with HNO_3 might be the most important as it affects the ozone budget of the upper troposphere, because there the photolysis of HNO_3 is a significant source of NO and NO_2, to which ozone sensitively responds. This reaction is also of significant interest because it converts barely soluble calcium carbonate into very soluble calcium nitrate, which can therefore dramatically affect the properties of dust as cloud condensation nuclei [*Krueger et al.*, 2003; *Laskin et al.*, 2005].

Several laboratory studies have been performed to understand and quantify these processes [*Hanisch and Crowley*, 2001; *Mamane and Gottlieb*, 1992; *Underwood et al.*, 2001]. In these studies, dust was exposed to the trace gas of interest in the form of single particles or powder samples. The use of bulk powder samples is accompanied with a large uncertainty of the particle surface area actually exposed to the trace gas, and the way these measurements should be interpreted is somewhat under debate (Usher et al. 2003). Single particle techniques are illustrative for changes in morphology and structure, but may not be sensitive enough to address kinetic issues at the low trace gas concentrations typically encountered in the environment. As an alternative, airborne mineral dust particles at atmospheric pressure could be used in laboratory studies. This method has been established for the study of heterogeneous reactions with several other aerosol systems [*Ammann et al.*, 1998; *Guimbaud et al.*, 2002; *Mozurkewich et al.*, 1987], with a variety of methods to determine mass transfer to the aerosol particles. The requirements for kinetic flow reactor studies are a well-defined size distribution and a constant output with time. Working with particle sizes below about 1μm is favorable for two reasons: mass transfer to aerosol particles is less affected by diffusion in the gas phase [*Fuchs and Sutugin*, 1970; *Kulmala and Wagner*, 2001], so that also fast uptake to aerosol particles can be addressed. Furthermore, flow reactor work is technically facilitated, because submicron particles are less subject to impaction losses in inlet/exit systems. So far, a dust aerosol generation system for this purpose has not been reported in the literature.

Applying strong shear forces in expanding flows (nozzles), mechanic uplifting using a brush, or fluidized bed disintegration are typical processes for powder resuspension. While in industrial applications, usually a substantial mass output is required, control of size distribution, stability and suspension in a chemically well defined carrier gas of relatively low flow rate is required in the context of interest here. Commercially available dust generators [*Blackford and Rubow*, 1986; *Marple et al.*, 1978] produce mainly coarse particles (particle diameter larger than 1 μm), which may not be completely deagglomerated to represent mineral dust aerosol typically undergoing long-range transport in the atmosphere. In this study, we present a dust aerosol generation system based on a new commercially available system. The system is characterized with respect to generation stability and some physical and chemical properties of the aerosol produced, and to what degree the product aerosol represents the chemical composition of the original powder processed. The choice of Arizona Test Dust as our test material for resuspension in this study has been motivated by the possibility to use it directly without any further pre-treatment, that it represents a naturally occurring dust type and that it has also been used previously in studies addressing related issues (e.g., [*Hanisch and Crowley*, 2001]).

4.3. Experimental

The material used in this study to produce airborne particles is Arizona Test Dust (Ultrafine Grade A1, Ellis Components, UK), specified in ISO12103-1 standard and obtained from naturally occurring sand from a specific area of desert in Arizona, USA. According to the manufacturer, this sand was jet milled to reduce its particle size. Jet milling uses high pressure compressed air to propel the sand particles in opposing directions so that they collide. The resulting dust was then passed through a classifier to produce the required particle size distribution of the powder.

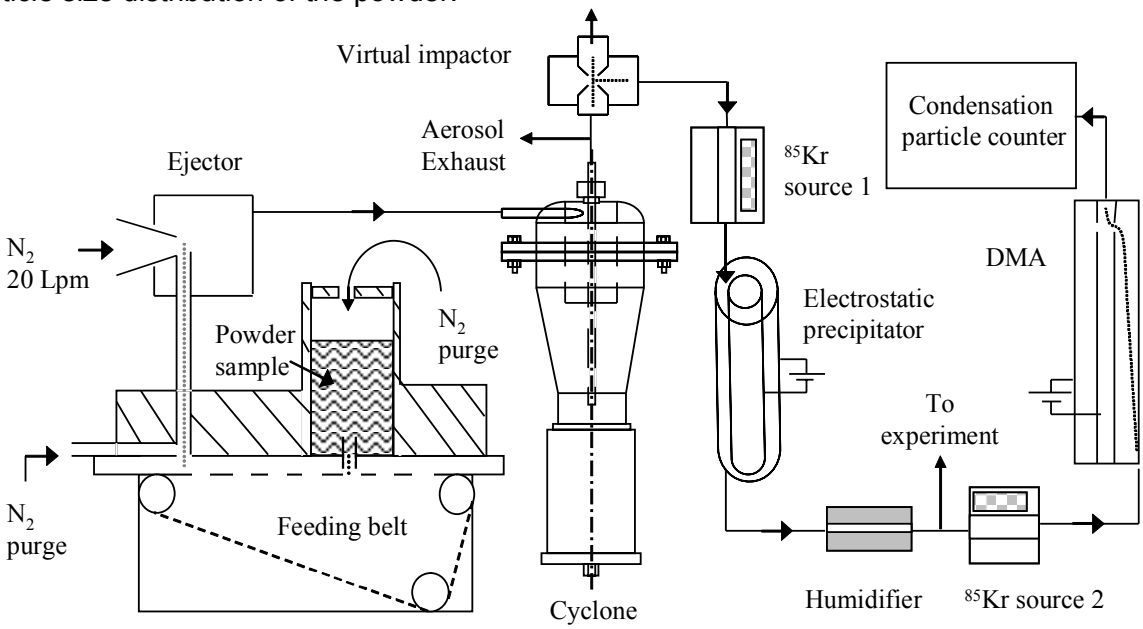

Fig. 4-1. Experimental setup to resuspend mineral dust into aerosol form and control the particle size distribution.

Our submicron mineral dust aerosol generation system consists of three stages: powder dispersion, particle size separation, control of particle charge and carrier gas (nitrogen). The setup is shown in Fig. 4-1. First, the sample powder is dispersed by a solid

aerosol generator (SAG, TOPAS GmbH, Germany). A special belt feeds the dust to the injector nozzle, which is a dual-stream injection nozzle (similar to standard ISO 5011:2000). The defined segments of the belt warrant a small but constant and reproducible supply of powder. Shear forces created in the injector nozzle at a flow rate of 20 $L \cdot min^{-1}$ disperse and disaggregate the powder to form particles. The resulting particle number concentration can be adjusted by setting the feeding belt speed over a wide range. Particle production can be stopped without changing the gas flow through the generator by stopping the belt movement. The original construction of the SAG by TOPAS allows the powder sample to come into contact with laboratory air through the opening of the dust container. Additionally, the laboratory air is admixed to the flow of resuspended dust through the opening of the dispersion unit. These two features of the manufacture design induce a contamination of the dust aerosol by the laboratory air. To solve this problem, we modified the original instrument by introducing a purge flow of nitrogen to the dust container, to the nozzle region and into the inner room of the housing (see Fig. 4-1). The resulting aerosol contains a significant amount of large particles. These particles readily sediment and hence could cause a problem due to deposition in the aerosol experiments envisaged with this source, which rely on a relatively narrow submicron size distribution. The coarse particles are removed by passing the 20 $L \cdot min^{-1}$ of aerosol flow through a homemade cyclone with a tangent inlet and axial discharge design (see Fig. 4-1). The dimensions of the cyclone are given in Table 4-1. The cyclone is immediately followed by a virtual impactor, where a final particle separation is achieved. This impactor is built according to the design by [*Marple et al.*, 1995] and has a cut-off diameter of 0.8 μm, removing particles above that size. The total input flow into the impactor is 2.2 $L \cdot min^{-1}$, the major exiting flow is 2 $L \cdot min^{-1}$ and the minor exiting flow is 0.2 $L \cdot min^{-1}$. The diameter of the impactor entrance nozzle is 0.8 mm and the diameter of the collection probe is 1 mm. The nozzle protrusion length and the spacing between the nozzle and the collection probe were both set to 1 mm. The construction of the cyclone and the impactor were optimised to facilitate disassembling the devices for routine cleaning.

Table 4-1. Standard dimensions [Buonicore and Davis, 1992] of the cyclone used in this study. All units are millimeters.

Dimensions	mm
Body diameter	68
Inlet diameter	4
Exit diameter	4
Vortex finder length	60
Body Length	63
Cone length	150
Dust outlet diameter	22

During dust dispersion, particles acquire a high electrical charge . This could cause an irreproducible particle loss to the walls of flow tubes consisting of insulating materials such as Teflon varieties necessary in experiments with reactive trace gases. To avoid this problem the aerosol is passed through a neutralizer (4 mCi ^{85}Kr source, denoted as Kr source no 1 in Fig. 4-1, inner volume 170 cm^3) to reduce the high particle charge, followed by an electrical precipitator (ESP). The ESP is a 29 cm long coaxial cylindrical condenser. A high voltage (5kV) is applied between the outer tube (3.8 cm diameter) and inner rod (1.9 cm diameter) allowing all charged particles below about 2μm diameter to deposit inside the precipitator. Only electrically conductive tubing is used to transport charged particles to this point.

The aerosol humidity could be adjusted by passing it through a vertically mounted tube with a H_2O permeable Goretex membrane (150 mm length, 6 mm i.d.) immersed in demineralised water. The relative humidity was measured by capacitance humidity sensors at room temperature.

Finally, the aerosol size distribution and number concentration was obtained by a Scanning Mobility Particle Sizer system (SMPS), which consisted of a ^{85}Kr neutralizer (denoted as Kr source no 2 in Fig. 4-1), a differential mobility analyzer DMA (model 3071, TSI) and a condensation particle counter CPC (model 3022, TSI). The system was operated at 3 $L \cdot min^{-1}$ sheath and 0.3 $L \cdot min^{-1}$ sample flow rates, respectively. Optionally the sheath flow could be humidified as the aerosol flow described above. The same relative humidity is maintained in both the DMA sheath air and in the aerosol flow since the aerosol liquid water content and consequently the particle diameter may be dependent on the relative humidity. Scanning time (300s) is long enough to get good counting statistics and a smooth particle spectrum. The performance of the system to resolve particle size was tested with the help of 40 nm (particle diameter) and 150 nm PSL particles (Duke Scientific Corporation, US). The SMPS system is configured to measure aerosol sizes from 20 to 800 nm. For sizing larger particles, an optical particle counter (OPC, GRIMM Labortechnik GmbH, Model 1.108) was used. That instrument was operated at 1.2 $L \cdot min^{-1}$ to measure the aerosol size distribution in the 0.3-20 μm size range. The averaging interval of the OPC was 60s. The instrument was calibrated by the manufacturer with polystyrene latex spheres (PSL). Application of both techniques allowed the measurement of the full size spectrum, which slightly exceeded the range covered by the SMPS system. Adequate control of even low numbers of larger particles is a prerequisite in experiments on trace gas uptake to particles as it strongly depends on surface area, and the larger particles may significantly contribute to the overall aerosol surface area.

Hygroscopic properties of the ATD particles were measured with a hygroscopicity tandem DMA (H-TDMA) instrument. A detailed description of the H-TDMA setup is given elsewhere [*Weingartner et al.*, 2002; *Weingartner et al.*, 2001] and thus will be given here in brief. A narrow size range of the polydisperse dry dust aerosol was selected with a first DMA. These monodisperse particles were humidified, and the resulting size of the humidified aerosol was measured by a SMPS consisting of a second DMA and a CPC. The RH was determined by measurement of the system temperature and sheath air dew point using dew point sensors. Two different H-TDMA operation modes were used [*Gysel et al.*, 2004]: During the hydration mode, the monodisperse dry particles were exposed to a well defined higher RH and experience strictly increasing RH conditions. During dehydration, the dry particles are first exposed to high RH (>95% during ~5s) and are then exposed to a lower RH (~15s) in which their final size was determined.

Resuspended dust aerosol was sampled on polycarbonate filters (Nuclepore) with 0.05μm pore size and 47 mm diameter. After collection, samples were analysed at the Laboratory of Material Behaviour of Paul Scherrer Institute using a Scanning-electron-microscope "Zeiss DSM 962". The SEM is equipped with an EDS System from Tracor Noran, the System "Voyager" with a Pioneer Detector. The electron gun has a simple tungsten filament, and the microscope can reach a resolution of 4 nm. The microscope was operated at a high voltage of 20 kV. Five sampled particles were analysed for elemental composition.

Elemental composition of ATD powder and submicron ATD aerosol was measured using inductively coupled plasma optical emission spectrometry (ICP-OES). Powder samples and dust particles collected on filters (MF-Millipore) were dissolved in HNO_3-HF-H_3BO_3-H_2O solution, heated overnight at 95°C and introduced into a VISTA-AX ICP-OES spectrometer (Varian Inc.).

The elemental composition of the particle surface was analysed with the help of X-ray Photoelectron Spectroscopy. This method is very surface sensitive due to the low escape depth of photoelectrons of a few nanometers beneath the sample surface. Resuspended particles were deposited on conductive silver fiber filters with 25 mm diameter. Several mass loadings on the filter were tested. The amount of 2-5 mg of dust per filter was found to be an

optimum in having complete coverage of the silver substrate while minimising charge build-up in the sample. XPS analysis was performed on an ESCALAB 220i XL instrument (Thermo VG Scientific). Binding energies were all referenced to the C 1s peak at 284.6 eV. In principle, the peak positions are specific for the chemical environment of each element. The samples were evacuated over night, but not heated.

The water soluble fraction of mineral dust was analysed by our Wet Effluent Diffusion Denuder / Aerosol Collector system, WEDDAC [*Zellweger et al.*, 1999]. The aerosol flow first passes through the wet effluent denuder, where water soluble components of the gas phase are absorbed. The aerosol particles pass through the denuder unaffected (due to their lower diffusion coefficient) and are then trapped in a mist chamber aerosol collector system, where the particles are exposed to a high water supersaturation. Both denuder and aerosol collector effluent aqueous solutions are concentrated on ion-exchange columns for the gas and particulate phase fractions, respectively. The columns are eluted into an ion-chromatography system (DIONEX) every 30 min. This technique provides a quasi-online analysis of the anionic fraction of the resuspended aerosol and of acidic gases eventually desorbing from the aerosol surface.

4.4. Results and discussion

The output stability is an important characteristic of an aerosol generator. Some instruments require some time to reach a steady state output and may show significant variation in the output upon repeated usage. These factors could limit the instruments application for studying heterogeneous reactions in flow tubes. The dust generator was tested by continuously running it over long time periods and also with intermittent stops of the feeding belt. Fig. 4-2 shows a typical on/off test series with relatively stable output during 6 hours and satisfying recovery behaviour. When the generator dust production was switched off and on again the aerosol concentration reached the same value as before within 15 minutes. The observed variation of particle number concentration of 14% (σ_{n-1}) and the aerosol surface area (11%) is higher than that of and the particle mean geometric diameter (3%).

The particle size spectrum was measured with the SMPS system by direct sampling (without dilution) of the aerosol flow. In accord with the cut-off characteristics of the virtual impactor, particles larger than 500 nm are effectively removed. Still, the SMPS measurement has shown a small number of large particles. The tail towards larger sizes of the spectrum was observed to be unresolved due to a limit of the SMPS sizing over 800 nm. To backup the SMPS measurement the optical particle counter (OPC) was used for particles larger than 300nm. The aerosol flow from the generator was diluted with particle free air by a factor of about 15 to decrease the particle concentration to $3.4 \cdot 10^4$ cm^{-3} to avoid exceeding the counting limit of the OPC. The measured aerosol size spectrum from both methods is shown in Fig. 4-3. It should be mentioned that the methods provide different size characteristics: optical particle diameter (OPC) and mobility diameter (SMPS). The relation between these parameters depends on particle geometrical shape and refraction index. The OPC was calibrated with the help of PSL spheres. The shape of mineral dust particles is obviously different from PSL spheres, while their refractive index (e.g., SiO_2:1.49, Al_2O_3: 1.77) might be comparable to that of PSL (1.59).

We observed that both techniques show a good agreement, at least within the logarithmic plot of Fig. 4-3 in the overlapping size range of 300-800 nm with a slight overestimation for the larger particle sizes by the SMPS system. Another study [*Stolzenburg et al.*, 1998] has also shown a good agreement of the optical and mobility diameters, though for very different kind of ambient and laboratory-generated aerosol particles. For the purpose

here, the most important result is that the OPC data show that the particle size distribution does not exhibit another mode, and drops rapidly with increasing particle diameter.

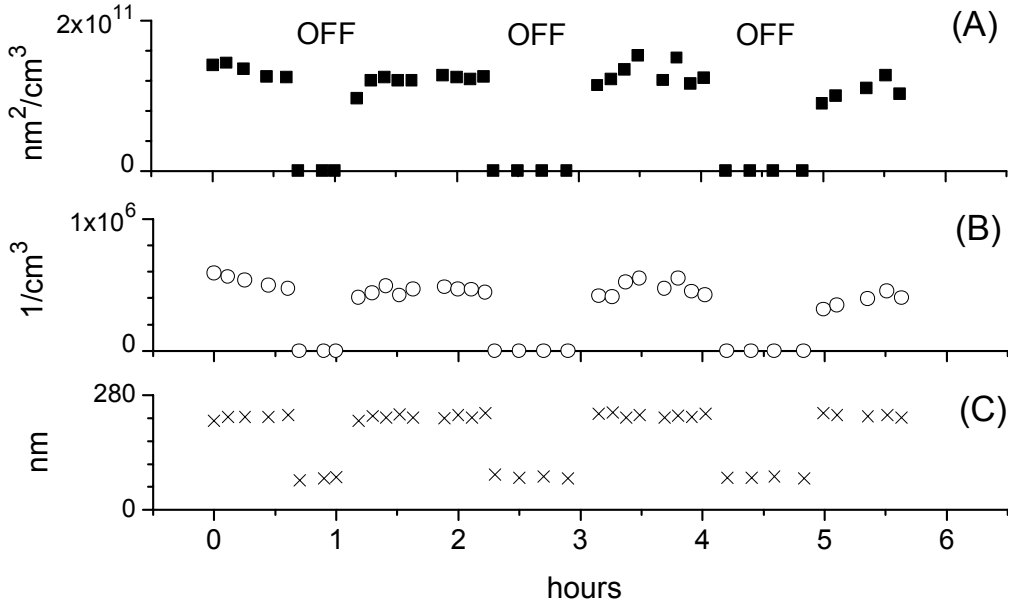

Fig. 4-2. Production stability and switch on/off test. Solid squares represent total aerosol surface area (panel A). Open circles represent particle number concentration (panel B). Crosses represent the particle mean geometric diameter (panel C). The labels "OFF" indicate the time intervals when the generator feeding belt was stopped.

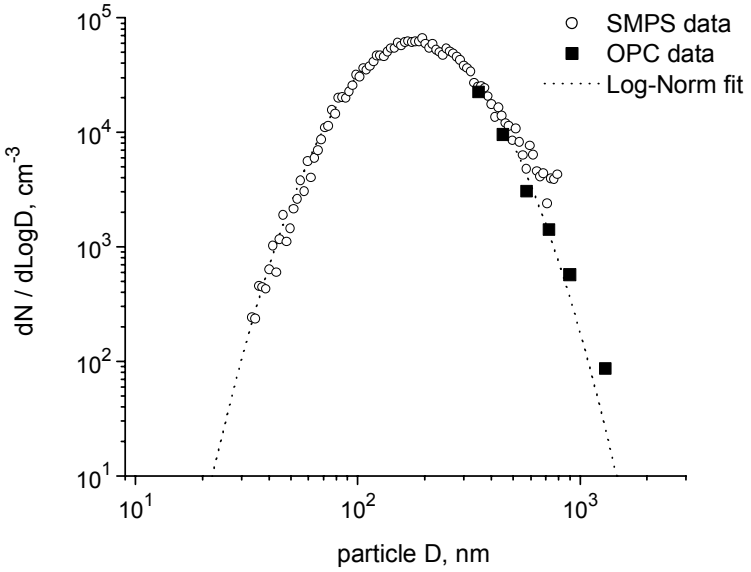

Fig. 4-3. Typical particle number size distribution measured by the SMPS system (open circles) and by the optical particle counter (solid squares). Measured data are fitted by a log-normal function (dashed line).

The observed size spectrum was fitted with a log-normal distribution by varying the geometric mean diameter D_g and the geometric standard deviation σ_g. Then, the other statistical parameters of the spectrum were calculated with the help of the Hatch-Choate equations for lognormal distributions of spherical particles [*Cooper*, 2001]. The log-normal fit function is

calculated for the combined data-set measured by SMPS and OPC. Table 4.2 shows the results in comparison with the parameters calculated by the SMPS software and based on SMPS data only.

Table 4-2. Spectral statistics of the resuspended mineral dust aerosol. All particle diameters are given in nanometers, aerosol surface area in nm^2/cm^3

	Lognormal fit	SMPS data
Measurement method	SMPS+OPC	SMPS
Dg	180	185
Dmean	204	212
Dmode	140	195
Dmedian	180	184
σg	1.65	1.74
Surface area	$6.40 \cdot 10^9$	$5.22 \cdot 10^9$

The total particle surface area was calculated using the log-normal fit function for the number size distribution and assuming spherical shape of the particles. This parameter was compared to the value given by the SMPS software, which assumes the same particle shape. The SMPS software shows a value smaller by about 25% (Table 4-2). It means that the sole use of the SMPS system would lead to a systematic 25% underestimation of particle surface area measurement due to the upper size limit of the SMPS system.

The dust generator output is controlled primarily by the speed of the conveyer belt (Fig. 4-4). Increasing the belt speed obviously provides more powder to the nozzle, which leads to higher concentrations of resuspended aerosol. The size of the resuspended particles (D_g) does not change because the separation devices remove the large particles, and the conditions at the nozzle do not change. Originally (by the manufacturer) the generator was designed for high mass output that could be achieved by providing large amounts of powder by the belt to the nozzle. In contrast, our purpose was to produce submicron mineral dust, which was achieved by varing the belt speed the range 1-15% of maximum speed. Increasing the belt speed further did not lead to accordingly higher concentrations of submicron particles, but rather to higher concentrations of large particles that are removed.

Hence, the combination of cyclone and virtual impactor proved to be a good choice for the size separation, the resuspended dust particles is in the designated submicron range. The production of mineral dust is stable with a sufficiently adjustable output.

The electrical properties of the resuspended dust aerosol were studied using the electrical precipitator and the neutralizer containing radioactive Kr-85. The aerosol flow was drawn through the electrical precipitator to the condensation particle counter (CPC), which measures the particle number concentration. When the voltage is not applied to the precipitator, the CPC measures the total particle concentration (charged and neutral). The concentration of only neutral particles was measured by passing the aerosol flow through the precipitator with the voltage applied. The measurements revealed that the resuspended aerosol leaving the nozzle and separation stages turned out to be highly charged. This is in accord with the study of [*Forsyth et al.*, 1998] reporting a high charge level of Arizona road dust dispersed by a fluidised bed dust generator. Similar to that study, we used a Kr-85 source (source 1 on Fig. 4-1) to neutralize the resuspended dust aerosol.

Passing the aerosol flow through the neutralizer decreased the concentration by about 40%, possibly due to losses inside the neutralizer and tubing. Using the measured aerosol size distribution and the symmetric Boltzman distribution of charges for aerosol particles [*Flagan*, 2001], we calculated that after passing through the radioactive source the aerosol should contain 31% of neutral particles. The experimentally measured value was 22% which means that neutralization was not efficient enough (probably due to the low residence time of 5s within the neutralizer), to completely reach ideal Boltzman equilibrium distribution charges.

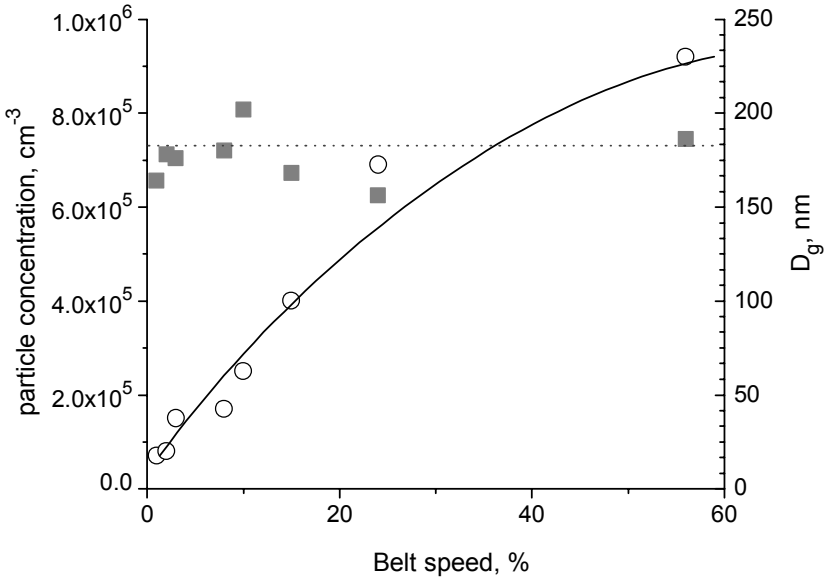

Fig. 4-4 Mineral dust generator output. Open circles present the particle number concentration, solid squares present the geometric mean particle diameter.

For the purpose of the present setup to provide a stable flow of a sufficient amount of neutral particles, it was not crucial to achieve an ideal equilibrium charge distribution, and therefore no further investigation was performed into this.

The hygroscopic properties of the submicron ATD particles were studied with the HTDMA. Experiments were performed at four different particle sizes, with dry mobility diameter D_0 = 55, 100, 250 and 400 nm, respectively. The measured humidograms at D_0 = 100 and 250 nm are shown in Fig. 4.5. The results obtained for particles with D_0 = 55 nm are not shown since they behaved very similar to those with D_0 = 100 nm, i.e. they also experienced a small hygroscopic growth of about 1% at RH = 90%. For the two larger sizes (D_0 = 250 and 400 nm) a different hygroscopic behavior was observed: During hydration, no water uptake (growth factor = 1.00) was measured up to 90 %RH. At RH > 90%, a distinct decrease of 1% in the hygroscopic growth factor was encountered. These points fit to the measurement performed in the dehydration mode. This diameter change is interpreted as a small restructuring of the larger agglomerates of dust to particles of smaller mobility diameter, under the influence of water vapor. Such a phenomenon was earlier also observed for soot particles [*Saathoff et al.*, 2003; *Weingartner et al.*, 1997]. The shrinking, which was more pronounced in the case of soot, was explained by capillary condensation in small angle cavities of aggregates. Capillary forces induced on any asymmetric part of the particles caused them to attain a more compact structure. In contrast, ATD particles smaller than 100-200 nm are not agglomerates and already substantially round, which can be seen in SEM images (Fig. 4-6). These particles do not undergo restructuring once exposed to RH above 90%.

Overall, the observed hygroscopic growth of the ATD particles is very small, as compared to aerosols composed of soluble salts. An evident explanation for such a behavior is the very small amount of soluble material associated with ATD mineral dust (see also below). Similar non-hygroscopic behavior of mineral dust particles was previously reported by [*Li-Jones et al.*, 1998; *Twomey*, 1977] measured the hygroscopic properties of African dust in the marine boundary layer using an integrating nephelometer. Their data also suggest that Saharan dust particles are essentially non-hygroscopic. Weingartner et al (2001) also found that during a Saharan dust event on a high alpine site 250 nm sized dust particles experience no hygroscopic growth. Note that processing of mineral dust with atmospheric trace gases

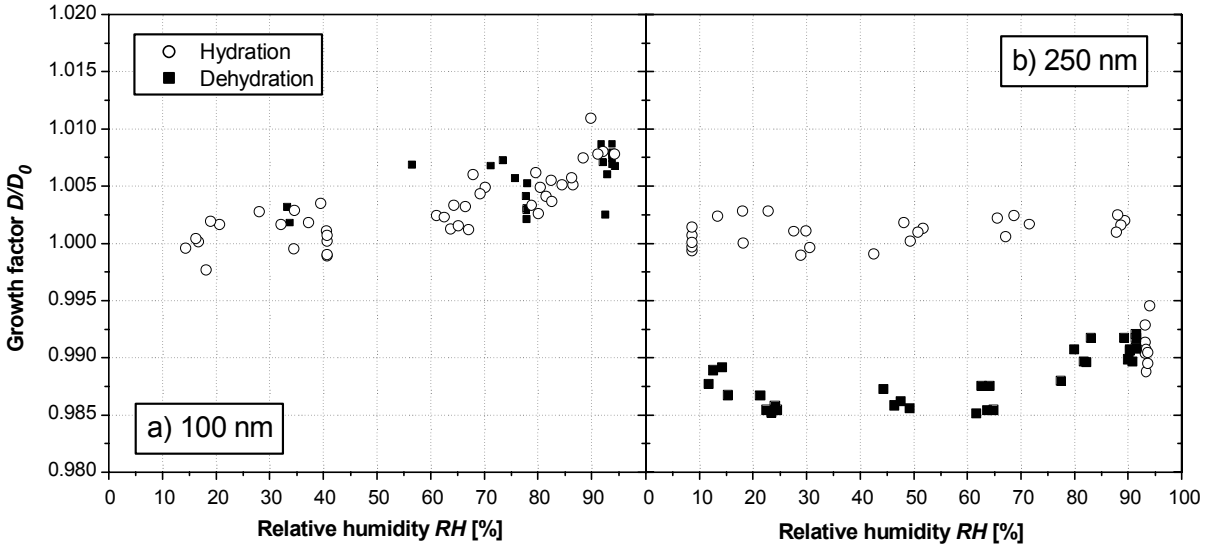

Fig. 4-5. Growth factors of D_0=100 and 250 nm ATD particles as a function of RH at 20°C. D_0 is the mobility size of monodisperse particles at the lowest RH. Hydration curve relates to the process when the dry particles are exposed to a well defined higher RH and experience strictly increasing RH conditions. Dehydration curve relates to the process when the dry particles are first exposed to high RH (>95%) and are then exposed to a lower RH in which their final size was determined.

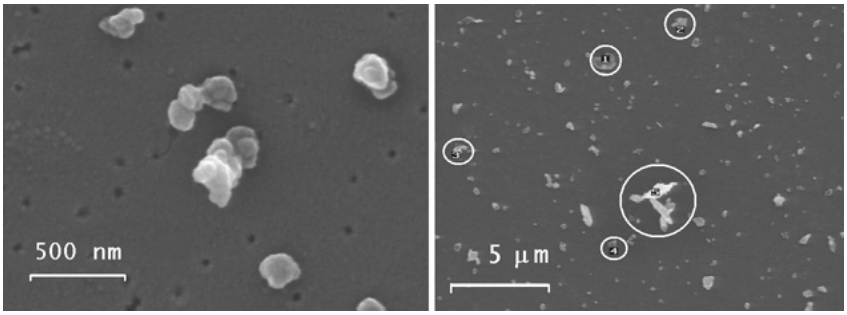

Fig. 4-6. Electron microscope images showing some of the mineral dust particles sampled. Size and shape distributions from this individual image is not representative of the dust aerosol as a whole. Particles marked with circles were analysed by EDX for the following crustal elements: Si, Al, Na, Mg, K and Fe.

could also substantially change this picture, when barely soluble mineral components are converted into very soluble products [*Krueger et al.*, 2003; *Laskin et al.*, 2005].

ATD mineral dust morphology was studied using scanning electron microscopy. Fig. 4-6 displays images of dust particles resuspended by the setup described above and deposited on a filter. It shows a heterogeneous mix of particles of different size and irregular shape. Some particles look like agglomerates either from incomplete disintegration during resuspension, or aggregation during sampling. Other particles (smaller than 200 nm) seem to be more compact, rather representing the primary mineral particles. The pictures somewhat overemphasizes the larger particles. On average, the pictures were consistent with the size distribution measured with the SMPS, with a mode at about 200 nm. A quantitative comparison of submicron aerosol composition with that of the original powder was obtained from ICP-OES measurements shown in Table 4-3. The notable difference between the two is the apparent depletion in the silica content in submicron particles. Several authors [*Gomes et al.*, 1990; *Reid et al.*, 2003] have shown that dust silica is mainly associated with coarse

particles (quartz, alumino-silicates). In line with this, in our system, Si-rich particles would be preferentially removed in the separation stages, leading to the depletion in the silica content (Table 4.3).

Table 4-3. Elemental composition of mineral dust expressed in % of atoms. * XPS data on Mg is not available because Mg anticathode was used as X-ray source.

	ATD powder ICP-OES	Particle bulk ICP-OES	Particle surface XPS
Na	2.3±0.2	2.9±0.2	2
Mg	2.1±0.2	4.7±0.2	*
Al	8.2±0.3	15.9±0.3	24
Si	79.1±1	63±1	63
K	1.7±0.2	3.1±0.2	3
Fe	2.2±0.1	4.9±0.2	3
Ca	4±0.2	4.8±0.2	5

Energy dispersive X-ray analysis (EDX) of a few particles as those shown in Fig. 4-6 was roughly consistent with the ICP-OES results (data not shown). It might be interesting to note that no substantial amount of Ca was found in the few particles analysed, while both the original powder and the average aerosol contains calcium. Obviously, the Ca containing minerals are distributed non-homogeneously among dust particles. Given the importance of calcium carbonate as a reactive component [*Fenter et al.*, 1995; *Goodman et al.*, 2000; *Hanisch and Crowley*, 2001], this reminds us that the heterogeneous reactivity of dust may be associated only with a certain particle fraction only.

XPS was employed to analyze the surface composition of a large ensemble of particles sampled into a layer a few particles thick on the silver fiber filter. A small shift in the position of the peaks (binding energy) provides information about the chemical environment of each element as the method probes the valence electrons. The analysis revealed (Table 4-3) that the samples were comparatively clean with regard to carbon contamination. Usually, samples exposed to air prior to analysis become rapidly contaminated with low volatile organic compounds resulting in the so called adventitious carbon-peak apparent with dominant intensity in all spectra [*Miller et al.*, 2002]. This peak is then usually used as reference to refer the kinetic energies of the other peaks to. In our samples, the intensity was surprisingly low, e.g. as compared to the blank filter substrate or as compared to other samples routinely used in the same apparatus. The ATD powder was exposed to air prior to introduction into the SAG. After sampling, the filters were stored in Ar until analysis. We therefore believe that most surfaces of our submicron aerosol have not been exposed to air before disaggregation. In addition, the XPS data indicated that calcium was present on the surface in the form of carbonate (based on the binding energy) rather than phosphate or nitrate. Comparison of the elemental composition suggests enrichment of Al at the surface.

Table 4-4. Mass concentration (in $\mu g \cdot m^{-3}$) of identified compounds in water-soluble fraction of mineral dust aerosol generated from ATD. Concentrations of acetate and formate are smaller than the detection limit of the method.

Compound	Concentration
Fluoride	0.1±0.05
Acetate	< 0.3
Formate	< 0.5
Chloride	0.7±0.1
Nitrate	0.2±0.1
Sulphate	41±0.5
Phosphate	3±0.3

The water soluble composition of mineral dust aerosol was measured by the Wet Effluent Diffusion Denuder system with anion chromatography detection. The mass concentrations measured are given in Table 4-4. Sulphate was the major anion, which is similar to the finding of [*Falkovich et al.*, 2001] in the dusts from the Sahara. In addition, Cl^-, PO_4^{3-}, small amounts of NO_3^- and fluoride anions were detected. Concentrations of the organic anions formate and acetate were small, and the corresponding chromatogram peaks were the same as in blank samples. Phosphate components of mineral dust are less soluble than others. The non-soluble components were retained in pre-filters in front of the preconcentrator columns. After switching off the aerosol production the concentration of phosphate was decreasing exponentially with time while other anions were washed out immediately. This behavior is similar to the dissolution of Sahara dust samples reported by [*Desboeufs et al.*, 1999]. Other water soluble components of the dust aerosol are extracted efficiently since the concentrations of anions scale linearly with the mineral dust mass aerosol concentration.

If we assume equal concentrations of cations and anions, then the water soluble fraction comprises only about 2% of the resuspended dust (by mass). Such a low water solubility of dust particles observed in our experiments is consistent with the non-hygroscopic behavior described earlier (Fig. 4-5). Note that also with regard to the water soluble components, the situation may dramatically change upon atmospheric processing.

4.5. Conclusions

A commercially available dust disperser has been modified and extended by size separating devices to produce a submicron aerosol prepared for heterogeneous chemical reaction studies. The adjustable output of the system is relatively constant with respect to aerosol number, surface and mass concentration. Submicron particles are produced with a log-normal shape of the size distribution. The system was used to produce and analyze aerosol from Arizona Test Dust, a widely used standard material representative of desert dust. Particle elemental composition is found to be similar for the particle surface and bulk, and in agreement with expectations from the size fractionated composition of the original powder. Resuspended dust particles show nonhygroscopic behaviour in a humid environment due to the low amount of soluble material associated with unprocessed dust particles. Interestingly, particles larger than 100-200 nm shrank about 1% (in mobility diameter) once exposed to RH > 90%. This was interpreted as a restructuring of the larger agglomerates of dust to the particles of smaller mobility diameter, under the influence of water vapor. The system described in this study, together with the chemical characterization employed, is ideal to provide atmospherically relevant mineral dust aerosols (from various authentic or chemically well-defined dust powder sources) for heterogeneous reaction studies in flow reactors.

Acknowledgements

Valuable technical support was provided by Mario Birrer. We thank R. Brütsch for the SEM, S. Köchli for the ICP-OES and Dr. B. Schnyder for the XPS measurements.

References

Ammann, M., Kalberer, K., Jost, D.T., Tobler, L., Rössler, E., Piguet, D., Gäggeler, H.W., and Baltensperger, U.: Heterogeneous production of nitrous acid on soot in polluted air masses, Nature, 395, 157 - 160, 1998.

Bauer, S.E., Balkanski, Y., Schulz, M., Hauglustaine, D.A., and Dentener, F.: Global modeling of heterogeneous chemistry on mineral aerosol surfaces: Influence on tropospheric ozone chemistry and comparison to observations, J. Geophys. Res.-Atmos., 109, doi:10.1029/2003JD003868, 2004.

Bian, H.S., and Zender, C.S.: Mineral dust and global tropospheric chemistry: Relative roles of photolysis and heterogeneous uptake, J. Geophys. Res.-Atmos., 108, doi:10.1029/2002JD003143, 2003.
Blackford, D.B., and Rubow, K.L.: A small-scale powder disperser, TIZ-Fachberichte, 110, 645-655, 1986.
Buonicore, A.J., and Davis, W.T., Air Pollution Engineering Manual, pp. 912, Air & Waste Management Association, Van Nostrand Reinhold, Pittsburgh, New York, 1992.
Cantrell, W., and Heymsfield, A.: Production of ice in tropospheric clouds - A review, Bull. Amer. Meteorol. Soc., 86, 795–807, 2005.
Cooper, D.W., Methods of Size Distribution Data Analysis and Presentation, in Aerosol measurement: Principles, Techniques, and Applications, edited by P.A. Baron, and K. Willeke, pp. 667-701, Wiley-InterScience. Inc., New York, 2001.
DeMott, P.J., Sassen, K., Poellot, M.R., Baumgardner, D., Rogers, D.C., Brooks, S.D., Prenni, A.J., and Kreidenweis, S.M.: African dust aerosols as atmospheric ice nuclei, Geophys. Res. Lett., 30, doi:10.1029/2003GL017410, 2003.
Desboeufs, K.V., Losno, R., Vimeux, F., and Cholbi, S.: The pH-dependent dissolution of wind-transported Saharan dust, J. Geophys. Res.-Atmos., 104, 21287-21299, 1999.
Falkovich, A.H., Ganor, E., Levin, Z., Formenti, P., and Rudich, Y.: Chemical and mineralogical analysis of individual mineral dust particles, J. Geophys. Res.-Atmos., 106, 18029-18036, 2001.
Fenter, F.F., Caloz, F., and Rossi, M.J.: Experimental-Evidence for the Efficient Dry Deposition of Nitric-Acid on Calcite, Atmos. Environ., 29, 3365-3372, 1995.
Flagan, R.C., Electrical Techniques, in Aerosol measurement: Principles, Techniques, and Applications, edited by P.A. Baron, and K. Willeke, pp. 537-568, Wiley-InterScience. Inc., New York, 2001.
Forsyth, B., Liu, B.Y.H., and Romay, F.J.: Particle charge distribution measurement for commonly generated laboratory aerosols, Aerosol Sci. Technol., 28, 489-501, 1998.
Fuchs, N.A., and Sutugin, A.G., Highly dispersed aerosols, 105 pp., Ann Arbor Science Publishers, Ann Arbor, 1970.
Gomes, L., Bergametti, G., Coudegaussen, G., and Rognon, P.: Submicron Desert Dusts - a Sandblasting Process, J. Geophys. Res.-Atmos., 95, 13927-13935, 1990.
Goodman, A.L., Underwood, G.M., and Grassian, V.H.: A laboratory study of the heterogeneous reaction of nitric acid on calcium carbonate particles, J. Geophys. Res.-Atmos., 105, 29053-29064, 2000.
Guimbaud, C., Arens, F., Gutzwiller, L., Gäggeler, H.W., and Ammann, M.: Uptake of HNO3 to deliquescent sea-salt particles: a study using the short-lived radioactive isotope tracer N-13, Atmos. Chem. Phys., 2, 249-257, 2002.
Gysel, M., Weingartner, E., Nyeki, S., Paulsen, D., Baltensperger, U., Galambos, I., and Kiss, G.: Hygroscopic properties of water-soluble matter and humic-like organics in atmospheric fine aerosol, Atmos. Chem. Phys., 4, 35-50, 2004.
Hanisch, F., and Crowley, J.N.: Heterogeneous reactivity of gaseous nitric acid on Al_2O_3, $CaCO_3$, and atmospheric dust samples: A Knudsen cell study, J. Phys. Chem. A, 105, 3096-3106, 2001.
Krueger, B.J., Grassian, V.H., Laskin, A., and Cowin, J.P.: The transformation of solid atmospheric particles into liquid droplets through heterogeneous chemistry: Laboratory insights into the processing of calcium containing mineral dust aerosol in the troposphere, Geophys. Res. Lett., 30, doi:10.1029/2002GL016563, 2003.
Kulmala, M., and Wagner, P.E.: Mass accommodation and uptake coefficients - a quantitative comparison, J. Aerosol Sci., 32, 833-841, 2001.
Laskin, A., Wietsma, T.W., Krueger, B.J., and Grassian, V.H.: Heterogeneous chemistry of individual mineral dust particles with nitric acid: A combined CCSEM/EDX, ESEM, and ICP-MS study, J. Geopyhs. Res., 110, doi:10.1029/2004JD005206, 2005.
Li-Jones, X., Maring, H.B., and Prospero, J.M.: Effect of relative humidity on light scattering by mineral dust aerosol as measured in the marine boundary layer over the tropical Atlantic Ocean, J. Geophys. Res.-Atmos., 103, 31113-31121, 1998.

Liao, H., and Seinfeld, J.H.: Global impacts of gas-phase chemistry-aerosol interactions on direct radiative forcing by anthropogenic aerosols and ozone, J. Geophys. Res.-Atmos., 110, doi:10.1029/2005JD005907, 2005.
Mamane, Y., and Gottlieb, J.: Nitrate Formation on Sea-Salt and Mineral Particles - a Single-Particle Approach, Atmos. Environ., 26, 1763-1769, 1992.
Marple, V.A., Liu, B.Y.H., and Rubow, K.L.: Dust Generator for Laboratory Use, Am. Ind. Hyg. Assoc. J., 39, 26-32, 1978.
Marple, V.A., Rubow, K.L., and Olson, B.A.: Diesel Exhaust Mine Dust Virtual Impactor Personal Aerosol Sampler - Design, Calibration and Field-Evaluation, Aerosol Sci. Technol., 22, 140-150, 1995.
Miller, D.J., Biesinger, M.C., and McIntyre, N.S.: Interactions of CO_2 and CO at fractional atmosphere pressures with iron and iron oxide surfaces: one possible mechanism for surface contamination, Surf. Interface Anal., 33, 299-305, 2002.
Mozurkewich, M., McMurry, P.H., Gupta, A., and Calvert, J.G.: Mass accommodation coefficient for HO_2 radicals on aqueous particles, J. Geophys. Res., 92, 4163-4170, 1987.
Penner, J.E., Andreae, M., Annegarn, H., Barrie, L., Feichter, J., Hegg, D., Jayaraman, A., Leaitch, R., Murphy, D., Nganga, J., and Pitari, G., Aerosols, their direct and indirect effects, in Climate Change 2001: The Scientific Basis. Contribution of Working Group I to the Assessment Report of the Intergovernmental Panel on Climate Change, edited by J.T. Houghton, Y. Ding, D.J. Griggs, M. Noguer, P.J. van der Linden, X. Dai, K. Maskell, and C.A. Johnson, pp. 291-348, Cambridge University Press, Cambridge, United Kingdom and New York, USA, 2001.
Putaud, J.P., van Dingenen, R., Dell'Acqua, A., Raes, F., Matta, E., Decesari, S., Facchini, M.C., and Fuzzi, S.: Size-segregated aerosol mass closure and chemical composition in Monte Cimone (I) during MINATROC, Atmos. Chem. Phys., 889-902, 2004.
Ramaswamy, V., Boucher, O., Haigh, J., Hauglustaine, D.A., Haywood, J., Myhre, G., Nakajima, T., Shi, G.Y., and Solomon, S., Radiative Forcing of Climate Change, in Climate Change 2001: The Scientific Basis. Contribution of Working Group I to the Assessment Report of the Intergovernmental Panel on Climate Change, edited by J.T. Houghton, Y. Ding, D.J. Griggs, M. Noguer, P.J. van der Linden, X. Dai, K. Maskell, and C.A. Johnson, pp. 351-416, Cambridge University Press, Cambridge, United Kingdom and New York, USA, 2001.
Reid, E.A., Reid, J.S., Meier, M.M., Dunlap, M.R., Cliff, S.S., Broumas, A., Perry, K., and Maring, H.: Characterization of African dust transported to Puerto Rico by individual particle and size segregated bulk analysis, J. Geophys. Res.-Atmos., 108, doi:10.1029/2002JD002935, 2003.
Saathoff, H., Naumann, K.H., Schnaiter, M., Schock, W., Mohler, O., Schurath, U., Weingartner, E., Gysel, M., and Baltensperger, U.: Coating of soot and $(NH_4)_2SO_4$ particles by ozonolysis products of alpha-pinene, J. Aerosol. Sci., 34, 1297-1321, 2003.
Sassen, K., DeMott, P.J., Prospero, J.M., and Poellot, M.R.: Saharan dust storms and indirect aerosol effects on clouds: CRYSTAL-FACE results, Geophys. Res. Lett., 30, doi:10.1029/2003GL017371, 2003.
Stolzenburg, M., Kreisberg, N., and Hering, S.: Atmospheric size distributions measured by differential mobility optical particle size spectrometry, Aerosol Sci. Technol., 29, 402-418, 1998.
Twomey, S., Atmospheric aerosols, 302 pp., Elsevier, Amsterdam, 1977.
Underwood, G.M., Song, C.H., Phadnis, M., Carmichael, G.R., and Grassian, V.H.: Heterogeneous reactions of NO_2 and HNO_3 on oxides and mineral dust: A combined laboratory and modeling study, J. Geophys. Res.-Atmos., 106, 18055-18066, 2001.
Weingartner, E., Gysel, M., and Baltensperger, U.: Hygroscopicity of aerosol particles at low temperatures. 1. New low-temperature H-TDMA instrument: Setup and first applications, Environ. Sci. Technol., 36, 55-62, 2002.
Weingartner, E., Henning, S., Gysel, M., Bukowiecki, N., and Baltensperger, U.: Hygroscopicity of aerosol particles at low temperatures, J. Aerosol Sci., S977-S978, 2001.
Weingartner, E., Keller, C., Stahel, W.A., Burtscher, H., and Baltensperger, U.: Aerosol emission in a road tunnel, Atmos. Environ., 31, 451-462, 1997.

5. Effect of humidity on nitric acid uptake on mineral dust aerosol particles

This chapter is a paper to which the author of this dissertation contributed and appears as a co–author. The author contributed to the construction of the processing chamber for the mineral dust and with hygroscopicity measurements of the HNO_3 processed mineral dust, as well as assistance during the manuscript writing process. Published in Atmospheric Chemistry and Physics, vol. 6, p. 2147-2160, 2006.

A. Vlasenko[1,2,] S. Sjogren[3], E. Weingartner[3], K. Stemmler[1], H. W. Gäggeler[1,2], M. Ammann[1]

[1]Laboratory of Radio- and Environmental Chemistry, Paul Scherrer Institute, Villigen PSI CH-5232, Switzerland

[2]Department for Chemistry and Biochemistry, University of Berne, Bern CH-3008, Switzerland

[3]Laboratory of Atmospheric Chemistry, Paul Scherrer Institute, Villigen PSI CH-5232, Switzerland

5.1. Abstract

This study presents the first laboratory observation of HNO_3 uptake by airborne mineral dust particles. The model aerosols were generated by dry dispersion of Arizona Test Dust (ATD), SiO_2, and by nebulizing a saturated solution of calcium carbonate. The uptake of ^{13}N-labelled gaseous nitric acid was observed in a flow reactor on the 0.2-2 s reaction time scale at room temperature and atmospheric pressure. The amount of reacted nitric acid was found to be a linear function of aerosol surface area. SiO_2 particles did not show any significant uptake, while the $CaCO_3$ aerosol was found to be more reactive than the ATD. Due to the smaller uncertainty associated with the reactive surface area in the case of suspended particles as compared to bulk powder samples, we believe that we provide an improved estimate of the uptake kinetics of HNO_3 to mineral dust. The uptake coefficient averaged over the first 2s of reaction time at a concentration of 10^{12} molecules cm^{-3} was found to increase with increasing relative humidity, from 0.022±0.007 at 12% RH to 0.113±0.017 at 73% RH , scaling along a water adsorption isotherm. The processing of the dust at 85% RH leads to a water soluble coating on the particles and enhances their hygroscopicity.

5.2. Introduction

Heterogeneous interactions between atmospheric trace gases and aerosols are important in several issues of atmospheric chemistry. The processing of atmospheric particles might affect the chemical and physical properties of the aerosol; on the other hand, it may also impact the global budget of important trace gas compounds. Among the many potential reactions occurring, the reaction of mineral dust aerosol with HNO_3 might be very important as it affects the ozone budget of the upper troposphere, because there the photolysis of HNO_3 is a significant source of NO and NO_2, to which ozone sensitively responds [*Bauer et al.*, 2004; *Bian and Zender*, 2003; *Dentener et al.*, 1996].

The heterogeneous reactions of mineral dust particles are also of significant interest because they could change the particle surface properties, which can therefore affect the properties of dust as cloud condensation or ice nuclei. The importance of this issue on a global scale has been demonstrated by several modelling studies [*Kärcher and Lohmann*, 2003; *Lohmann et al.*, 2004]. Laskin et al (2005) reported field evidence of complete, irreversible processing of particles containing solid calcium carbonate and quantitative formation of liquid calcium nitrate particles, apparently as a result of the heterogeneous reaction of calcium carbonate with gaseous nitric acid. Such conversion of insoluble material to soluble material strongly affects the radiative properties of these aerosol particles as well as their ability to act as cloud condensation nuclei. Recent ambient studies have shown the ability of Saharan dust aerosol particles to form ice crystals in cirrus clouds [*DeMott et al.*, 2003; *Sassen et al.*, 2003]. Currently, the question to what degree processing of dust particles by trace gases affects heterogeneous ice nucleation is subject of laboratory and field investigations [*Archuleta et al.*, 2005].

Mineral dust is a complicated mixture of different minerals, and its reactivity with trace gases obviously depends on the composition. To understand the mechanism of the heterogeneous interaction with dust one could study the reactions with each of the components. However, the reactive behaviour of complex mixtures is not only a superposition of the behaviour of their individual components. In addition, in practice it would be a hard task to complete due to the complexity of the dust composition. Therefore, in the case of HNO_3, many studies have concentrated on identifying the most reactive components, among which is $CaCO_3$, and assessing their reactivity. [*Fenter et al.*, 1995; *Goodman et al.*, 2001; *Hanisch and Crowley*, 2001; *Krueger et al.*, 2004]. In the present work, the heterogeneous reactivity of $CaCO_3$ and SiO_2 has been compared to the reactivity of the Arizona Test Dust (ATD) aerosol particles. These components are chosen since quartz is one of the major (by weight) constituent of the dust in general and in the ATD in particular; and calcite is suggested to be one of the most reactive constituents of the dust [*Usher et al.*, 2003]. While many other studies focussed on Ca rich authentic dusts, ATD used in the present study is among the Ca poorer, though not less abundant forms of dust.

In this study, a dry dispersion generation method was used to produce submicron mineral dust aerosol and to measure the kinetics of the heterogeneous reaction with gaseous nitric acid with the aerosol particles in gas suspension. To our knowledge it is the first time that such a method was used for the production of a surrogate for atmospheric mineral dust in combination with a kinetic flow-tube technique. This approach is an alternative to the published studies of heterogeneous interactions in a Knudsen cell or with single particle techniques.

This study concentrates on basic uptake data and its dependence on relative humidity as well as the consequences on the hygroscopic properties of the dust particles. Ongoing, more detailed kinetic experiments will be reported elsewhere.

5.3. Experimental

The experimental method used is similar to the ones reported previously [*Ammann*, 2001; *Guimbaud et al.*, 2002]. Nitric acid labelled with a short-lived radioactive isotope ^{13}N is mixed with the aerosol particles in a flow reactor. After a certain reaction time, gas phase and particulate phase products are separated and trapped in a parallel-plate denuder and in a filter, respectively. The concentration of each species is measured by counting the number of ^{13}N decays in each trap per unit time. In this way, the loss of nitric acid from the gas phase and its irreversible uptake by the aerosol particle surface are measured simultaneously. The scheme of the setup is given in Fig. 5-1. Apart from the kinetic experiments, ATD aerosol particles were also processed by gaseous HNO_3 in a larger reactor. Hygroscopic properties of dust particles were studied before and after HNO_3 exposure using a HTDMA system described below.

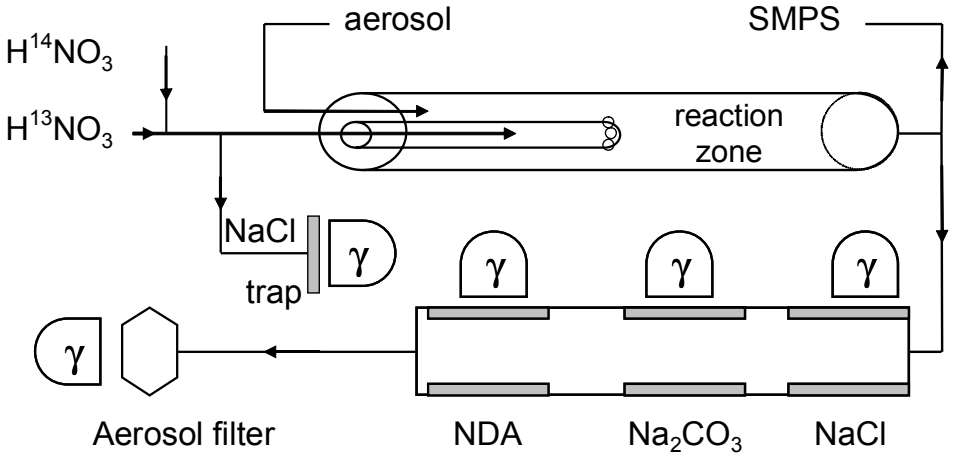

Fig. 5-1. Schematic diagram of the flow reactor and detection system.

Production of HNO_3

The production of ^{13}N in the form of ^{13}NO has been described in detail elsewhere [*Ammann*, 2001]. In brief, the ^{13}N isotope is produced via the reaction $^{16}O(p, \alpha)^{13}N$ in a gas-target, which is set up as a flow cell, through which 20% O_2 in He pass at 1l /min stp at 2.5 atm, and which is continuously irradiated by 15 MeV protons provided by the accelerator facilities at Paul Scherrer Institute. The primary ^{13}N molecules and radicals are reduced to ^{13}N labelled NO over a TiC catalyst immediately after the target cell. The resulting gas is continuously transported to the laboratory through a 580 m capillary. There, a small fraction of this flow (typically 25 ml/min) is mixed with nitrogen as carrier gas (1 lpm) in our experiments. Additional amounts of non-labelled NO can be added from a certified cylinder (10 ppm in N_2) to vary the total concentration of NO within a range of 1 ppb to 1 ppm. NO is oxidized to NO_2 by reaction with ozone in a flow reactor with a volume of 2 liters. Ozone is generated by passing a mixture of synthetic air in nitrogen through a quartz tube irradiated by a mercury penray UV lamp (185 nm wavelength). HNO_3 is produced from the reaction of NO_2 with OH radicals; the flow containing NO_2 is humidified to 40% relative humidity and irradiated by a second 172 nm excimer UV lamp to produce OH radicals, which rapidly convert a large fraction of NO_2 to HNO_3 (see results section).

Aerosol particle generation

In this study, two types of aerosol generation methods were employed: dry dispersion from a powder and atomisation of an aqueous solution. The dispersion of Arizona Test Dust and detailed characterisation of the resulting aerosol is published elsewhere [*Vlasenko et al.*, 2005]. Here only a short description of the technique is given. In a first step, the sample powder is dispersed by a solid aerosol generator (Topas GmbH, Dresden, Germany). Therein, a special belt feeds the dust to an injector nozzle in order to provide a constant input. Shear forces created in the injector disperse and disaggregate the powder to form submicron particles. In a second step, the remaining coarse particles are removed by a cyclone and a virtual impactor. This method is used to produce submicron particles from Arizona Test Dust (Ellis Components, England) and silica (Aerosil 200, Degussa, Germany). Calcium carbonate aerosol was generated by nebulizing a saturated aqueous $CaCO_3$ solution (Model 3075, TSI, USA). The resulting droplets are dried by passing the flow through a diffusion dryer. Charged particles from both aerosol sources are removed by passing the flow through an electrical precipitator. Finally, the aerosol flow is conditioned to a certain relative humidity. The humidifier is a vertically mounted tube with a H_2O permeable Goretex membrane (150 mm length, 6 mm i.d.) immersed in demineralised water. The relative humidity was measured by capacitance detectors at room temperature. The aerosol number concentration, size distribution and total aerosol surface area are controlled by a Scanning Mobility Particle Sizer (SMPS, TSI, USA). The size spectra of the aerosols obtained are given in Fig. 5-2. One can see that the particle concentration was largest for silica aerosol and lowest for the calcium carbonate particles.

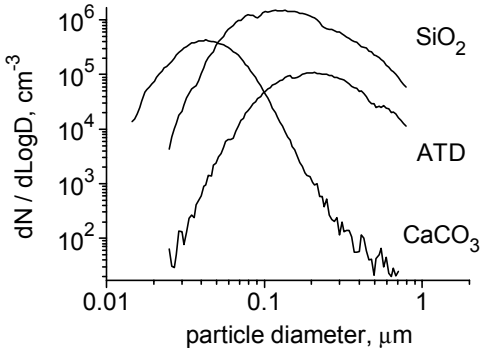

Fig. 5-2. Size distribution of aerosol particles used to study the heterogeneous reaction with gaseous nitric acid.

Flow reactor for kinetic experiments

Mineral dust aerosol and nitric acid flows are mixed to react in the flow tube reactor with cylindrical geometry. The reactor is a PFA Teflon tube of 8 mm inner diameter and 10 mm outer diameter. The PFA Teflon material has been chosen to minimise the losses and retention of HNO_3 on the surface [*Neuman et al.*, 1999]. Gaseous nitric acid is introduced via an injector along the axis of the flow reactor. The injector is a PFA tube (i.d. 4mm), which could be moved along the axis of the reactor. The position of the injector determines the gas-aerosol contact or reaction time. When the injector is pushed all the way in to the maximum position inside the flow reactor then the reaction time is minimum (0.2 s) and vice versa (2 s). The end of the injector tube is supplied with a special plug so that the gas enters the flow reactor through small openings at the end of the injector, perpendicular to the flow of aerosol. This is used to facilitate rapid mixing of the flows, which is critical for exactly controlling the reaction time. The degree of mixing was checked by measurement of the aerosol particle concentration upstream and downstream of the injection point by extracting a small flow with a small capillary pushed in from the opposite end of the reactor. The particle concentration

was decreased immediately after the mixing with the gas flow in accord with the dilution factor of the corresponding volumetric flows. The flow tube is operated under laminar flow conditions, and it is assumed that the laminar flow profile is established a few cm downstream of the injector. The outer flow tube is replaced after each 6 hours of operation to avoid wall losses of HNO_3 driven by the particles deposited on the inner wall. The system is kept at room temperature. The relative humidity of the flow is continuously measured downstream of the reactor.

Detection system

The flow leaving the flow reactor was directly entering the parallel-plate denuder system. The latter captures the gaseous species HNO_3, HONO, NO_2 on different chemically selective coatings by lateral diffusion. Note that this denuder train also effectively scrubs HNO_3 reversibly adsorbed to the particles. The sub-micron aerosol particles have a small diffusivity and pass through the denuder without being collected. Gaseous nitric acid is taken up in the first denuder section coated with NaCl. HONO is collected in the next section coated with Na_2CO_3, while NO_2 is absorbed in the third section by reaction with NDA (N-(1-naphtyl) ethylene diamine dihydrochloride) mixed with KOH. These coatings are freshly prepared after each 6 hours of operation. Generation of HNO_3 by reaction of NO_2 with OH is accompanied by ozone production under UV radiation. High concentrations of O_3 are not desirable because ozone reacts with the NDA-coating and depletes the capacity of the coating to absorb NO_2. To minimise this effect the parameters of the HNO_3 generation (UV radiation exposure and amount of synthetic air) are optimised in a way to keep the output concentration of O_3 at minimum (below 30 ppb).

After passing the denuder, the aerosol particles are captured by a glass fiber filter. To each trap (the coatings and filter) a separate CsI scintillator crystal with integrated PIN diode is attached (Carroll and Ramsey, USA) which detects the gamma quanta emitted after decay of the ^{13}N atoms. The detector signal is converted to the flux of the gaseous species into the trap using the inversion procedure reported elsewhere [*Guimbaud et al.*, 2002; *Kalberer et al.*, 1996; *Rogak et al.*, 1991]. This flux is proportional to the concentration of the species in the gas phase.

An additional NaCl-trap is used to monitor the concentration of gaseous HNO_3 in a small side flow before entering the reactor. The trap consists of a quartz-fiber filter, soaked with a saturated aqueous NaCl solution and dried. Also to this trap, a scintillator device as that described above is attached. This measurement provides a “reference” for the generation of gaseous nitric acid and reduces the uncertainty related to the instability of the flux of ^{13}N arriving in the laboratory. The relative counting efficiency of each detector is determined by accumulating a certain amount of $H^{13}NO_3$ in the “reference” trap and exposing it to each of the other detectors attached to the denuder sections and the particle filters in a way that closely mimics the geometrical configuration at each trap. The concentration of non-labelled NO and NO_2 is monitored by a chemiluminescence analyser (Ecophysics, Switzerland). Further details of the preparation of the coatings, trap and filter efficiencies, and the performance of the detection system are published elsewhere [*Ammann*, 2001; *Guimbaud et al.*, 2002].

Mineral dust processing and measurement of hygroscopic properties.

Apart from the kinetic experiments, ATD aerosol particles were also processed by gaseous HNO_3 in a laminar flowtube reactor at room temperature and atmospheric pressure over longer time scales. The mean residence time of the aerosol in this reactor was 3 min at a flowrate of 0.3 lpm. Relative humidity in the reactor was monitored by a capacitance detector. To vary the relative humidity in the reactor chamber, the aerosol flow passes through the humidifier (identical to the one described above). The flow of HNO_3 was maintained by passing a 0.2 lpm flow of nitrogen through a bubbler, which contained a nitric acid solution in

H_2O (0.1 M) at 12°C. Half of this flow was directed to a molybdenum converter held at 400°C and then to a NO chemiluminescence detector to monitor the concentration of nitric acid in the gas phase [*Joseph and Spicer*, 1978]. The concentration of gaseous HNO_3 detected in this way was 3×10^{13} molecules cm^{-3} at 298K. The other half of the HNO_3 flow is mixed with the ATD aerosol flow (0.2 lpm) prior to the reactor entrance. After the reaction chamber, the aerosol flow was drawn through a NaOH coated denuder tube to remove HNO_3 from the gas phase. The hygroscopic properties of the processed ATD aerosol was measured by a Hygroscopicity Tandem Differential Mobility Analyzer (HTDMA) system described elsewhere [*Weingartner et al.*, 2002]. Briefly, in this instrument, the aerosol is first dried to a low RH (< 5%) and fed into the first differential mobility analyzer (DMA) where a monodisperse particle size fraction is selected (diameter $D = D_o$). Then, the aerosol is exposed to higher RH during ~60 s, and the resulting new particle size distribution is determined with a second DMA combined with a condensation particle counter. This instrument is capable of measuring the hygroscopic growth factor (GF) defined as the relative particle diameter increase from dry to humidified state, D/D_o. A prehumidifier (RH=95%) is included or bypassed in order to measure hygroscopic growth factors during dehydration or hydration.

Table 5-1. Flow reactor parameters and measurement conditions.

Parameter	Value
Reaction time	0.2-2 s
Concentration $H^{13}NO_3$ (labelled)	~10^6 cm^{-3}
Concentration of HNO_3 (not labelled)	10^{11}-10^{12} cm^{-3}
Pressure	~ 1 atm
Relative humidity	12-73 %

5.4. Results and discussion

Procedure of the kinetic experiments

The time profiles of the NO_2, HNO_3(g), HNO_3 (γ-reference) and HNO_3(aerosol) concentrations during an individual uptake experiment is illustrated in Fig. 5-3 and described in detail below. The experiment starts with equilibrating the system by running all gas flows without the admission of ^{13}N-labelled nitrogen dioxide (0-12 min time interval). At this time the background signals of the gamma detectors are recorded. Then at 12 minute, a small flow of $^{13}NO_2$ is admitted to the main gas flow. The NDA coating of the denuder starts to absorb nitrogen dioxide from the gas phase, accompanied by an increasing number of decays observed in this trap (panel A, dashed line). This growing signal is inverted to the flux of ^{13}N labelled molecules into this trap, which is proportional to the concentration of the $^{13}NO_2$ in the gas phase (panel A, solid line). Because this flux is calculated based on the difference of two consecutive activity measurements only, the inverted data (solid line) show more apparent scatter than the raw activity signals (dashed line). Prior to the reactive absorption in the NDA-trap the nitrogen dioxide molecules travel along the NaCl and Na_2CO_3 traps. Due to reversible adsorption and some slow conversion to HNO_3 and HONO, some of the ^{13}N atoms are also being absorbed on these traps, which leads to a small increase of the corresponding detector signals (panel B: solid line). For the same reason, the signal at the “reference” trap detector is increased (panel B, dashed line). The efficiency of the NO_2 absorption in the NDA-trap is not

entirely 100%, so that a small fraction of NO_2 may penetrate the denuder to the aerosol filter and manifests itself as a slight increase of the signal (panel C). Note that this penetrating fraction may be extremely low but may still allow a detectable signal.

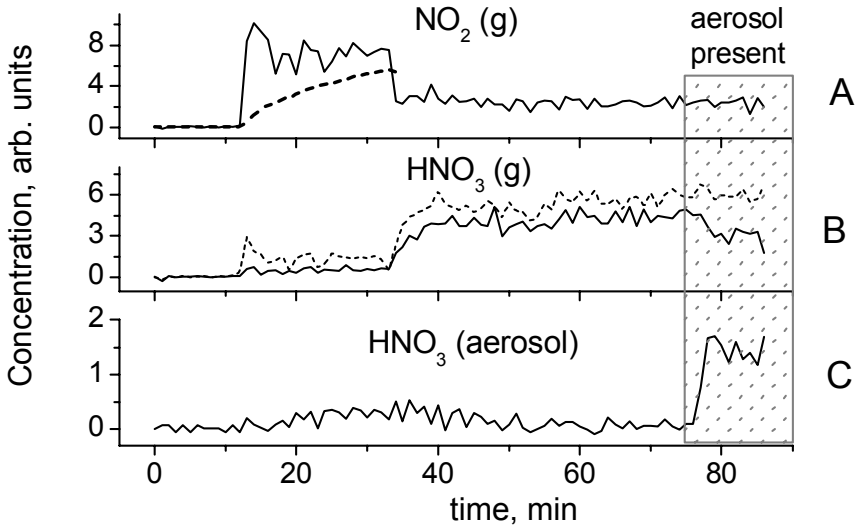

Fig. 5-3. Online record of an uptake experiment. Panel A: dashed line represents the signal of detector at the NDA-trap and solid line corresponds to the concentration of nitric dioxide. Panel B: the dashed line represents the "reference" gas phase concentration of HNO_3 (concentration before entering the reactor) and the solid line corresponds to the concentration after the reactor. Panel C: the solid line represents the concentration of nitric acid on the aerosol surface. The grey bar (75-90 min) corresponds to the time when aerosol was present in the flow reactor. The HNO_3 gas phase concentration in the flow tube was 10^{11} cm^{-3} and RH 33%.

At 33 min of the experiment, the production of HNO_3 is started by switching on the UV lamp for OH production to convert NO_2 into HNO_3. As a result, the detector signal of the NDA-trap decreases by about a factor of three (panel A, solid line). It indicates that two thirds of the labelled NO_2 molecules were oxidized to HNO_3. We use this conversion factor to calculate the overall concentration of nitric acid in the gas phase by applying the same factor for the conversion of non-labelled NO_2, the concentration of which is measured by the chemiluminescence detector. The increase of the HNO_3 concentration is detected at the NaCl denuder (panel B, solid line) and in the reference trap (panel B, dashed line).

The mineral dust particles are introduced to the flow reactor at 75 min of the experiment. The gas phase nitric acid concentration drops (panel B, solid line) due to reaction with the aerosol surface, while the concentration of the particulate HNO_3 increases (panel C). As noted above, the signal associated with particulate HNO_3 is due to HNO_3 irreversibly taken up to the particles. HNO_3 desorbing from the particles faster than 0.1 s would be detected as gas phase HNO_3 in the first denuder. No increase of the signals in the other denuders has been observed during the presence of aerosol, so that not significant amounts of HNO_3 desorbing on the time scale of a second while travelling along the denuder train had been associated with the aerosol. A significant loss of HNO_3 from the particles on the filter on the time scale of minutes would have resulted in a lack of mass closure for HNO_3.

Using the procedure given here, uptake to aerosol particles can be measured as a function of reaction time, HNO_3 concentration in the flow tube and relative humidity. The algorithm to derive the value of the uptake coefficient from the measurements shown in Fig. 5-4 is described below.

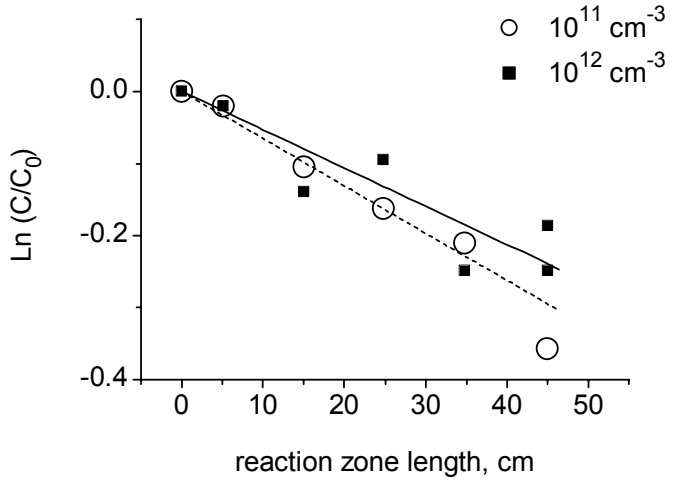

Fig. 5-4. Concentration of $H^{13}NO_3$ leaving the flow reactor in absence of aerosol at different injector positions, normalized by the initial concentration. Circles and squares represent the data points measured at 10^{11} cm^{-3} and 10^{12} cm^{-3}, respectively, of HNO_3 in flow tube and 33% RH. Lines are fits to the data according to the model explained in the text.

Calculation of the uptake coefficient

The uptake coefficient is usually defined as the ratio between the net flux of molecules from the gas phase to the aerosol particles and the gas-kinetic collision flux of the molecules to the surface of the particles.

$$\gamma = \frac{J_{net}}{J_{coll}} \qquad \textbf{(5-1)}$$

The observations from an individual experiment shown in the previous section allow determining the rate of change of gas-phase and particulate phase concentrations. In principle, the mechanism leading to the net transfer of HNO_3 to an irreversibly bound product in the particulate phase can be very complex. Nevertheless, to obtain first insights into the kinetics, the uptake coefficient can be estimated in a first order approach similar to that reported earlier [*Guimbaud et al.*, 2002]. Note that this approach assumes a constant (quasi-steady state) uptake to the aerosol during the residence time of the aerosol in the flow reactor. Because, as noted above, reversibly adsorbed HNO_3 is not detected in the aerosol phase, the uptake coefficient obtained this way is the probability that an HNO_3 molecule colliding with the dust surface is irreversibly reacting with a dust component. Therefore, initial loss from the gas phase could be stronger than the quasi-steady state uptake coefficient assumed in this approach. The rate equation for the depletion of radioactively labelled HNO_3 from the gas phase in the cylindrical flow tube is given by

$$-\frac{dC_g}{dt} = (k_w + k_p)C_g \qquad \textbf{(5-2)}$$

where C_g is the average concentration of HNO_3 in gas phase. k_w is the constant which describes the pseudo first order loss of $H^{13}NO_3$ from the gas phase due to its adsorption to the walls of the reactor. k_p is the constant, which describes the heterogeneous reaction between gaseous nitric acid and aerosol particles. The presence of the wall-loss is rather specific for the radioactively labelled molecules used in this study and will be discussed in detail in the next section. Integration of the Eq.(5-2) with respect to time gives the concentration of $H^{13}NO_3$ molecules in the gas phase as a function of time:

$$C_g(t) = C_g^{t=0} \exp\{-(k_w + k_p)t\} \quad \textbf{(5-3)}$$

where $C_g^{t=0}$ is the initial concentration at time zero. k_w can be obtained from the measurement of the concentration of $H^{13}NO_3$ (g) as a function of time in absence of aerosol (k_p=0). The loss rate of $H^{13}NO_3$ (g) in presence of the aerosol then allows determining k_p.

The kinetics of appearance of $H^{13}NO_3$ in the particulate phase is given by:

$$C_p(t) = C_g^{t=0} \frac{1 - e^{-(kw+kp)t}}{1 + \frac{k_w}{k_p}} \quad \textbf{(5-4)}$$

where $C_p(t)$ is the concentration of $H^{13}NO_3$ in the particulate phase.

In practice, we used Eq.(5-4) and not Eq.(5-3) to calculate the constant k_p, because the experimental measurement of C_p is more accurate than that of C_g. The heterogeneous constant k_p is related to the effective uptake coefficient γ_{eff} according to following equation:

$$k_p = \frac{\gamma_{eff} S_p \omega}{4} \quad \textbf{(5-5)}$$

where S_p is the aerosol surface to volume ratio, ω is the mean thermal velocity of HNO_3 given by $\omega=(8RT/(\pi M))^{1/2}$, R is the gas constant, T is the absolute temperature and M is the molar weight of HNO_3.

The value of S_p was measured in the experiment by the SMPS and the values of k_p and ω could be calculated using the equations listed above.

The value of the effective uptake coefficient, calculated in this way, depends slightly on the aerosol particle size, because gas phase diffusion affects the rate of transfer to larger particles more strongly than that to smaller particles. The diffusion correction was made using Eq.(5-6) and Eq. (5-7) [*Pöschl et al.*, 2005].

$$\frac{1}{\gamma} = \frac{1}{\gamma_{eff}} - \frac{0.75 + 0.28Kn}{Kn(1 + Kn)} \quad \textbf{(5-6)}$$

$$Kn = \frac{6D}{\omega d_p} \quad \textbf{(5-7)}$$

where D is the diffusion coefficient of HNO_3, d_p is aerosol particle diameter and *Kn* is the Knudsen number. Note that for the experiments reported in this study, the correction was always below 5% as discussed below.

Retention of $H^{13}NO_3$ on the flow reactor wall

The observations show that there is a steady state drop of the gas phase concentration of $H^{13}NO_3$ during passage through the flow reactor even without aerosol. As already pointed out by Guimbaud et al. (2002), this is not due to an irreversible chemical loss of HNO_3 on the wall, but rather due to retention driven by adsorption and desorption. When considering the non-labelled HNO_3 molecules, this effect leads to the well-known slow response time of this sticky gas measured at the reactor outlet when switching it on and off. At low concentrations, the observed response time is directly related to the average residence time of individual molecules in the flow tube. If this residence time is comparable to the half-life of the radioactive ^{13}N-tracer, 10 min., a drop in the $H^{13}NO_3$ concentration along the flow tube can be observed, while the concentration of the non-labelled HNO_3 concentration remains constant, if equilibrium with the wall is established.

The details of lateral diffusion, adsorption, desorption, and radioactive decay are lumped into the pseudo-first order decay constant k_w. Therefore, Eq.(5-3) with k_p=0, was used to fit the experimentally observed $H^{13}NO_3$(g) concentration drop in absence of aerosol as shown in Fig. 5-4 for two examples. Typical residence times of HNO_3 derived from these loss curves are about 4 min. k_w obtained from these fits significantly decreased with increasing HNO_3 concentration, possibly because saturation coverage of HNO_3 on the PFA Teflon surface was reached above 10^{12} molecules cm^{-3}. k_w was also observed to increase with increasing relative humidity. This might be related to higher surface coverage by H_2O molecules at higher relative humidity and the formation of surface-adsorbed nitric acid–water complexes.

Apart from these effects, k_w also varied to some degree from tube to tube. Therefore, each time some parameter of the experimental system was changed or a new PFA flow tube was installed, a new measurement of k_w was performed.

Effect of aerosol surface area and "diffusion resistance"on uptake

The dependence of the amount of $H^{13}NO_3$ taken up on the aerosol of the aerosol surface area was investigated at an HNO_3 concentration in the gas phase of 10^{12} cm^{-3}, RH of 33% and reaction time of 1.9 s. The aerosol surface area was varied by changing the dust generator output, which results in a change of the particle number concentration but not particle size.

Fig. 5-5 shows the number of HNO_3 molecules reacted per cm^3 as a function of the particle surface area per cm^3. The error bars represent the 1σ deviation of data about the mean. The amount of nitric acid reacted on the surface should be a linear function of the particle surface area, as long as $(k_w + k_p)t < 1$, so that $C_p(t) \approx C_g{}^{t=0} k_p t$, and for fixed reaction time t, $C_p \propto S_p$. This confirms that our experiment lies well within pseudo-first order kinetics and that the availability of HNO_3 is not limiting the uptake.

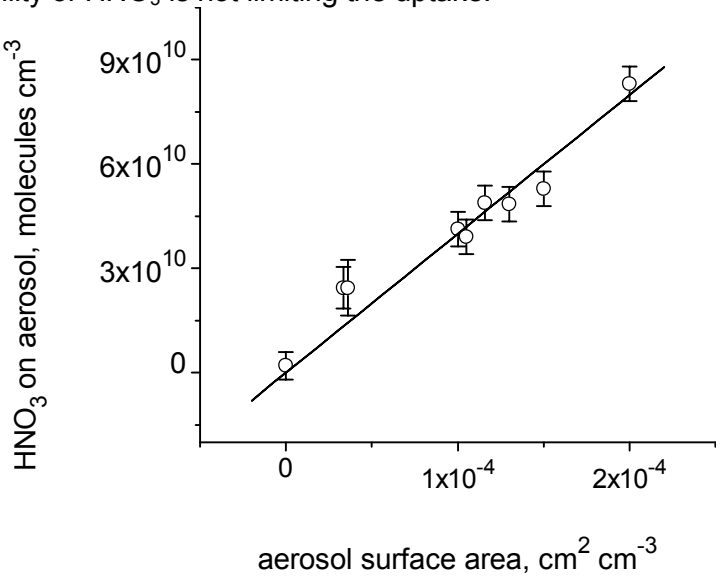

Fig. 5-5. HNO_3 reacted with ATD particles as a function of specific aerosol surface area. The nitric acid gas phase concentration in the flow tube was 10^{12} cm^{-3} and RH 33%.

To estimate the limitation of uptake by the diffusion of HNO_3 in the gas phase we use the expressions (5-6) and (5-7). The HNO_3 diffusion coefficient D has been taken as 0.118 cm^2s^{-1} [*Durham and Stockburger*, 1986], which had been measured at atmospheric pressure,

298 K and 5-95% relative humidity. The "diffusion limitation" effect is stronger for higher values of the uptake coefficient. Based on Eq.(5-6) and Eq.(5-7), the maximum correction γ/γ_{eff} is 1.5 at 1 micrometer particle diameter for γ_{eff} =0.1. When integrated over the full aerosol spectrum of ATD, the correction is about 5% or less for smaller values of γ.

Uptake coefficient on Arizona Test Dust aerosol

The experimental data of the $H^{13}NO_3$ (g) concentration drop and the corresponding gain of $H^{13}NO_3$ (p) in the aerosol phase shown in Fig. 5-6 was fitted using Eq. (5-4) and Eq. (5-5), with k_p as independent variable. The constant k_p was varied using the least square method to achieve the best agreement between the data points of the concentration in the aerosol phase and model curve, calculated by Eq. (5-4), because, as noted above, the changes in the aerosol phase could be detected with better accuracy than those in the gas phase. The result is given in Fig. 5-6 and Table 5-2. The fit and the data agree quite well. One should notice that within accuracy of the experiment the drop of the HNO_3(g) concentration due to uptake to the aerosol corresponds to the growth of the HNO_3(p) signal. Most of the discrepancy between data and model has been assigned to the instability of aerosol generation. For instance, the deviation of the data points from the fit at 1.9 s reaction time in the example shown in Fig. 5-6 is due to an increase of the aerosol surface area recorded by the SMPS system at that time and as a result a higher uptake to the aerosol phase and stronger depletion of the HNO_3 concentration in the gas phase.

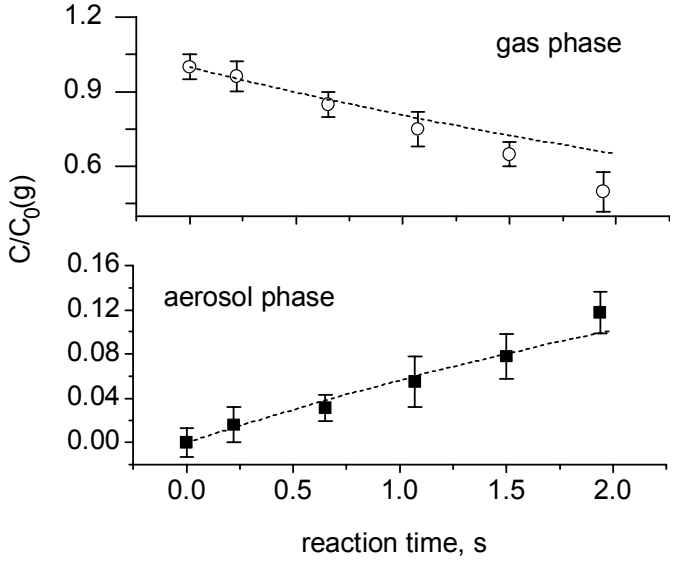

Fig. 5-6. Change of the HNO_3 concentration in the gas (open circles) and particulate (solid squares) phases as a function of reaction time. Experimental data are represented as the concentrations normalized by the concentration in the gas phase at reaction zero time. The dashed lines are the model fits. The HNO_3 gas phase concentration in the flow tube was 10^{11} cm^{-3} and RH 33%. The error bars represent the 1σ deviation of data about the mean.

Table 5-2. Conditions of the uptake experiments and the results of the fits to the data.

Parameter	HNO_3 concentration in the gas phase in flow reactor, molecules cm^{-3}	
	$(1\pm0.5)\times10^{11}$	$(10\pm1)\times10^{11}$
RH, %	33±1	33±1
$S_p \times10^{-5}$, cm^2 cm^{-3}	8.6±0.5	12.9±0.3
k_w, s^{-1}	0.152±0.002	0.110±0.003
k_p, s^{-1}	0.063±0.005	0.025±0.005
γ_{eff}	0.10±0.01	0.03±0.01
γ	0.105±0.01	0.03±0.01

The uptake coefficient is found to be a function of HNO_3 concentration in the gas phase (Table 5-2). At higher concentration of nitric acid in the flow tube the uptake coefficient drops by more than a factor of three. Previous work on this and similar heterogeneous reaction systems indicate that the HNO_3+mineral dust reaction could be considered as a two stage process: adsorption of HNO_3 on the dust surface followed by a reaction of the adsorbed HNO_3 with a basic surface site (surface OH—group on aluminosilicate or similar minerals or bulk $CaCO_3$). Therefore, the decrease of the uptake coefficient, which is an average over the two seconds reaction time, could be either due to the depletion of the reaction sites or due to saturation of the adsorbed precursor [*Ammann et al.*, 2003]. The available data points at HNO_3(g) concentration 10^{12} cm^{-3} still fit the model (which assumes an average uptake coefficient over the time scale of the experiment) reasonably well, so that depletion of the reactants during the early periods of the reaction time is likely not the reason for the concentration dependence. While the amount of HNO_3 found on the particle surface after two seconds of about 2×10^{14} molecules cm^{-2} could be considered close to a monolayer surface coverage, the degree with which components contained in the bulk of the particles can react and thus extend the capacity of the particles to react is not known. Therefore, this apparent non-first order behavior of the rate of product appearance indicates that the simple approach adopted here is not sufficient to retrieve a reliable parameterization of the kinetics. A more extended kinetic data set associated with proper kinetic modeling is necessary to extract the parameters describing the elementary processes of the uptake process. This will be part of a follow-up study of this, while here we concentrate on the humidity dependence.

Uptake coefficient on SiO_2 and $CaCO_3$ aerosols

In an attempt to understand the mechanism of the heterogeneous reaction between HNO_3 and the ATD and for the purpose of comparison with other studies, we also made experiments of uptake of HNO_3 to silica and calcite aerosol particles.

Fig. 5-7 shows the uptake of the gaseous nitric acid to silica and $CaCO_3$ aerosol particles. To simplify the discussion of this comparison, we show the raw data in the same way as discussed above. The experiment starts with recording the background detector signal, as shown in Fig. 5-3. After 20 minutes, the aerosol is introduced into the flowtube, adjusted to a reaction time of 1.9s. One may see that the detector signal level does not change with the introduction of SiO_2 particles at a statistically significant level. This means that silica aerosol seems rather inert with respect to reaction with HNO_3. Assuming the detection limit at 3σ of the background noise level of the signal of the γ-detector at the aerosol filter and taking into account the measured SiO_2 aerosol surface area of 10^{11} cm^2 cm^{-3}, an upper limit to the uptake coefficient of 5×10^{-4} is obtained.

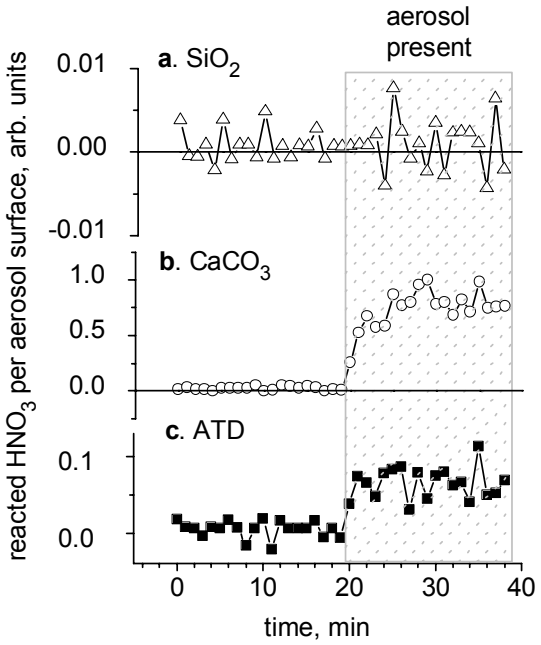

Fig. 5-7. Online record of uptake experiments between gaseous HNO_3 and aerosol particles of different materials. Panel a, b and c represent the reactions with the aerosol composed of silica, calcium carbonate and Arizona Test Dust, respectively. The time period 0-20 min corresponds to the background readings of the detector. The grey bar (20-40 min) corresponds to the time when aerosol was present in the flow reactor. The HNO_3 gas phase concentration in the flow tube was 10^{12} cm^{-3} and RH 33%.

This result is in agreement with the Knudsen cell study of Underwood et al. (2001) who reported the uptake of HNO_3 to a SiO_2 surface "too low to be measured". Goodman et al. (2001) studied the heterogeneous reaction of silica powder with gaseous nitric acid using transmission FT-IR spectroscopy and classified the SiO_2 as a non-reactive neutral oxide with respect to this reaction. The authors also concluded that the adsorption of nitric acid on silica surface is reversible at 296 K. This is also in agreement with the data of the present study because HNO_3 reversibly adsorbed to the SiO_2 particles in the flowtube is desorbed in the denuder and not detected in the aerosol phase. This reversible nature of HNO_3 adsorption on silica surfaces was also reported by Dubowski et al. (2004) who found no significant amounts of covalently bonded nitrate on glass and quartz surface after exposure to HNO_3.

In contrast, $CaCO_3$ particles are more reactive with respect to nitric acid than ATD, as also shown in Fig. 5-7. The uptake to $CaCO_3$ is almost 4 times higher than to ATD. This is not surprising, since the reactivity of $CaCO_3$ with HNO_3 is well known, while ATD contains only little $CaCO_3$ but much more of the less reactive silica and alumino-silicates. This is in agreement with the studies of Krueger et al. (2003, 2004), which showed the formation of $Ca(NO_3)$ in single $CaCO_3$ and authentic dust particles as a reaction product at conditions close to the experimental conditions of this study (RH 38%, HNO_3 concentration 4.6×10^{11} molecules cm^{-3}). To some extent the nature of the mineral surface under the humid conditions of the present study could be rationalized from the way how the major mineral constituents are expected to dissolve in near neutral or acidic aqueous solution [*Desboeufs et al.*, 2003; *Schott and Oelkers*, 1995]:

$$SiO_2(quartz) + 2H_2O \quad \Leftrightarrow \quad H_4SiO_4 \qquad \textbf{(5-8)}$$

$$Albite + H^+ \Leftrightarrow H_{1/3}Al_{1/3}SiO_{8/3}(hydrogenet\,ed\ albite) + Na^+(K^+) \qquad \textbf{(5-9)}$$

$$H_{1/3}Al_{1/3}SiO_{8/3} + H^+ + (n-2/3)H_2O \Leftrightarrow (SiO_2 \cdot nH_2O) + 1/3\,Al^{3+} \quad \textbf{(5-10)}$$

$$CaCO_3(calcite) + H^+ \Leftrightarrow HCO_3^- + Ca^{2+} \quad \textbf{(5-11)}$$

This list of reactions is not complete and one should also consider the dissolution of minor components of the ATD: microcline, illite, etc. Most of these minerals dissolve similar to albite and some could additionally release Mg^{2+} cations. Exposure of ATD to HNO_3 under humid conditions certainly helps promoting these hydrolysis processes by providing protons. Even though these hydrolysis processes might not be complete on the surface, especially at relatively low humidity, partial solvation might be enough for providing a reactive site to HNO_3.

Effect of humidity on uptake

The hydrolysis reactions (5-8) to (5-11), which might promote the surface (and eventually also bulk) reactivity of dust towards HNO_3, are directly suggesting that a significant humidity dependence should exist. The effect of variation in relative humidity on the uptake coefficient was investigated using a fixed HNO_3 concentration of 10^{12} molecules cm^{-3} and a fixed reaction time of 1.9 s. The data displayed in Fig. 5-8 indeed show that γ increases steadily from 0.022±0.007 at 12% RH to 0.113±0.017 at 73% RH. A possible explanation to this is the increasing amount of H_2O adsorbed on the surface of ATD particles, which may promote the hydrolysis processes. Some information on the amount of water associated with ATD aerosol can be obtained from the hygroscopic growth of ATD aerosol particles investigated in a previous study [*Vlasenko et al.*, 2005].

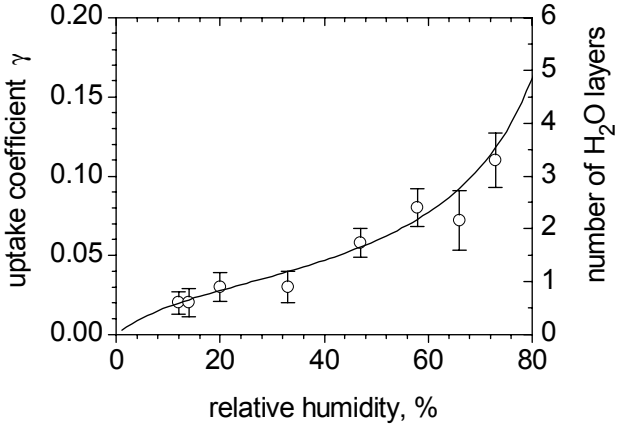

Fig. 5-8. Uptake coefficient of nitric acid to ATD mineral dust aerosol as a function of relative humidity. Open circles represent the experimental values of the uptake coefficient reaction time 1.9 s, the concentration of nitric acid in the flow tube was $10^{12}cm^{-3}$). The solid line represents a BET isotherm (Eq. 5-8, c=8) for water adsorption, scaled to match the uptake data.

The main conclusion was that the ATD particles adsorb water under increasing RH conditions, to some degree related to the presence of water soluble material. However, the small size changes did not allow retrieving a well resolved water adsorption isotherm. For bulk oxide materials it has been shown that several monolayers of water can be formed on the surfaces of SiO_2, Al_2O_3 and $CaCO_3$ with increasing relative humidity [*Al-Abadleh and Grassian*, 2003; *Goodman et al.*, 2001; *Goodman et al.*, 2000]. Similar behavior was shown for water adsorption on a borosilicate glass surface [*Dubowski et al.*, 2004; *Sumner et al.*, 2004]. These authors have adapted the BET equation [*Adamson*, 1982] to describe water adsorption on the surface of solids. We used the same approach to calculate the isotherm for the adsorption of water by

$$\Theta_{H_2O} = \frac{c\,RH}{(1-RH)(1-(1-c)RH)} \qquad \textbf{(5-12)}$$

One can see in Fig. 5-8 that this isotherm can be well fitted to the experimental data of the uptake coefficient of HNO_3 on ATD. This observation continues the row of "BET isotherm like" humidity dependent heterogeneous reactions on solid surfaces: HNO_3(g)+NaCl(s) [*Davies and Cox*, 1998], HNO_3(g)+$CaCO_3$(s) [*Goodman et al.*, 2000], NO_2+1,2,10-anthracenetriol (s) [*Arens et al.*, 2002] and NO_2+borosilicate glass [*Finlayson-Pitts et al.*, 2003], in all of which hydrolysis of the substrate provides the reactive components. This contrasts other heterogeneous processes, such as oxidation reactions [*Adams et al.*, 2005; *Pöschl et al.*, 2001], in which water adsorption competes with the adsorbing gaseous reactant, so that humidity has an inhibiting or no effect on the overall process. Furthermore, the increase of the uptake coefficient with humidity measured in this study is consistent with data from the ACE-Asia field campaign, where the mass accommodation coefficient of HNO_3 on ambient dust was found to depend on RH [*Maxwell-Meier et al.*, 2004].

Comparison to literature data

Several aspects should be considered, when comparing the uptake data of the present study to those currently available in the literature as listed in Table 5-3. Our data suggest a strong humidity dependence of the uptake coefficient, while the previously available kinetic studies were all performed under completely dry conditions. If we would extrapolate our data along the water adsorption isotherm to very low humidity (0.1% RH) in Fig. 5-8, we expect the uptake coefficient to get into the range of 10^{-3} for ATD, and a similar shift might be expected for the uptake on $CaCO_3$, if we would assume a similar dependence on humidity. Hanisch et al. (2001) report an about a factor of 2 change in the uptake coefficient on $CaCO_3$ measured under dry conditions, when water remaining after evacuation was further removed by baking the dust powder.

Table 5-3. Uptake coefficient measured for aerosol particles of different composition. KC, DRIFTS and FT are abbreviations of Knudsen Cell, Diffuse reflectance infrared spectroscopy and Flow Tube reactors, respectively. Only average values of uptake coefficients and orders of magnitude HNO_3 concentrations are given for conciseness.

***values are given for nonheated and heated sample respectively. ** uptake measured at RH 33%.**

Study	Reactor	Sample	HNO_3 Conc, cm^{-3}	Composition		
				SiO_2	$CaCO_3$	ATD
Fenter et al. 1995	KC	powder	10^{10}-10^{13}		0.15	
Goodman et al. 2001 Goodman et al. 2000	DRIFTS KC	powder powder	10^{14}-10^{15} 10^{12}	10^{-9}	 2.5×10^{-4}	
Johnson et al. 2005	KC	powder	10^{11}		2×10^{-3}	
Hanisch et al. 2001	KC	powder	10^{14}-10^{15} 10^{11}-10^{12}		0.18, 0.1*	 0.06
Seisel et al. 2004	DRIFTS	powder	10^{11}-10^{12}			0.012
this work**	FT	aerosol	10^{12} 10^{11}	$<5\times10^{-4}$	0.11	0.03 0.11

A second aspect relates to the issue of surface area to normalize the uptake according to equation (2). The significant disagreement between the values reported by Goodman et al. (2000) and by Johnson et al. (2005) on the one hand and those reported by Fenter et al. (1995) and Hanisch et al. (2001) on the other are due to different ways of taking into account internal surface areas of the powders used. Goodman et al. (2000) measured the specific area of $CaCO_3$ powder with a BET method and applied the Keyser-Moore-Leu model [*Keyser*

et al., 1991] to account for the contribution by the internal surface area, while Fenter and Hanisch referred to the geometric sample surface area to calculate the collisional flux in the molecular flow regime to the external powder surface. In our study with suspended aerosol particles, we estimate the reactive surface area from the measurement of the mobility diameter (measured by SMPS) and assuming that the particles are spherical, even though it has been shown [*Vlasenko et al.*, 2005] that the ATD particles used in this study are not perfectly spherical and could be to some degree agglomerates, especially for particle sizes larger than 200 nm. Experimentally, the relation between the surface of aerosol agglomerates available for reaction and the surface measured by SMPS is only known for a perfectly sticking (γ=1) species, namely ^{211}Pb atoms. Rogak et al. (1991) experimentally proved that the mobility diameter measured by SMPS is equal to the "mass transfer" diameter not only for spherical particles but also for complex agglomerates, namely soot. Other existing theoretical approaches to account for the additional internal surface of aerosol agglomerates rely strongly on empirical parameters [*Naumann*, 2003; *Xiong et al.*, 1992]. In the absence of a more accurate way to evaluate the true dust surface area (available for reaction with HNO_3) we used the surface area measured by the SMPS system to calculate the uptake coefficient. Bearing in mind that only part of all the particles are slightly agglomerated (particles larger than 200 nm) we guess a not more than 20% systematic underestimation of the dust surface area given by the SMPS. Therefore, the apparent agreement of the uptake coefficients observed under humid conditions of this study with those of Hanisch and Fenter for $CaCO_3$ and Hanisch and Seisel for ATD under very dry conditions might be accidental, And our data might be in closer agreement with the Goodman and Johnson data than it would seem at first glance.

Implications for the hygroscopic properties of ATD aerosol

One of the atmospherically relevant consequences of the heterogeneous interaction between HNO_3(g) and mineral dust is the associated change of hygroscopic properties of the dust particles. Fig. 5-9 shows the hygroscopic growth of ATD particles before and after reaction with gaseous nitric acid and water vapor.

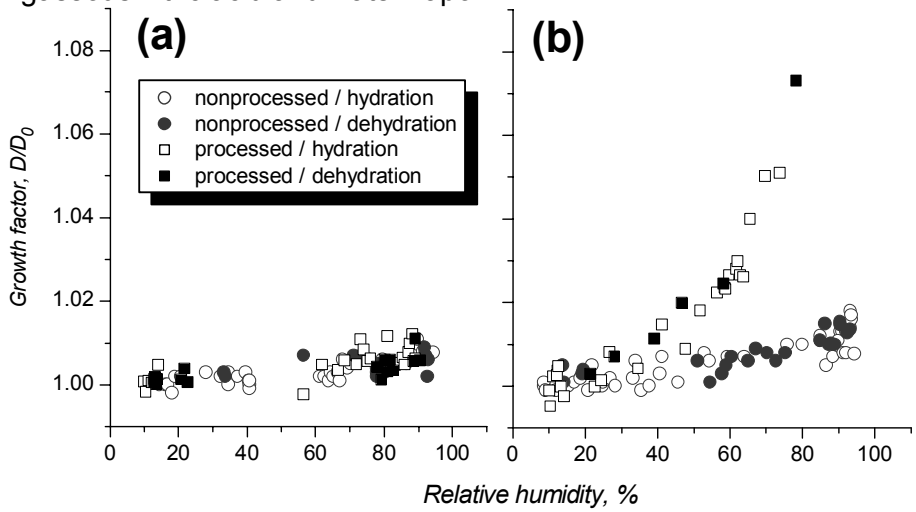

Fig. 5-9. Hygroscopic growth of ATD particles before (circles) and after (squares) reaction with gaseous nitric acid (3×10^{13} molecules cm^{-2}) and water vapour. (a): circles represent ATD particles with D_0=100nm before reaction, squares represent particles of the same size after reaction with HNO3 at 30% RH. (b): circles represent ATD particles before reaction, squares represent ATD particles after reaction with HNO_3 at 85% RH. D_0 is the mobility size of monodisperse particles at lowest RH at 20°C. Open and solid symbols correspond to hydration and dehydration curves, respectively.

When dust particles are exposed to HNO_3 (3×10^{13} molecules cm^{-3}) for 3 min at 30% relative humidity the hygroscopic properties do not change significantly (Fig. 5-9(a)). The exposure in this experiment corresponds to the integrated exposure of an atmospheric dust particle to 0.1-1ppb of HNO_3 during a typical life-time of 1-10 days, even though we are aware that in view of the concentration dependence observed this might be an over-simplification. The ATD hygroscopicity is significantly changed after weathering the particles at the same concentration of HNO_3 and 85% RH. Fig. 5-9(b) shows that after the exposure the particle diameter is increased by 7% while increasing the humidity from 10% to 78%. This finding is consistent with the kinetic data that show a strong effect of humidity on the speed and extent of processing of the dust particles by HNO_3 (Fig. 5.8). Even though the formation of a liquid phase is thermodynamically not favored (for the pure HNO_3-H_2O system) under our conditions, we nevertheless assume that the concomitant exposure to nitric acid and high humidity of 85% over longer time scales promotes the significant dissolution of the particle surface material through reactions (5-9) to (5-12) [*Desboeufs et al.*, 2003; *Schott and Oelkers*, 1995]. *Desboeufs et al.* (1999) studied the dissolution rates of different elements from Sahara dust at different pH and reported the increasing solubility sequence Si<Mg<Ca<K<Na. From these data we concluded that the uptake of HNO_3 from the gas phase to mineral dust particles at 85% RH increases the acidity of the adsorbed water layers and strongly promotes the dissolution of major minerals. The weathering of silica is believed to be small on a time scale of our experiment (3 min). In our experiments, after the processing the aerosol was dried, and possibly separate phases of Ca/Mg/Na nitrates are formed on the particles. *Laskin et al. (*2005) interpreted the increase the O,N atomic content of the Ca-rich mineral dust particles after HNO_3(g) exposure as formation of calcium nitrate. We use the assumption (that the reaction product is $Ca(NO_3)_2$) to calculate the amount of product built up after processing of ATD with gaseous nitric acid. Using the approach of *Saathoff et al.* (2003) and assuming spherical shape of particles and independent additive hygroscopic behaviour of the different components one may calculate the volume fraction of $Ca(NO_3)_2$ coating on the processed particles according to the following equation:

$$\varepsilon = \frac{GF_{proc}^3 - GF_{nonproc}^3}{GF_{Ca(NO3)2}^3 - GF_{nonproc}^3} \qquad \textbf{(5-13)}$$

where GF_{proc} and $GF_{nonproc}$ are hygroscopic growth factors of the processed and nonprocessed ATD particles, respectively. $GF_{Ca(NO3)2}$ is a hygroscopic growth factor of pure calcium nitrate, which is quite similar to the other soluble nitrates in dust (sodium nitrate and magnesium nitrate).

Using the measured values of the hygroscopic growth factors (Fig. 5-9(b)) for the ATD and the literature value for the calcium nitrate hygroscopic growth [*Tang and Fung*, 1997] as a proxy for the behaviour of the soluble nitrates, we calculate a 8% volume fraction of $Ca(NO_3)_2$ in the processed particles. Expressed as an external coating, this corresponds to an about 1 nm thick layer. This rough estimate shows that several monolayers of hygroscopic reaction products could be formed on the surface of the ATD particles as a result of processing with gaseous nitric acid. Note that extrapolation of our processing experiment to atmospheric conditions is only valid under the assumption that the degree of processing is a function of the integrated exposure only and not a function of HNO_3 concentration during the exposure.

5.5. Atmospheric Implications

The major atmospheric implication of this study is the experimentally determined humidity dependence of the heterogeneous uptake on the dust aerosol. It has been shown that increasing the relative humidity promotes the uptake of nitric acid. However, recent modeling studies [*Bauer et al.*, 2004; *Bian and Zender*, 2003; *Tang et al.*, 2004] consider the heterogeneous reactivity of the dust independent of relative humidity. While the order of magnitude of the uptake coefficient used by Bauer et. al. (2004) based on the data of Hanisch and Crowley (2001) obtained under very dry conditions (RH<1%) is similar to what we report here, we strongly suggest that a humidity dependent uptake coefficient scaling along a water isotherm as shown in Fig. 3.8 could be used in modeling studies. Implementing this dependence into global dust models will certainly reduce their uncertainty.

Another atmospherically relevant outcome of the present study is the experimental evidence that extensive processing of mineral dust by HNO_3(g) and possibly other acidic gases results in significant hygroscopic growth. The enhanced water uptake by dust particles increases their interaction with solar radiation. To illustrate this effect we estimate an increase of the dust single scattering albedo (SSA). SSA is the commonly used measure of the relative contribution of absorbing aerosol to extinction and is a key variable in assessing the climatic effect of the aerosol [*Seinfeld et al.*, 2004]. Assuming that the processing does not change the refractive index (n=1.52, k=0.00133) of the dust shown on Fig. 5-9(b) and only increases the particle size we estimate 3% increase of the SSA for the aged dust at 550 nm wavelength of incident light. This calculation is very crude but indicates the potential of the dust aging process to affect the radiation balance of the planet.

Acknowledgements

We would like to thank Mario Birrer for his excellent technical support. We also greatly acknowledge the staff of the PSI accelerator facility for their efforts to provide stable proton beam.

References

Adams, J.W., Rodriguez, D., and Cox, R.A.: The uptake of SO_2 on Saharan dust: a flow tube study, Atmos. Chem. Phys., 5, 2679-2689, 2005.

Adamson, A.W.: Physical Chemistry of Surfaces, John Wiley & Sons, New York, 1982.

Al-Abadleh, H.A., and Grassian, V.H.: FT-IR study of water adsorption on aluminum oxide surfaces, Langmuir, 19, 341-347, 2003.

Ammann, M.: Using ^{13}N as tracer in heterogeneous atmospheric chemistry experiments, Radiochim. Acta, 89, 831-838, 2001.

Ammann, M., Pöschl, U., and Rudich, Y.: Effects of reversible adsorption and Langmuir-Hinshelwood surface reactions on gas uptake by atmospheric particles, Phys. Chem. Chem. Phys., 5, 351-356, 2003.

Archuleta, C.M., DeMott, P.J., and Kreidenweis, S.M.: Ice nucleation by surrogates for atmospheric mineral dust and mineral dust/sulfate particles at cirrus temperatures, Atmos. Chem. Phys., 5, 2617-2634, 2005.

Arens, F., Gutzwiller, L., Gäggeler, H.W., and Ammann, M.: The reaction of NO_2 with solid anthrarobin (1,2,10-trihydroxy- anthracene), Phys. Chem. Chem. Phys., 4, 3684-3690, 2002.

Bauer, S.E., Balkanski, Y., Schulz, M., Hauglustaine, D.A., and Dentener, F.: Global modeling of heterogeneous chemistry on mineral aerosol surfaces: Influence on tropospheric ozone chemistry and comparison to observations, J. Geophys. Res.-Atmos., 109, doi:10.1029/2003JD003868, 2004.

Bian, H.S., and Zender, C.S.: Mineral dust and global tropospheric chemistry: Relative roles of photolysis and heterogeneous uptake, J. Geophys. Res.-Atmos., 108, doi:10.1029/2002JD003143, 2003.

Davies, J.A., and Cox, R.A.: Kinetics of the heterogeneous reaction of HNO_3 with NaCl: Effect of water vapor, J. Phys. Chem. A, 102, 7631-7642, 1998.
DeMott, P.J., Sassen, K., Poellot, M.R., Baumgardner, D., Rogers, D.C., Brooks, S.D., Prenni, A.J., and Kreidenweis, S.M.: African dust aerosols as atmospheric ice nuclei, Geophys. Res. Lett., 30, doi:10.1029/2003GL017410, 2003.
Desboeufs, K.V., Losno, R., and Colin, J.L.: Relationship between droplet pH and aerosol dissolution kinetics: Effect of incorporated aerosol particles on droplet pH during cloud processing, J. Atmos. Chem., 46, 159-172, 2003.
Desboeufs, K.V., Losno, R., Vimeux, F., and Cholbi, S.: The pH-dependent dissolution of wind-transported Saharan dust, J. Geophys. Res.-Atmos., 104, 21287-21299, 1999.
Dubowski, Y., Sumner, A.L., Menke, E.J., Gaspar, D.J., Newberg, J.T., Hoffman, R.C., Penner, R.M., Hemminger, J.C., and Finlayson-Pitts, B.J.: Interactions of gaseous nitric acid with surfaces of environmental interest, Phys. Chem. Chem. Phys., 6, 3879-3888, 2004.
Durham, J.L., and Stockburger, L.: Nitric-Acid Air Diffusion-Coefficient - Experimental-Determination, Atmos. Environ., 20, 559-563, 1986.
Fenter, F.F., Caloz, F., and Rossi, M.J.: Experimental-Evidence for the Efficient Dry Deposition of Nitric-Acid on Calcite, Atmos. Environ., 29, 3365-3372, 1995.
Finlayson-Pitts, B.J., Wingen, L.M., Sumner, A.L., Syomin, D., and Ramazan, K.A.: The heterogeneous hydrolysis of NO_2 in laboratory systems and in outdoor and indoor atmospheres: An integrated mechanism, Phys. Chem. Chem. Phys., 5, 223-242, 2003.
Goodman, A.L., Bernard, E.T., and Grassian, V.H.: Spectroscopic study of nitric acid and water adsorption on oxide particles: Enhanced nitric acid uptake kinetics in the presence of adsorbed water, J. Phys. Chem. A, 105, 6443-6457, 2001.
Goodman, A.L., Underwood, G.M., and Grassian, V.H.: A laboratory study of the heterogeneous reaction of nitric acid on calcium carbonate particles, 105, 29053-29064, 2000.
Guimbaud, C., Arens, F., Gutzwiller, L., Gäggeler, H.W., and Ammann, M.: Uptake of HNO_3 to deliquescent sea-salt particles: a study using the short-lived radioactive isotope tracer N-13, Atmos. Chem. Phys., 2, 249-257, 2002.
Hanisch, F., and Crowley, J.N.: Heterogeneous reactivity of gaseous nitric acid on Al_2O_3, $CaCO_3$, and atmospheric dust samples: A Knudsen cell study, J. Phys. Chem. A, 105, 3096-3106, 2001.
Joseph, D.W., and Spicer, C.W.: Chemiluminescence Method for Atmospheric Monitoring of Nitric-Acid and Nitrogen-Oxides, Anal. Chem., 50, 1400-1403, 1978.
Kalberer, M., Tabor, K., Ammann, M., Parrat, Y., Weingartner, E., Piguet, D., Rössler, E., Jost, D.T., Türler, A., Gäggeler, H.W., and Baltensperger, U.: Heterogeneous chemical processing of $^{13}NO_2$ by monodisperse carbon aerosols at very low concentrations, J. Phys. Chem., 100, 15487-15493, 1996.
Kärcher, B., and Lohmann, U.: A parameterization of cirrus cloud formation:Heterogeneous freezing, J. Geopyhs. Res., 108, 4402-4417, 2003.
Keyser, L.F., Moore, S.B., and Leu, M.T.: Surface-Reaction and Pore Diffusion in Flow-Tube Reactors, J. Phys. Chem., 95, 5496-5502, 1991.
Krueger, B.J., Grassian, V.H., Cowin, J.P., and Laskin, A.: Heterogeneous chemistry of individual mineral dust particles from different dust source regions: the importance of particle mineralogy, 38, 6253-6261, 2004.
Lohmann, U., Karcher, B., and Hendricks, J.: Sensitivity studies of cirrus clouds formed by heterogeneous freezing in the ECHAM GCM, J. Geophys. Res.-Atmos., 109, doi:10.1029/2003JD004443, 2004.
Maxwell-Meier, K., Weber, R., Song, C., Orsini, D., Ma, Y., Carmichael, G.R., and Streets, D.G.: Inorganic composition of fine particles in mixed mineral dust-pollution plumes observed from airborne measurements during ACE-Asia, J. Geophys. Res.-Atmos., 109, 2004.
Naumann, K.H.: COSIMA - a computer program simulating the dynamics of fractal aerosols, J. Aerosol. Sci., 34, 1371-1397, 2003.
Neuman, J.A., Huey, L.G., Ryerson, T.B., and Fahey, D.W.: Study of inlet materials for sampling atmospheric nitric acid, Environ. Sci. Technol., 33, 1133-1136, 1999.
Pöschl, U., Letzel, T., Schauer, C., and Niessner, R.: Interaction of ozone and water vapor with spark discharge soot aerosol particles coated with benzo[a]pyrene: O-3 and H2O adsorption, benzo[a]pyrene degradation, and atmospheric implications, 105, 4029-4041, 2001.

Pöschl, U., Rudich, Y., and Ammann, M.: Kinetic model framework for aerosol and cloud surface chemistry and gas-particle interactions: Part 1 – general equations, parameters, and terminology, Atmos. Chem. Phys. Discuss., 5, 2111–2191, 2005.

Rogak, S.N., Baltensperger, U., and Flagan, R.C.: Measurement of mass transfer to agglomerate aerosols, Aerosol Sci. Technol., 14, 447-458, 1991.

Saathoff, H., Naumann, K.H., Schnaiter, M., Schock, W., Mohler, O., Schurath, U., Weingartner, E., Gysel, M., and Baltensperger, U.: Coating of soot and $(NH_4)_2SO_4$ particles by ozonolysis products of alpha-pinene, J. Aerosol. Sci., 34, 1297-1321, 2003.

Sassen, K., DeMott, P.J., Prospero, J.M., and Poellot, M.R.: Saharan dust storms and indirect aerosol effects on clouds: CRYSTAL-FACE results, Geophys. Res. Lett., 30, doi:10.1029/2003GL017371, 2003.

Schott, J., and Oelkers, E.H.: Dissolution and Crystallization Rates of Silicate Minerals as a Function of Chemical Affinity, Pure Appl. Chem., 67, 903-910, 1995.

Seinfeld, J.H., Carmichael, G.R., Arimoto, R., Conant, W.C., Brechtel, F.J., Bates, T.S., Cahill, T.A., Clarke, A.D., Doherty, S.J., Flatau, P.J., Huebert, B.J., Kim, J., Markowicz, K.M., Quinn, P.K., Russell, L.M., Russell, P.B., Shimizu, A., Shinozuka, Y., Song, C.H., Tang, Y.H., Uno, I., Vogelmann, A.M., Weber, R.J., Woo, J.H., and Zhang, X.Y.: ACE-ASIA - Regional climatic and atmospheric chemical effects of Asian dust and pollution, Bull. Amer. Meteorol. Soc., 85, 367-380, 2004.

Sumner, A.L., Menke, E.J., Dubowski, Y., Newberg, J.T., Penner, R.M., Hemminger, J.C., Wingen, L.M., Brauers, T., and Finlayson-Pitts, B.J.: The nature of water on surfaces of laboratory systems and implications for heterogeneous chemistry in the troposphere, Phys. Chem. Chem. Phys., 6, 604-613, 2004.

Tang, I.N., and Fung, K.H.: Hydration and Raman scattering studies of levitated microparticles: $Ba(NO_3)_2$, $Sr(NO_3)_2$, and $Ca(NO_3)_2$, J. Chem. Phys., 106, 1653-1660, 1997.

Tang, Y.H., Carmichael, G.R., Kurata, G., Uno, I., Weber, R.J., Song, C.H., Guttikunda, S.K., Woo, J.H., Streets, D.G., Wei, C., Clarke, A.D., Huebert, B., and Anderson, T.L.: Impacts of dust on regional tropospheric chemistry during the ACE-Asia experiment: A model study with observations, J. Geophys. Res.-Atmos., 109, 2004.

Usher, C.R., Michel, A.E., and Grassian, V.H.: Reactions on Mineral Dust, Chem. Rev., 103, 4883-4939, 2003.

Vlasenko, A., Sjogren, S., Weingartner, E., Gäggeler, H.W., and Ammann, A.: Generation of submicron Arizona test dust aerosol: Chemical and hygroscopic properties, Aerosol Sci. Technol., 39, 452-460, 2005.

Weingartner, E., Gysel, M., and Baltensperger, U.: Hygroscopicity of aerosol particles at low temperatures. 1. New low-temperature H-TDMA instrument: Setup and first applications, Environ. Sci. Technol., 36, 55-62, 2002.

Xiong, Y., Pratsinis, S.E., and Weimer, A.W.: Modeling the Formation of Boron-Carbide Particles in an Aerosol Flow Reactor, Aiche J., 38, 1685-1692, 1992.

6. Hygroscopicity of the submicrometer aerosol at the high-alpine site Jungfraujoch, 3580 m asl, Switzerland

Published on the Atmospheric Chemistry and Physics Discussions (ACPD) website, the first publication stage of ACP, 19.09.2007.

S. Sjogren[a], M. Gysel[a], E. Weingartner[a], M. R. Alfarra[a], J. Duplissy[a], J. Cozic[a], J. Crosier[b], H. Coe[b] and U. Baltensperger[a]

[a]*Laboratory of Atmospheric Chemistry, Paul Scherrer Institut, CH-5232 Villigen, Switzerland*
[b]*School of Earth, Atmospheric and Environmental Science, University of Manchester, UK*

6.1. Abstract

Data from measurements of hygroscopic growth of submicrometer aerosol with a hygroscopicity tandem differential mobility analyzer (HTDMA) during four campaigns at the high alpine station Jungfraujoch (JFJ), Switzerland, are presented. The campaigns took place during the years 2000, 2002, 2004 and 2005, each lasting approximately one month. In parallel, size resolved chemical composition measurements with an aerosol mass spectrometer were done. A hygroscopic closure was done with the composition data using the Zdanovskii-Stokes-Robinson relation. In general, quantitative agreement between measured and modeled data was found, with some discrepancies caused by instrumental noise at low aerosol loadings. Hygroscopic growth factors (GF, i.e. the relative change in particle diameter from dry diameter, D_0, to diameter measured at higher relative humidity, RH) are presented for three distinct air mass types, namely for: 1) free tropospheric winter conditions, 2) planetary boundary layer influenced air masses (during a summer period) and 3) Saharan dust events (SDE). The GF values at 85% RH (D_0=100 nm) were 1.40±0.11 and 1.29±0.08 for the first two situations while for SDE a bimodal GF distribution was often found. No phase changes were observed when the RH was varied between 10-90%, and the continuous water uptake could be well described with a single-parameter empirical model. The frequency distributions of the average hygroscopic growth factors and the width of the retrieved growth factor distributions (indicating whether the aerosol is internally or externally mixed) are presented, which can be used for modeling purposes.

6.2. Introduction

Aerosol particles in the atmosphere affect the earth's radiation balance in various ways (e.g. Solomon et al., 2007). Firstly, aerosol particles absorb and scatter radiation. This *direct aerosol effect* is influenced by the hygroscopicity of the aerosol particles, which is determined mainly by their chemical composition. Secondly, the tendency for cloud formation and resulting cloud properties similarly depend on chemical composition as well as on size distribution of the aerosol particles (e.g. McFiggans et al., 2006). Thus the cloud albedo and the radiative properties of cloud droplets are influenced; this is termed the *indirect aerosol effect*. The presence of particulate water allows for physical processes (e.g., shape modification) or heterogeneous chemical reactions, which in turn influences the chemical composition. These processes are commonly referred to as the ageing of aerosols.

Aerosols and their properties, such as hygroscopicity, are currently modeled in global climate models (GCMs), mostly to better predict the scattering properties and size distribution under varying humidity conditions (Randall et al., 2007). Relatively few measurements of background aerosol from the lower free troposphere exist (e.g. Kandler & Schutz, 2007). To increase available data and validation possibilities four measurement campaigns at the high alpine site Jungfraujoch (JFJ), with a duration of about one month each, are presented here. During 2000, 2002, 2004 and 2005 the CLACE (CLoud and Aerosol Characterization Experiment) field studies were performed within international collaborations, including both summer and winter seasons. The general goals of the field campaigns were i) a physical, chemical, and optical characterization of the aerosol at the JFJ in order to better quantify the direct aerosol effect, and ii) an investigation of the interaction of aerosol with clouds, for a better quantification of the indirect effect. The cloud forming processes were studied under different meteorological conditions, with a special focus on aerosol-cloud partitioning in mixed-phase clouds (Cozic et al., 2007b; Verheggen et al., 2007). Further topics were the physical and chemical characterization of ice nuclei (Cozic et al., 2007a; Mertes et al., 2007), and the processes responsible for the formation of new particles in the free troposphere. Instrumentation was deployed to characterize the aerosol size distribution (scanning particle mobility sizer and optical particle counter), size segregated chemical composition (Aerodyne aerosol mass spectrometer, AMS) and hygroscopicity (hygroscopicity tandem differential mobility analyzer, HTDMA). In this study AMS and HTDMA results will be analyzed in greater detail.

Atmospheric aerosol components can be classified into inorganic and organic fractions (e.g. Kanakidou et al., 2005). The hygroscopic properties of most inorganic salts present in the atmospheric aerosol are known. Of the many organic species identified in the aerosol (e.g. Putaud et al., 2004), the hygroscopic properties of quite a few substances have been investigated. Inorganic salts (for instance ammonium sulfate (AS) and sodium chloride (NaCl)) can show a hysteresis behavior during uptake and loss of water, i.e. by exhibiting a difference between the deliquescence and efflorescence relative humidities (DRH/ERH), and with a higher water content of the deliquesced than the effloresced particles in this relative humidity (RH) range. Conversely, organic constituents of the aerosol often do not show efflorescence which can contribute to an uptake of water at lower RH than the DRH of inorganic salts. A method for characterizing water uptake is the HTDMA (Liu et al., 1978; Rader et al., 1986; Weingartner et al., 2002b). The set-up used in three of the campaigns was a low-temperature HTDMA (-10°C during the winter campaigns and 0.5°C during the summer campaign), and in the winter campaign 2005 measurements were done at laboratory temperature (25-33°C). Furthermore, measurements with an AMS supplied time- and mass-resolved chemical composition of sulfate, nitrate, ammonium and organics during the campaigns 2002, 2004 and 2005. The hygroscopic growth was predicted with the Zdanovskii-Stokes-Robinson (ZSR) relation using the measured composition from the AMS (Gysel et al., 2006; Stokes et al., 1966), and compared with the hygroscopicity measured by the HTDMA.

6.3. Methods

6.3.1. Site and air mass types

The JFJ is a European high-alpine background site located on an exposed mountain col in the Bernese Alps, Switzerland, at 3580 meters altitude (46.33 °N, 7.59 °E). Throughout the year the station is within clouds about one third of the time (Baltensperger et al., 1998). During winter it is predominantly in lower free tropospheric air masses. During summer the aerosol sampled is influenced by injections of air from the planetary boundary layer (PBL) (Baltensperger et al., 1997; Nyeki et al., 2000). The station is surrounded by glaciers and rocks, and no local vegetation is present. The JFJ boasts the highest European (electrical) railway station and is easily accessible throughout the year. Within the World Meteorological Organization (WMO) Global Atmosphere Watch (GAW) program continuous measurements of aerosol parameters are performed at the JFJ site since 1995. The research station is also part of the Swiss National Monitoring Network for Air Pollution (NABEL) and the Swiss Meteorological Institute (SMI).

The aerosol loading at the JFJ shows an annual cycle with highest concentrations in August to July and minimum concentrations in January to February (e.g. Cozic et al., 2007c; Nyeki et al., 1998; Weingartner et al., 1999). Based on comparison with the continuous aerosol measurements that are available for the JFJ since 1995, campaigns in 2000 and 2004 appear as typical winter conditions (with low aerosol concentration present in the free troposphere), while the campaign in 2002 is typical of summer conditions, and the 2005 campaign can be considered as spring-like conditions, with features situated in between winter and summer. In the following, the data are separated accordingly to these cases: non-disturbed lower free tropospheric winter conditions (abbreviated FT) and PBL influenced summer conditions (abbreviated PBL INF). Further, at times the JFJ is influenced by Saharan dust events (SDE). These events were detected according to the method described by Coen et al. (2004), which shows that during SDE the Angström exponent of the single scattering albedo is negative. This method was also corroborated by size resolved ion chromatography, where, during dust events, ~6% of the total calcium concentration was found in the PM_1 samples. Thus, a third type of air mass (abbreviated SDE) is distinguished here. The criterion used for SDE was when the Angström exponent was less than -0.1 for more than three hours. Conversely non-disturbed FT air masses were defined as the periods where the Angstrom exponent was positive, and furthermore 1 h around each SDE was removed from the data to avoid transition periods.

6.3.2. Measurements

Several different inlets were used during the experiments. In this study a heated *total inlet* (25°C) was used, which was designed to evaporate the condensed water from cloud hydro-meteors thus sampling the sum of all particles including both cloud droplet residual and interstitial particles. Calculations for this setup showed that cloud droplets smaller than 40 µm can be sampled at wind speeds up to 20 ms^{-1} (Weingartner et al., 1999). An *interstitial inlet* was operated with a PM_1 or $PM_{2.5}$ cyclone and sampled only the interstitial submicron-sized aerosol, with hydro-meteors being precipitated in the cyclone. The difference in response downstream of the two different inlets provides insight into the fractionation of aerosol particles between the cloud phase and the interstitial phase.

Table 6-1 lists the dates for the campaigns as well as details of instruments used and setup of the HTDMA.

Table 6-1. Overview of the campaigns.

		Dry diameter, D_0 [nm]		
2000 – Winter		50	100	250
Date	21.02 to 27.03.2000			
Number of scans* at constant RH		1698	1855	1648
Number of humidograms		11	15	11
T setting HTDMA, inlet type	-10°C, interstitial, PM_1			
2002 – Summer				
Date	08.07 to 17.07.2002			
Number of scans* at constant RH		528	746	517
Number of humidograms		4	43	4
T setting HTDMA, inlet type	0.5°C, interstitial, PM_1			
2004 – Winter				
Date	01.03 to 01.04.2004			
Number of scans* at constant RH		499	1767	1295
Number of humidograms		4	4	4
T setting HTDMA, inlet type	-10°C (as well as shortly 20°C), interstitial, $PM_{2.5}$			
2005 - Spring-like				
Date	13.02 to 16.03.2005			
Number of scans* at constant RH		306	1533	162
Number of humidograms		6	6	6
T setting HTDMA, inlet type	25°C, total inlet			

*each scan had a duration of 300 s.

6.3.3. AMS (Aerosol Mass Spectrometer)

An Aerodyne quadruple AMS (Jayne et al., 2000) was used to provide on-line, quantitative measurements of the total mass and size distributed non refractory chemical composition of the submicron ambient aerosol at a high temporal resolution. The instrument works by sampling air through an aerodynamic lens to form a particle beam in a vacuum and accelerating the focused beam of particles as a function of their momentum towards a tungsten heater (550°C) that flash vaporizes the particles. The volatilization stage is performed adjacent to an electron impact ionizer (about 70 eV) and the ions are analyzed by a quadruple mass spectrometer (QMA 410, Balzers, Liechtenstein) with unit mass-to-charge (*m/z*) resolution. In typical field operation, the AMS alternates between two modes: (i) in the mass-spectrum (MS) mode the averaged chemical composition of the non-refractory (NR) aerosol ensemble is determined by scanning the *m/z* spectrum with the quadruple mass

spectrometer, without size resolved information, (ii) using the aerosol time-of-flight (ToF) mode selected *m/z* representative of key chemical components can be resolved as a function of the vacuum aerodynamic diameter of the particles. More detailed descriptions of the AMS measurement principles and various calibrations (Canagaratna et al., 2007; Jayne et al., 2000), its modes of operation (Jimenez et al., 2003) and data processing and analysis (Allan et al., 2004; Allan et al., 2003) are available. The AMS supplies the concentrations of inorganic ions, i.e. sulfate, nitrate and ammonium. It has been reported that these ions account for 96% of the composition of inorganic ions at the JFJ (Cozic et al., 2007c; Henning et al., 2003; Krivacsy et al., 2001). Furthermore the total concentration of the organic content is supplied, although no detailed speciation is possible. Mass loadings at the JFJ site are generally low. Therefore 3-h averages were calculated as a compromise between counting statistics and time resolution.

6.3.4. Black carbon concentration

During the first two campaigns 2000 and 2002 the black carbon (BC) concentration was measured with an AE 31 Aethalometer (at wavelength λ = 880 nm) (Weingartner et al., 2003). During the last two campaigns BC was measured with a multiple angle absorption photometer (MAAP, at wavelength λ = 630 nm) as well with an AE 31 Aethalometer (at λ = 880 nm). A mass absorption efficiency of 7.6 m^2g^{-1} for winter and 11.1 m^2g^{-1} for summer was used for the MAAP data (Cozic et al., 2007c). BC concentrations from the aethalometer were determined accordingly, taking advantage of a high correlation between these two instruments during simultaneous measurements (Cozic et al., 2006). As no size resolved BC measurements were available it was assumed that the BC fraction in each size range was independent of size and thus equal to the BC fraction in PM1 (defined as the sum of the AMS and the BC data). The choice of the mass absorption efficiency for the BC concentration and the assumption of size independence are not critical due to the low sensitivity of the hygroscopicity closure to these values.

6.3.5. HTDMA (Hygroscopicity Tandem Differential Mobility Analyzer)

Briefly, the HTDMA functions as follows: a differential mobility analyzer (DMA1) selects a monodisperse aerosol size cut with mobility diameter, D_0, under dry conditions. The aerosol then passes through a humidifier with a controlled higher RH, and the mobility diameter D is measured with a second DMA (DMA2). The two DMAs are similar to the TSI 3071 type. The relevant RH in DMA2 was determined by measurement of the system temperature and the DMA2 excess sheath air dew point using a dew point mirror (model 2002 Dewprime, EdgeTech). The accuracy of the RH measurement at higher RH is for example 85±1.1%, assuming no temperature gradients in the DMA2. The residence time of the sampled aerosol at the set RH was >20 s before size measurement (Sjogren et al., 2007). The HTDMAs were employed in slightly different ways during the different campaigns (see Table 6-1). In general the HTDMA measured at constant RH, set to 85%. On occasions the RH-dependence of the hygroscopic growth was investigated by both increasing and decreasing the RH in DMA2 between 10 and 85%. These are known as the dehydration and hydration modes of operation, respectively. This allows for detecting potential hysteresis effects in the hygroscopic growth behavior with distinct efflorescence and deliquescence transitions. The hydration mode, where the mono-modal dry particles were exposed to a monotonically increasing RH in the HTDMA prior to the size measurement in DMA2 (allowing measurements of DRH), was applied during all campaigns, and is also the mode of operation used during measurements at constant RH. The dehydration mode, where the dry particles are first exposed to RH>80% using a pre-humidifier before monotonically lowering the RH towards the RH in DMA2 (Gysel et al., 2004; Sjogren et al., 2007), was mainly applied during the 2004 winter campaign (allowing measurements of ERH).

The hygroscopic growth factor (GF) indicates the relative increase in mobility diameter of particles due to water absorption at a certain RH, and is defined as

$$GF(RH) = \frac{D(RH)}{D_0} \ , \qquad \textbf{(6-1)}$$

where *D(RH)* is the mobility diameter at a specific RH and D_0 is the particle mobility diameter measured under dry conditions (91% of the data were with DMA1 at RH<15%. However to increase available data we included periods where the RH in DMA1 was up to 35%, the water uptake being no more than 3% at 35% RH for the ambient aerosol). Mobility diameter growth factors obtained with an HTDMA are only equal to volume equivalent growth factors if the particles do not change their shape during water uptake. This assumption is justified as the hygroscopicity was characterized by a continuous growth curve for the majority of the time (see below), thus the particles can be considered liquid and consequently roughly spherical at all measured RH. During the first three campaigns both DMAs and the humidifier were inserted in a well-circulated water bath, ensuring constant temperature as indicated. The aerosol line was cooled and insulated from the outside of the building to the entry of the first DMA. This ensured that no artifacts during the sampling occurred (i.e. volatilization of semi-volatile material), as the measurements were performed close to ambient temperatures (Gysel et al., 2002; Weingartner et al., 2002b). During the campaign 2005 the first DMA was maintained at the laboratory temperature (25-33°C) and only DMA2 was kept at a constant temperature in a water bath (22.8°C) (Sjogren et al., 2007). This was done because of the functionality of the HTDMA used, and because it was deduced from the three first campaigns that temperature artifacts were negligible (i.e. compared to measurement uncertainties). The HTDMA data were averaged to 3h, in order to match the AMS time series. The performance of the instruments was verified with extensive testing with AS and NaCl before the campaigns. During 2004 and 2005 these salts were also measured at JFJ. The growth of AS and NaCl particles was compared with the theoretical prediction using the Aerosol Diameter-Dependent Equilibrium Model (ADDEM) (Topping et al., 2005a; Topping et al., 2005b), and corresponded to within less than 0.04 in GF at 85% RH.

Inversion algorithm

Atmospheric particles of a defined dry size typically exhibit a range of growth factors or even clearly separated growth modes, because of external mixing or variable relative fractions of different compounds in individual particles (hereinafter referred to as quasi-internally mixed). Growth factor probability distributions *c(GF)=dC/dGF* are retrieved from each measurement, and normalised such that $C = \int c(GF)dGF = 1$. The inversion method applied to the raw data (Gysel et al., in prep.) has similarities to the inversion algorithm described by Cubison et al. (2005). The distribution *c(GF)* is also inverted from the measurement distribution into contributions from fixed classes of narrow growth factor ranges, but instead of using a linear inversion, c(*GF*) is fitted to the actual measurements using a full TDMA transfer forward model. A bin resolution of ΔGF=0.15 was chosen for the inversion because of counting statistics. The AMS provides chemical composition data for the entire submicron aerosol particle ensemble in the air sample, whereas no information on the mixing state of individual particles is obtained. Inverted growth factor distributions *c(GF)* obtained with the HTDMA provide some information on the mixing state. The ensemble mean growth factor *GF** is defined as the 3rd-moment mean growth factor of *c(GF)*. *GF** represents the growth factor that would be observed if the absorbed water were equally distributed among all particles, even in the case of several distinct growth modes. Thus *GF** is the quantity to be compared with growth factor predictions based on composition data obtained by the AMS (see below). Thus even if the measured GF is broad or even clearly bimodal *GF** would represent the hygroscopicity as predicted from the AMS data as long as the AMS can measure all the relevant chemical components in both modes. This is not the case if some of the material sampled is composed of a refractory component such as dust or sea salt that cannot be observed by the AMS.

The standard deviation σ of the inverted growth factor distribution *c(GF)* is used as a measure for the spread of growth factors. With a bin resolution of ΔGF=0.15 as chosen here for the HTDMA data inversion, the σ that would be obtained for a perfectly internally mixed aerosol with a well defined growth factor (i.e. σ =0) is between 0.06 and 0.10 depending on the bin positions relative to the *GF**. The σ obtained with pure ammonium sulfate at 85% RH is <0.05, when inverting the data with high resolution. Therefore any $\sigma \leq 0.10$ indicates absence of distinct growth modes, i.e. a quasi-internal mixture with limited spread of growth factors, while any $\sigma \geq 0.15$ shows that the aerosol is externally mixed or quasi-internally mixed with substantial spread of growth factors. We use the σ not only to describe the spread of a single mode, but also in the sense of describing a broader distribution, or describing cases which are clearly bimodal. Two HTDMA measurement examples (red) and corresponding inverted growth factor distributions (green) as well as the inverted growth distribution reprocessed through the HTDMA forward model (blue) are shown in Fig. 6-1. Panel A shows an aerosol observed during undisturbed FT conditions with *GF**=1.28 and σ =0.08, indicating that it was internally mixed. Panel B shows an aerosol observed during an SDE with σ =0.22. This aerosol is obviously externally mixed with two distinct modes at GF=1.070 and GF=1.488, whereof the former can be attributed to mineral dust. The *GF** is 1.227 and is not representative of the hygroscopic behavior of the aerosol but would be the value to compare with the predicted hygroscopicity from the ensemble chemical composition, which would need to take mineral dust into account. In this case the blue line does not exactly follow the measurement because of the limited resolution of the inversion. However, better results cannot be obtained even with increasing the resolution, because the measurement uncertainties are too big at such a low number of measured counts.

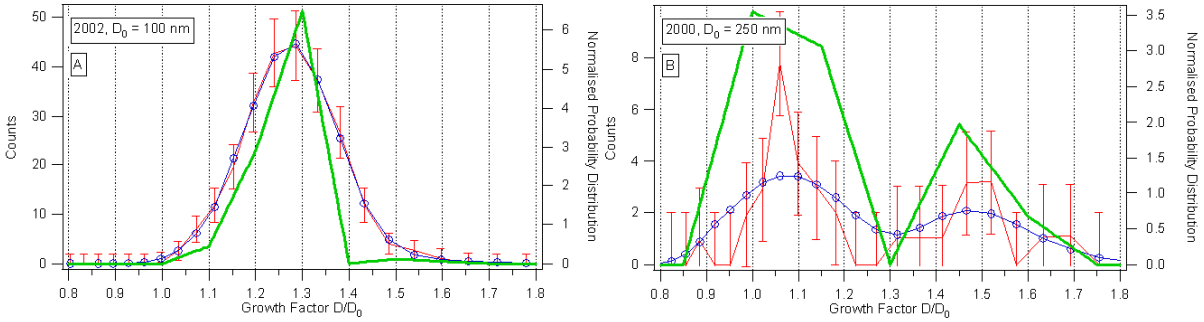

Fig. 6-1. Typical examples of growth factor distributions of 100 nm particles (GF=1.28) and σ=0.08 (Panel A, 12.7.2002 18:00) and of 250 nm particles during a SDE (Panel B, 17.3.2000 20:24), with a first mode at GF=1.070 and a second mode at GF=1.488 (overall σ=0.22). The red line and points (left axis) refer to measured particle counts, the green line is the inverted GF distribution (right axis) and the blue line inverted growth distribution reprocessed through the forward model (left axis). Error bars indicate the estimated counting uncertainty of the measurement.

6.3.6. Correction of HTDMA data to 85% RH

The measurements were generally done at 85% RH. To obtain a more complete time series data set, data between 80 and 90% RH were corrected to 85% RH using the following equation:

$$k(GF, a_W) = \frac{(GF^3 - 1)(1 - a_W)}{a_W} \Leftrightarrow GF_{RH=85\%}(a_W, k) = \left(1 + k\frac{a_W}{1 - a_W}\right)^{1/3} \qquad \textbf{(6-2)}$$

where k captures all solute properties. a_w is the water activity. First the k-value was calculated from the measured GF and RH (left hand side of Eq. 6-2), and then the corresponding corrected GF at 85% was calculated using this k (right hand side of Eq. 6-2). Eq. (6-2) is equivalent to Eq. (4) in the paper by Gysel et al. (2004) with

$k = (M_W \rho_S i_S)/(\rho_W M_S)$, where M_w is the molar mass and ρ_w the density of water, and M_s the molar mass, ρ_s the density and i_s the van't Hoff factor of the solute. Eq. (6-2) is also equivalent to Eq. (1) in the paper by Dick et al. (2000) with $a = k$ and $b = c = 0$, where a, b, and c are their model parameters. More details about the theoretical background of the functionality of Eq. (6-2) are given in Kreidenweis et al. (2005). Using a constant k-value for RH corrections is equivalent to a constant van't Hoff factor, which means constant deviation from ideal behavior. This assumption is justified for differences of ±5% RH as chosen here.

6.3.7. ZSR relation

The hygroscopic growth factor of a mixture (GF_{mixed}) can be estimated from the growth factors of the individual components of the aerosol and their respective volume fractions, ε, with the ZSR relation (Gysel et al., 2004; Stokes et al., 1966):

$$GF_{mixed} = \left(\sum_k \varepsilon_k GF_k^3 \right)^{1/3}, \quad \textbf{(6-3)}$$

where the summation is performed over all compounds present in the particles. The model assumes that: the particles are spherical; ideal mixing behavior (i.e. no volume change upon mixing); and independent water uptake of the organic and inorganic components. The volume fractions ε_i for the components in the particles were calculated as

$$\varepsilon_i = \frac{(w_i / \rho_i)}{\sum_k (w_k / \rho_k)}, \quad \textbf{(6-4)}$$

where w_i is the mass fraction and ρ_i the density of component i.

The AMS measured size-resolved component mass during the last three campaigns: 2002, 2004 and 2005. We compared the fraction of particles in the range 88-196 nm vacuum aerodynamic diameter (d_{va}) from the AMS with the measured 100 nm mobility diameter (d_{mob}) from the HTDMA. The range was chosen so that the volume difference was equal on each side of 100 nm, (i.e. 49-122 nm in d_{mob}). The chosen width of the size range is a compromise between size resolution and signal statistics. The mobility diameter can be calculated from the aerodynamic diameter as follows (Zelenyuk et al., 2006), with the assumption that the particles are spherical (χ_v=1, dynamic shape factor in the free molecular regime):

$$d_{mob} = \frac{\rho_0}{\rho_p} \frac{d_{va}}{\chi_v}, \quad \textbf{(6-5)}$$

Where ρ_0 is standard density (1000 kg m^{-3}) and ρ_p is the particle density. The particle density was calculated from the bulk composition averaged over the campaigns and was 1565 kg m^{-3}. In general the hygroscopicity, predicted with ZSR relation, is more sensitive to substances with higher GF than the ones closer to 1.0 due to the cubic weighting. Thus it is more important to accurately predict the hygroscopicity of the pure inorganic salts, than the organic or the soot components. A second factor of importance is the fraction of the more hygroscopic substances. All individual growth factors and densities used were taken from literature (see Table 6-2).

Table 6-2. GF's for pure substances and physical properties used (Bulk properties, Topping et al., 2005a).

Substance	GF (at a_w = 0.85)	Density [kg m^{-3}]
$(NH_4)_2SO_4$	1.56	1769
NH_4HSO_4	1.62	1780
NH_4NO_3	1.59	1720
H_2SO_4	1.88	1830
BC	1.0	2000
Organics	1.20[a]	1400[b]

[a]The growth factor of the organics was chosen to give a best fit between measurement and model. This value is in accordance with the GF measured for secondary organic aerosol (SOA) (Duplissy, J., Gysel, M., Alfarra, M. R., Dommen, J., Metzger, A., Prevot, A. S. H., Weingartner,E., Laaksonen, A., Raatikainen, T., Good, N., Turner, S. F., McFiggans, G. and Baltensperger, U.: The cloud forming potential of secondary organic aerosol under near atmospheric conditions, Geophys. Res. Lett., submitted, 2007; Baltensperger et al., 2005).

[b]The density of organics was chosen to represent oxidized organics in aged atmospheric aerosol (Alfarra et al., 2006; Dinar et al., 2006).

6.3.8. Neutralization of aerosol

If one considers the major ions present in the JFJ PM_1 aerosol, and the ones with concentrations available from the AMS and filters, namely SO_4^{2-}, NO_3^-, NH_4^+, the aerosol mixture was mostly neutralized (Cozic et al., 2007c). However, occasionally the measured ammonium concentration was insufficient to fully neutralize the sulfuric acid, indicating an acidic aerosol. Then it was assumed that an equilibrium with first NH_4HSO_4 and subsequently H_2SO_4 was formed. As expected during cases with incomplete neutralization the NO_3^- values were low. Note that this choice of sulfate salts is crucial for a correct application of the ZSR mixing rule, i.e. choosing only a combination of H_2SO_4 and $(NH_4)_2SO_4$ to match the measured sulfate and ammonium concentrations would result in significant prediction errors (Gysel et al., 2006). Splitting the sulfate salts based on the measured ammonium may not be highly accurate, but it indicates at least whether the aerosol is neutralized or acidic. The mass fractions of the different components are shown in the time series in Fig. 6-4.

6.4. Results

6.4.1. Hygroscopicity at the JFJ

The RH-dependence of GF was measured by variation of the RH in the HTDMA between 10 and 85%. Figure 6-2 shows three typical humidograms examples showing the features observed at the JFJ. Generally a continuous growth without differences between hydration and dehydration operating mode was found, thus indicating absence of phase changes. This does not exclude existence of efflorescence at RH<10%, because our measurements were technically limited to RH>~10%. Such continuous growth is expected and has been reported for complex mixtures with an increasing number of organic components (Marcolli et al., 2004; Marcolli & Krieger, 2006). The aerosol at the JFJ seems to exist predominantly as dissolved liquid or amorphous particles. Furthermore, the growth curves can be well described with the single-parameter (*k*) semi-empirical model given in Eq. 6-2, as can be seen from the solid lines in Fig. 6-2. The growth curves were also fitted with an empirical power law fit $GF=(1-a_w)^{\gamma}$ (Swietlicki et al., 2000), dashed lines in Fig. 6-2, but for this model we found consistently larger χ^2-residuals than with the former model. As can be seen from Fig. 6-2, 6-3 and 6-4 the magnitude of the hygroscopic growth at the JFJ varies substantially over time, but the RH-dependence at any time can be captured with a single parameter (*k*).

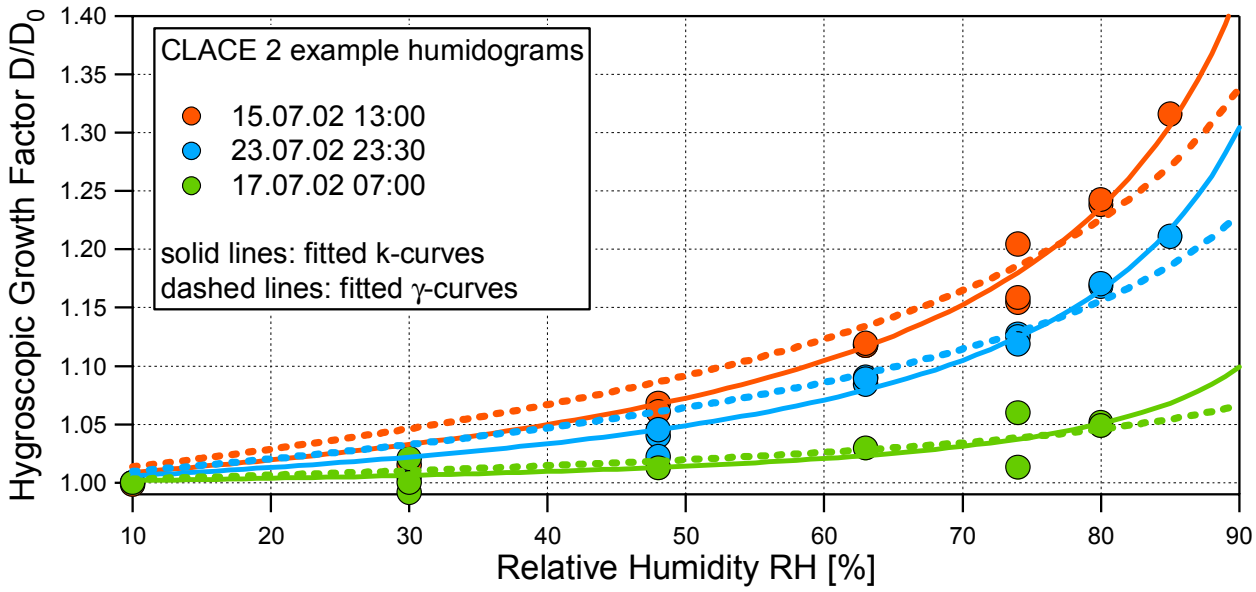

Fig. 6-2. Typical humidograms of particles with D_0 = 100 nm sized particles during July 2002 (the other campaigns gave similar results). The hygroscopicity at the JFJ varies with varying season and origin of air parcels, but the water uptake at a specific time can be well described as a function of RH with a single-parameter model (solid lines).

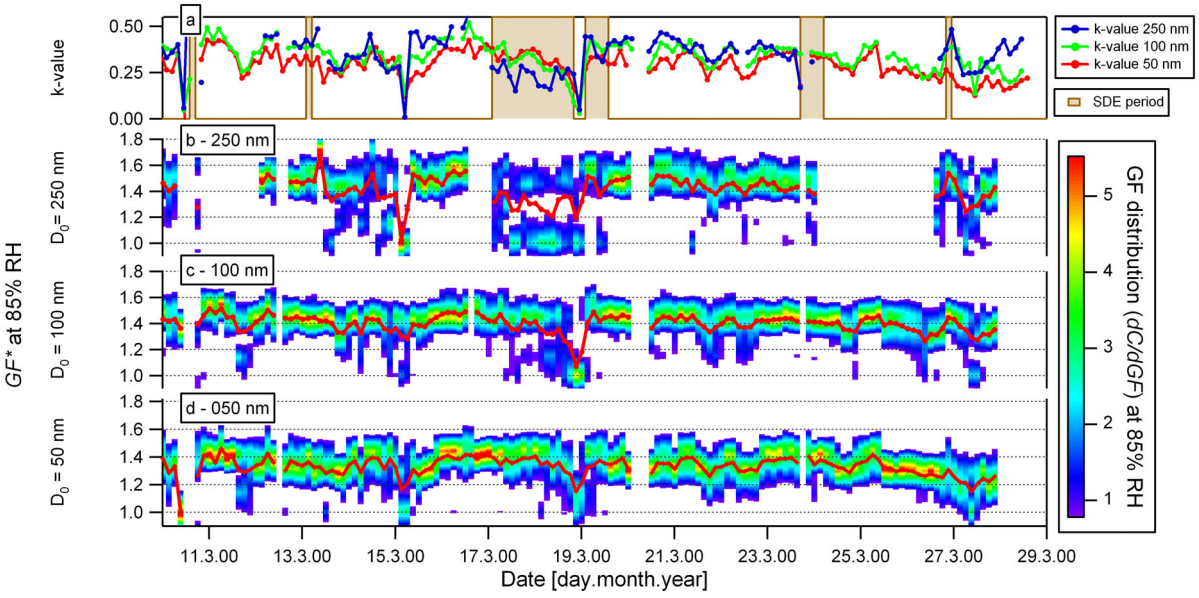

Fig. 6-3. Temporal evolution of GF distributions for GF all measured sizes (50, 100, 250 nm) at RH=85%, during year 2000. Panel a shows the *k*-values indicating the solubility of the aerosol. The red lines on panels b, c and d represent the ensemble mean growth factor *GF.**

Figure 6-3 shows the temporal evolution of GF distributions for a period of the campaign in 2000. Several SDE were observed, as indicated with the shaded areas in panel a. During undisturbed FT conditions, a size dependence of the growth factor can be seen, with larger growth for larger particles. This feature, which has previously been shown by Weingartner et al. (2002b), was also observed during the other campaigns and is attributed to a size dependent chemical composition. This is confirmed by larger *k*-values at larger dry diameters (top panel of Fig. 6-3), which are a measure of the hygroscopicity without the influence of the Kelvin effect. The ensemble *k*-values have been calculated from the ensemble mean growth factor *GF** using Eq. 6-2, whereas the water activity corresponding to the measured RH has been calculated assuming surface tension of pure water. It is

hypothesized that smaller particles contain a larger fraction of organic compounds from secondary organic aerosol (SOA) formation. Such a dependence was confirmed by AMS measurements during summer 2002 (Alfarra, 2004). During major SDE two distinct growth modes can be seen for the 250 nm particles, while no clear change in hygroscopic behavior is seen for the 50 nm particles. This is also reflected in strongly decreasing *k*-values at D_0=250 nm, while little or no changes occur at D_0=100 and 50 nm. Thus mineral dust particles are only found at larger sizes. As during SDE larger sized particles are more externally mixed, the reduction of the *k*-value in these periods only reflects the influence of the increasing amount of particles, presumably mineral dust, with lower hygroscopicity, not the *k*-value of each mode.

In summer, a strong diurnal variation is typically found in most aerosol variables (Lugauer et al., 2000). During the 2002 campaign this diurnal variation was also present in the observed mass loadings, though to a slightly lesser extent (Alfarra, 2004). However, the mass fractions of different components did not vary to a large degree during this diurnal variation, resulting in a fairly constant hygroscopicity on a timescale of hours seen both in the HTDMA results and in the closure (Fig. 6-4). However, more data with days showing a strong diurnal variation are required for a conclusive description of this influence. As can be seen from the *GF** values in Table 6-3, the summer campaign is characterized by lower hygroscopicity, due to a higher organic loading (68% in summer compared to 42% in winter). This is most probably due to higher emission rates of SOA precursors and higher photo-oxidation activity, which can also be transported upwards through valley venting.

Figure 6-4 shows the predicted growth and *GF** for the campaigns 2002, 2004 and 2005 (no high time resolution composition data were available for 2000). A growth factor for organic compounds of 1.2 at a_w=0.85, corresponding to 1.182 for a 100 nm particle at 85% RH was used in this work, which is in agreement with smog chamber experiments of organic aerosols (Duplissy et al., 2007; Baltensperger et al., 2005). The sensitivity to this value was tested by comparing the model fit to the data over several values of GF_{org} and 1.2 at a_w = 0.85 gave the best fit with a slope of 1, though the fit is relatively insensitive as the influence of GF_{org} is relatively low compared to the influence of the inorganic fraction. The mass spectrum delivered by the AMS at the Jungfraujoch is characterized by a relatively low *m/z* 57 signal indicating that little unprocessed primary organic material is present and that the majority of the organics are composed of oxidized organic mater (Alfarra et al., 2006; Zhang et al., 2007). During SDE there will be an increased fraction of mostly insoluble mineral dust material (Vlasenko et al., 2006) which is not detected in the AMS. This will lead to an increase in the predicted GF compared to the measured one. However, during 2004 some SDE were detected when both instruments were in operation, but the residuals from measured minus predicted hygroscopicity for these SDE were similar to FT conditions. Probably the mass fraction of mineral dust components were not sufficiently high in the sizes <250 nm to significantly influence the ensemble mean growth factor *GF**.

Recently, Gysel et al. (2006) have found significant discrepancies between measured and predicted GFs if substantial mass fractions of ammonium nitrate were present. They concluded that the most likely cause for the discrepancies was an evaporation artifact of ammonium nitrate in the HTDMA, which was operated at ~25 °C and with a residence time of ~60 s. No systematic prediction bias for data points with high ammonium nitrate mass fraction was found in the data set presented here. An important difference is that the HTDMA measurements of this study were mostly done at low temperatures (T=-10 to 0.5°C) and the residence time was kept short (in the order of 20 s), thus minimizing potential evaporation artifacts.

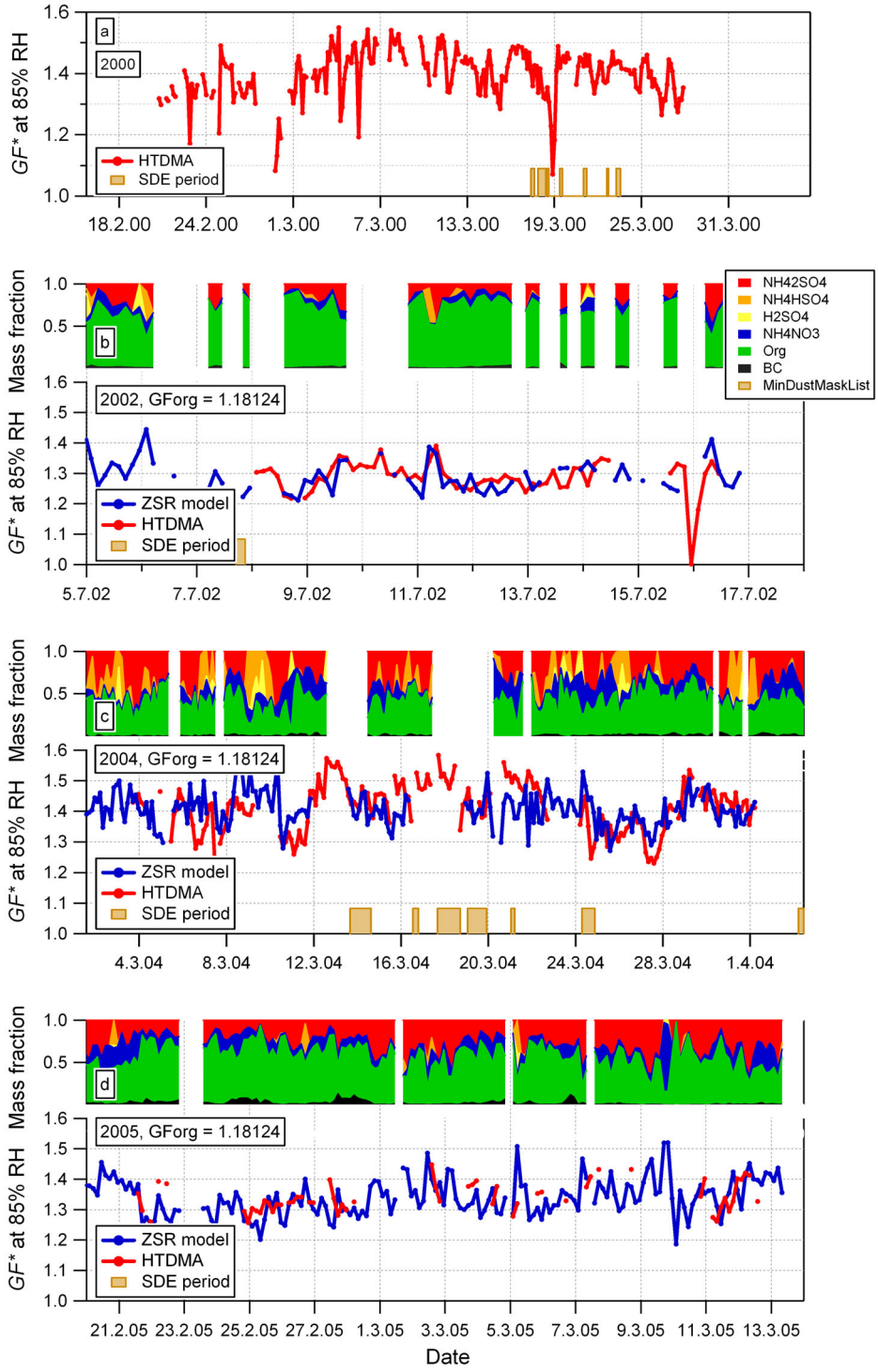

Fig. 6-4. Time series of the *GF for D_0=100 nm particles at JFJ for each campaign measured (each lower panel), as well as the chemical composition (each top panel). The predicted *GF** from composition data is shown as the blue line in the GF panels and the measured in red. During winter 2000 no high time resolution composition data were available.**

6.4.2. Frequency distributions of GF^* *and σ*

Panels A, D and G of Fig. 6-5 show the averages of the normalized measured GF distributions for each dry size studied and for each air mass category. The air mass types distinguished in this analysis are the SDE, the non-disturbed FT conditions as well as the cases influenced by injections from planetary boundary layer air (i.e., during summer, PBL

INF). These averaged growth distributions illustrate the mean number fraction of particles in a defined air mass type exhibiting a certain growth factor, unlike Fig. 6-1 which shows snapshot growth distributions for a specific time. Thus the averages do not necessarily indicate the mixing state of the aerosol as the temporal variability increases the spread. Most of the time at JFJ one expects to encounter non-disturbed FT conditions or PBL INF during summer. It has been shown in Coen et al. (2004) that SDE are present only 5% of the time (yearly average). For the FT conditions the 50 and 100 nm particles appear internally mixed, however with a small fraction of particles with a GF between 1.0-1.2, which is not easily resolved with the inversion considering the instrument limits and the low mass loading. For the 50-nm particles this shoulder at low GFs is less pronounced, but this is to some extent a consequence of the smaller hygroscopicity of the main mode, which is slightly overlapping with this shoulder. Kandler et al. (2007) also reported GF values for March 2000 at the JFJ (measured at 90% RH at ~20°C), which are in agreement with the GFs shown here. Kandler et al. (2007) indicated a bimodal distribution for all sizes, however they do not show the relative number fractions in each mode, which, if small for the lower GF mode, would be in agreement with our data. The PBL INF measurements show a more homogeneous GF distribution, but the hygroscopicity is also lower. SDE only occurred during the two winter campaigns, and for these cases the D_0 = 250 nm particles showed an increase of non-hygroscopic particles in a distinct mode with a GF of 1.0. The hygroscopic properties of the D_0 = 50 and 100 nm particles do not differ between SDE / FT. Panels B, E, and H of Fig. 6-5 show the frequency distribution of *GF**, from which the mean *GF** presented in Table 6-3 has been calculated. The hygroscopicity for summer indicates a similar chemical composition for different sizes, while during winter the hygroscopicity increases with size.

Panels C, F and I of Fig. 6-5 show the frequency distribution of σ averaged for each of the relevant periods. The σ of individual scans can be used to distinguish between quasi-internally mixed aerosols with limited growth factor spread ($\sigma \leq 0.1$) and externally or quasi-internally mixed aerosols with substantial spread ($\sigma \geq 0.15$). The frequency distribution of σ thus indicates the fraction of time of each period that a certain mixing state (σ) is encountered. The most frequent spread observed in summer is σ ~0.125 which is internally mixed, whereas larger spread is seen in winter FT conditions. This can be attributed to a larger separation of the main growth mode from the minor fraction of particles with growth factors <1.2. For the same reason the spread also increases with particle size in winter with σ ~0.1, 0.125 and 0.15 for 50, 100 and 250 nm particles, respectively. This indicates that even under FT conditions observed during winter the aerosol contains a fraction of particles which appear to remain less processed and thus less hygroscopic also at a remote location. The mineral dust during SDE mostly influences the larger particles with D_0=250 nm, as already exemplified in Figs. 6-3 and 6-5A. Here it has to be stressed that different scenarios can end up with a bimodal shape of the mean GF distribution as shown in Fig. 6-5A. Either the GF distribution is always bimodal with similar number fractions of particles in both modes, or only monomodal but the GF distribution are observed with the mode centered at GF~1.0 or GF~1.45 during 50% of the time each. Frequent occurrence of $\sigma \geq 0.2$ and *GF**=1.3-1.5 for D_0=250 nm during SDE indicates that the former alternative with simultaneous presence of non-hygroscopic mineral dust and more hygroscopic background particles, both in comparable number fractions, dominates. No clear influence of SDE on σ and *GF** is seen at 50 and 100 nm confirming the finding from panels D and G.

The frequency distributions of the GF^* and σ can be used to simulate internally or quasi- internally mixed hygroscopic behavior of particles in different air masses encountered at the JFJ. Additionally to the frequency distributions it has to be known whether GF^* and σ are dependent on each other. We explored the relationship between the two distributions, but no dependence between *GF** and σ was found. This is different from results found by Aklilu and Mozurkewich (2004) in Lower Fraser Valley, British Colombia, who have reported a horseshoe-shaped relationship with maximum σ values at intermediate GF.

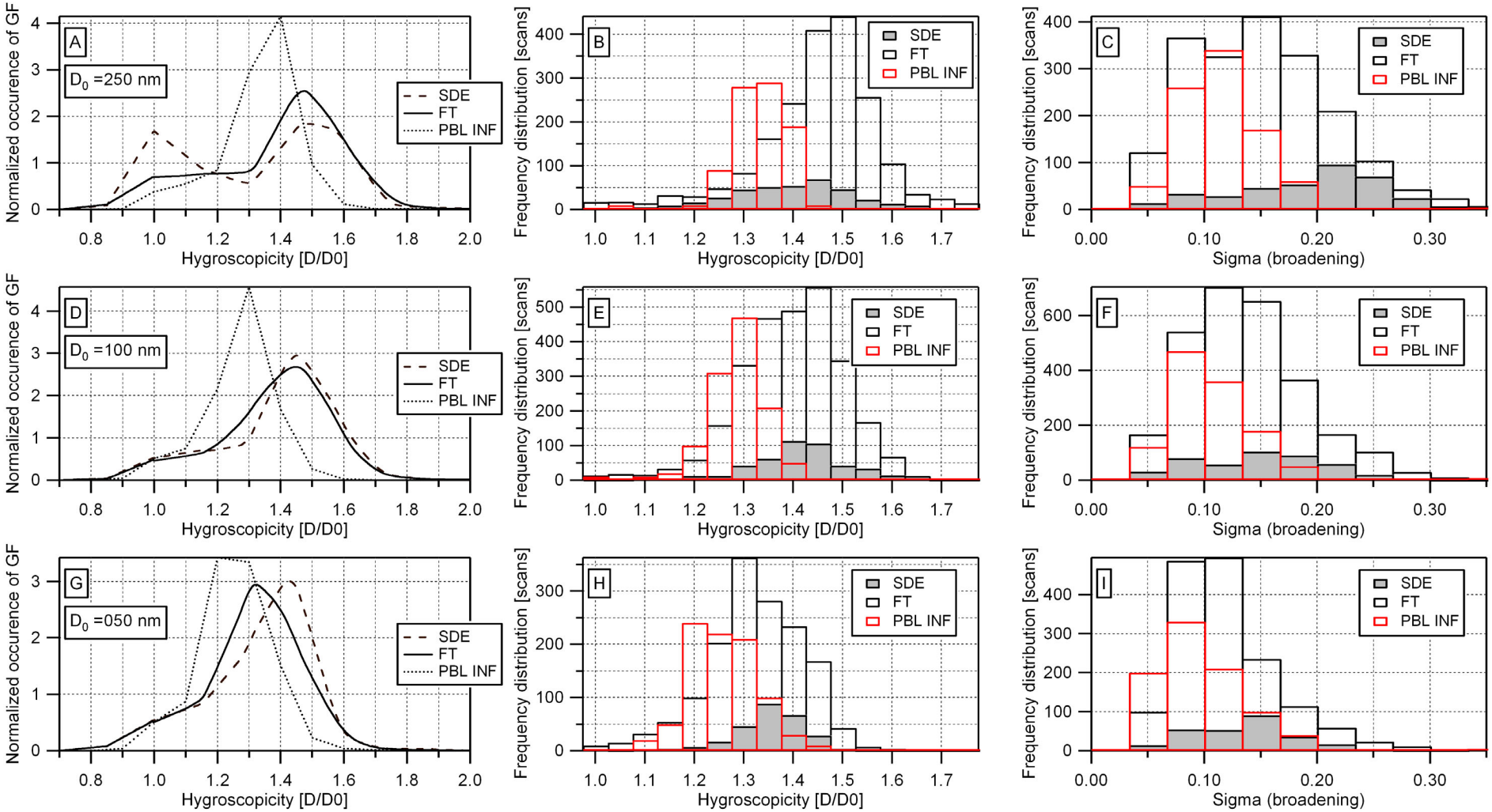

Fig. 6-5. From top row to bottom, the dry sizes D_0 = 250, 100, 50 nm are presented. First column shows the GF distribution for SDE, FT and PBL INF conditions. Second column shows the frequency distribution of GF^*. Third column shows the frequency distribution of the spread of the scans, σ.

Table 6-3. Summary of averages of GF and σ for the campaigns.

Campaign date	Feb-Mar 2000			July 2002			Mar 2004			Feb-Mar 2005		
Season		Winter			Summer			Winter			Spring-like	
Dry sizes [nm]	50	100	250	50	100	250	50	100	250	50	100	250
Average *GF** at 85% RH	1.33	1.40	1.41	1.26	1.29	1.35	1.34	1.40	1.47	1.30	1.35	1.42
-Std.dev.	0.091	0.104	0.133	0.090	0.076	0.081	0.122	0.112	0.114	0.081	0.076	0.076
N (3h averages)	1698	1855	851	528	746	517	499	1767	1295	306	1533	162
σ	0.13	0.15	0.19	0.08	0.10	0.12	0.11	0.13	0.15	0.17	0.16	0.16
-Std.dev. of σ	0.041	0.046	0.070	0.045	0.043	0.043	0.050	0.055	0.063	0.095	0.058	0.089
Median *GF** at 85% RH	1.34	1.41	1.44	1.25	1.29	1.36	1.33	1.41	1.48	1.31	1.34	1.41

6.5. Conclusions

A statistical analysis of measurements from four field campaigns of about one month each at the high alpine site Jungfraujoch is presented. During the winter season when the station was in the undisturbed free troposphere, the average GF measured with an HTDMA was 1.40±0.11 at 85% RH for 100 nm particles. During the summer season, due to higher SOA formation, the GF was 1.29±0.08 at 85% RH. During mineral dust events GF distributions were partly bimodal for D_0 = 250 nm particles. The frequency distributions of the width of the retrieved growth factor (internally/externally mixed) distributions are presented, which can be used to compare with simulations of the hygroscopic behavior of the aerosol encountered at the JFJ. The hygroscopicity was also predicted using the ZSR mixing rule along with chemical composition data. The ZSR mixing model can qualitatively describe the variability of measured hygroscopicity of submicrometer particles. However, due to low loadings at the JFJ (apart from times when influenced by PBL), the spread in error of the predicted GF from the chemical composition as well as the error for the HTDMA measurement is on average +/- 0.1, which makes it difficult to verify the absolute hygroscopicity values. The most important factor for the modeling is the accuracy in GFs of the inorganics and their composition. It is also important to consider the separation of SO_4^{2-} into ammonium sulfate, ammonium bisulfate and sulfuric acid.

Acknowledgements

This work was supported by the Swiss National Science Foundation Switzerland (grant n° 200021-100280), MeteoSwiss in the framework of the Global Atmosphere Watch Program as well as the EC project ACCENT. The UMan measurements were supported by the UK Natural Environment Research Council. We thank the International Foundation High Altitude Research Stations Jungfraujoch and Gornergrat (HFSJG), who made it possible for us to carry out our experiments at the High Altitude Research Station at Jungfraujoch, and also the caretakers at the station.

References

Aklilu, Y. A., & Mozurkewich, M. (2004). Determination of external and internal mixing of organic and inorganic aerosol components from hygroscopic properties of submicrometer particles during a field study in the Lower Fraser Valley. *Aerosol Science and Technology*, *38*, (2), 140-154.

Alfarra, M. R., Paulsen, D., Gysel, M., Garforth, A. A., Dommen, J., Prevot, A. S. H., Worsnop, D. R., Baltensperger, U., & Coe, H. (2006). A mass spectrometric study of secondary organic aerosols formed from the photooxidation of anthropogenic and biogenic precursors in a reaction chamber. *Atmospheric Chemistry and Physics*, *6*, 5279-5293.

Allan, J. D., Delia, A. E., Coe, H., Bower, K. N., Alfarra, M. R., Jimenez, J. L., Middlebrook, A. M., Drewnick, F., Onasch, T. B., Canagaratna, M. R., Jayne, J. T., & Worsnopf, D. R. (2004). A generalised method for the extraction of chemically resolved mass spectra from aerodyne aerosol mass spectrometer data. *Journal of Aerosol Science*, *35*, (7), 909-922.

Allan, J. D., Jimenez, J. L., Williams, P. I., Alfarra, M. R., Bower, K. N., Jayne, J. T., Coe, H., & Worsnop, D. R. (2003). Quantitative sampling using an Aerodyne aerosol mass spectrometer: 1. Techniques of data interpretation and error analysis (vol 108, art no 4090, 2003). *Journal of Geophysical Research-Atmospheres*, *108*, (D9).

Ansari, A. S., & Pandis, S. N. (1999). Prediction of multicomponent inorganic atmospheric aerosol behavior. *Atmospheric Environment*, *33*, (5), 745-757.

Badger, C. L., George, I., Griffiths, P. T., Braban, C. F., Cox, R. A., & Abbatt, J. P. D. (2006). Phase transitions and hygroscopic growth of aerosol particles containing humic acid and mixtures of humic acid and ammonium sulphate. *Atmospheric Chemistry and Physics*, *6*, 755-768.

Baltensperger, U., Gaggeler, H. W., Jost, D. T., Lugauer, M., Schwikowski, M., Weingartner, E., & Seibert, P. (1997). Aerosol climatology at the high-alpine site Jungfraujoch, Switzerland. *Journal of Geophysical Research-Atmospheres*, *102*, (D16), 19707-19715.

Baltensperger, U., Schwikowski, M., Jost, D. T., Nyeki, S., Gäggeler, H. W., & Poulida, O. (1998). Scavenging of atmospheric constituents in mixed phase clouds at the high-alpine site Jungfraujoch part I: Basic concept and aerosol scavenging by clouds. *Atmospheric*

Environment, *32*, (23), 3975-3983.
Baltensperger, U., Kalberer, M., Dommen, J., Paulsen, D., Alfarra, M. R., Coe, H., Fisseha, R., Gascho, A., Gysel, M., Nyeki, S., Sax, M., Steinbacher, M., Prevot, A. S. H., Sjogren, S., Weingartner, E., & Zenobi, R. (2005). Secondary organic aerosols from anthropogenic and biogenic precursors. *Faraday Discussions*, (130), 265-278.
Biskos, G., Paulsen, D., Russell, L. M., Buseck, P. R., & Martin, S. T. (2006). Prompt deliquescence and efflorescence of aerosol nanoparticles. *Atmospheric Chemistry and Physics*, *6*, 4633-4642.
Canagaratna, M. R., Jayne, J. T., Jimenez, J. L., Allan, J. D., Alfarra, M. R., Zhang, Q., Onasch, T. B., Drewnick, F., Coe, H., Middlebrook, A., Delia, A., Williams, L. R., Trimborn, A. M., Northway, M. J., DeCarlo, P. F., Kolb, C. E., Davidovits, P., & Worsnop, D. R. (2007). Chemical and microphysical characterization of ambient aerosols with the aerodyne aerosol mass spectrometer. *Mass Spectrometry Reviews*, *26*, (2), 185-222.
Chan, M. N., & Chan, C. K. (2005). Mass transfer effects in hygroscopic measurements of aerosol particles. *Atmospheric Chemistry and Physics*, *5*, 2703-2712.
Choi, M. Y., & Chan, C. K. (2002). Continuous measurements of the water activities of aqueous droplets of water-soluble organic compounds. *Journal of Physical Chemistry A*, *106*, (18), 4566-4572.
Chuang, P. Y. (2003). Measurement of the timescale of hygroscopic growth for atmospheric aerosols. *Journal of Geophysical Research-Atmospheres*, *108*, (D9), art. no.-4282.
Coen, M. C., Weingartner, E., Schaub, D., Hueglin, C., Corrigan, C., Henning, S., Schwikowski, M., & Baltensperger, U. (2004). Saharan dust events at the Jungfraujoch: detection by wavelength dependence of the single scattering albedo and first climatology analysis. *Atmospheric Chemistry and Physics*, *4*, 2465-2480.
Colberg, C. A., Luo, B. P., Wernli, H., Koop, T., & Peter, T. (2003). A novel model to predict the physical state of atmospheric H2SO4/NH3/H2O aerosol particles. *Atmospheric Chemistry and Physics*, *3*, 909-924.
Colberg, C. A., Krieger, U. K., & Peter, T. (2004). Morphological investigations of single levitated H2SO4/NH3/H2O aerosol particles during deliquescence/efflorescence experiments. *Journal of Physical Chemistry A*, *108*, (14), 2700-2709.
Cozic, J., Verheggen, B., Mertes, S., Baltensperger, U., & Weingartner, E. (2007a). Field observation of black carbon enrichment in atmospheric ice particle residuals suggesting a potential ice nucleating capability. *In preparation*.
Cozic, J., Verheggen, B., Mertes, S., Connolly, P., Bower, K., Petzold, A., Baltensperger, U., & Weingartner, E. (2007b). Scavenging of black carbon in mixed phase clouds at the high alpine site Jungfraujoch. *Atmospheric Chemistry and Physics*, *7*, (7), 1797-1807.
Cozic, J., Verheggen, B., Mertes, S., Connolly, P., Bower, K., Petzold, A., Baltensperger, U., & Weingartner, E. (2006). Scavenging of black carbon in mixed phase clouds at the high alpine site Jungfraujoch. *Atmos. Chem. Phys. Discuss.*, *6*, 11877–11912.
Cozic, J., Verheggen, B., Weingartner, E., Crosier, J., Bower, K., Flynn, M., Coe, H., Henning, S., Steinbacher, M., Collaud Coen, M., Petzold, A., & Baltensperger, U. (2007c). Chemical composition of free tropospheric aerosol for PM1 and coarse mode at the high alpine site Jungfraujoch. *Atmospheric Chemistry and Physics Discussions*, *Submitted*.
Cubison, M. J., Coe, H., & Gysel, M. (2005). A modified hygroscopic tandem DMA and a data retrieval method based on optimal estimation. *Journal of Aerosol Science*, *36*, (7), 846-865.
Cubison, M. J. (2005). *Design, Construction and Use of a Hygroscopic Tandem Differential Mobility Analyser*, PhD thesis, University of Manchester, Manchester.
Davis, E. J., Buehler, M. F., & Ward, T. L. (1990). The Double-Ring Electrodynamic Balance for Microparticle Characterization. *Review of Scientific Instruments*, *61*, (4), 1281-1288.
Dick, W. D., Saxena, P., & McMurry, P. H. (2000). Estimation of water uptake by organic compounds in submicron aerosols measured during the Southeastern Aerosol and Visibility Study. *Journal of Geophysical Research Atmospheres*, *105*, (D1), 1471-1479.
Dinar, E., Mentel, T. F., & Rudich, Y. (2006). The density of humic acids and humic like substances (HULIS) from fresh and aged wood burning and pollution aerosol particles. *Atmospheric Chemistry and Physics*, *6*, 5213-5224.
Graber, E. R., & Rudich, Y. (2006). Atmospheric HULIS: How humic-like are they? A comprehensive and critical review. *Atmospheric Chemistry and Physics*, *6*, 729-753.
Gysel, M., Crosier, J., Topping, D. O., Whitehead, J. D., Bower, K. N., Cubison, M. J., Williams, P. I., Flynn, M. J., McFiggans, G. B., & H., C. (2006). Closure between measured and modelled

particle hygroscopic growth during TORCH2 implies ammonium nitrate artefact in the HTDMA measurements. *Atmos. Chem. Phys. Discuss.*, *6*, (6), 12503-12548.

Gysel, M., Weingartner, E., Nyeki, S., Paulsen, D., Baltensperger, U., Galambos, I., & Kiss, G. (2004). Hygroscopic properties of water-soluble matter and humic-like organics in atmospheric fine aerosol. *Atmospheric Chemistry and Physics*, *4*, 35-50.

Gysel, M., Weingartner, E., & Baltensperger, U. (2002). Hygroscopicity of aerosol particles at low temperatures. 2. Theoretical and experimental hygroscopic properties of laboratory generated aerosols. *Environmental Science & Technology*, *36*, (1), 63-68.

Hämeri, K., Charlson, R., & Hansson, H. C. (2002). Hygroscopic properties of mixed ammonium sulfate and carboxylic acids particles. *Aiche Journal*, *48*, (6), 1309-1316.

Hennig, T., Massling, A., Brechtel, F. J., & Wiedensohler, A. (2005). A tandem DMA for highly temperature-stabilized hygroscopic particle growth measurements between 90% and 98% relative humidity. *Journal of Aerosol Science*, *36*, (10), 1210-1223.

Henning, S., Weingartner, E., Schwikowski, M., Gaggeler, H. W., Gehrig, R., Hinz, K. P., Trimborn, A., Spengler, B., & Baltensperger, U. (2003). Seasonal variation of water-soluble ions of the aerosol at the high-alpine site Jungfraujoch (3580 m asl). *Journal of Geophysical Research-Atmospheres*, *108*, (D1).

IPCC (2001). *Climate Change 2001: The Scientific Basis*, Cambridge Univ. Press, New York.

Jayne, J. T., Leard, D. C., Zhang, X. F., Davidovits, P., Smith, K. A., Kolb, C. E., & Worsnop, D. R. (2000). Development of an aerosol mass spectrometer for size and composition analysis of submicron particles. *Aerosol Science and Technology*, *33*, (1-2), 49-70.

Jimenez, J. L., Jayne, J. T., Shi, Q., Kolb, C. E., Worsnop, D. R., Yourshaw, I., Seinfeld, J. H., Flagan, R. C., Zhang, X. F., Smith, K. A., Morris, J. W., & Davidovits, P. (2003). Ambient aerosol sampling using the Aerodyne Aerosol Mass Spectrometer. *Journal of Geophysical Research-Atmospheres*, *108*, (D7).

Joutsensaari, J., Vaattovaara, P., Vesterinen, M., Hämeri, K., & Laaksonen, A. (2001). A novel tandem differential mobility analyzer with organic vapor treatment of aerosol particles. *Atmospheric Chemistry and Physics*, *1*, 51-60.

Kanakidou, M., Seinfeld, J. H., Pandis, S. N., Barnes, I., Dentener, F. J., Facchini, M. C., Van Dingenen, R., Ervens, B., Nenes, A., Nielsen, C. J., Swietlicki, E., Putaud, J. P., Balkanski, Y., Fuzzi, S., Horth, J., Moortgat, G. K., Winterhalter, R., Myhre, C. E. L., Tsigaridis, K., Vignati, E., Stephanou, E. G., & Wilson, J. (2005). Organic aerosol and global climate modelling: a review. *Atmospheric Chemistry and Physics*, *5*, 1053-1123.

Kandler, K., & Schutz, L. (2007). Climatology of the average water-soluble volume fraction of atmospheric aerosol. *Atmospheric Research*, *83*, (1), 77-92.

Kärcher, B., & Lohmann, U. (2003). A parameterization of cirrus cloud formation: heterogeneous freezing. *Journal of Geophysical Research*, *108*, (D14), 4402-4416.

Kerminen, V. M. (1997). The effects of particle chemical character and atmospheric processes on particle hygroscopic properties. *Journal of Aerosol Science*, *28*, (1), 121-132.

Kiehl, & Trenberth (1997). Earth's annual global mean energy budget. *Am. Met. Soc*, *78*, (197–208).

Kiss, G., Tombacz, E., Varga, B., Alsberg, T., & Persson, L. (2003). Estimation of the average molecular weight of humic-like substances isolated from fine atmospheric aerosol. *Atmospheric Environment*, *37*, (27), 3783-3794.

Kreidenweis, S. M., Koehler, K., DeMott, P. J., Prenni, A. J., Carrico, C., & Ervens, B. (2005). Water activity and activation diameters from hygroscopicity data - Part I: Theory and application to inorganic salts. *Atmospheric Chemistry and Physics*, *5*, 1357-1370.

Krieger, U. K., & Braun, C. (2001). Light-scattering intensity fluctuations in single aerosol particles during deliquescence. *Journal of Quantitative Spectroscopy & Radiative Transfer*, *70*, (4-6), 545-554.

Krivacsy, Z., Gelencser, A., Kiss, G., Meszaros, E., Molnar, A., Hoffer, A., Meszaros, T., Sarvari, Z., Temesi, D., Varga, B., Baltensperger, U., Nyeki, S., & Weingartner, E. (2001). Study on the chemical character of water soluble organic compounds in fine atmospheric aerosol at the Jungfraujoch. *Journal of Atmospheric Chemistry*, *39*, (3), 235-259.

Kumar, S. (1989). The characteristic time to achieve interfacial phase equilibrium in cloud drops. *Atmospheric Environment*, *23*, 2299-2304.

Liu, B. Y. H., Pui, D. Y. H., Whitby, K. T., Kittelson, D. B., Kousaka, Y., & McKenzie, R. L. (1978). The Aerosol Mobility Chromatograph: a new detector for sulfuric acid aerosols. *Atmospheric Environment*, *12*, 99-104.

Liu, Y. C., Wang, Q., Wu, T., & Zhang, L. (2005). Fluid structure and transport properties of water inside carbon nanotubes. *Journal of Chemical Physics*, *123*, (23).

Lugauer, M., Baltensperger, U., Furger, M., Gäggeler, H. W., Jost, D. T., Nyeki, S., & Schwikowski, M. (2000). Influences of vertical transport and scavenging on aerosol particle surface area and radon decay product concentrations at the Jungfraujoch (3454 m above sea level). *Journal of Geophysical Research Atmospheres*, *105*, (D15), 19869-19879.

Marcolli, C., Luo, B. P., & Peter, T. (2004). Mixing of the organic aerosol fractions: Liquids as the thermodynamically stable phases. *Journal of Physical Chemistry A*, *108*, (12), 2216-2224.

Marcolli, C., & Krieger, U. K. (2006). Phase changes during hygroscopic cycles of mixed organic/inorganic model systems of tropospheric aerosols. *Journal of Physical Chemistry A*, *110*, (5), 1881-1893.

McFiggans, G., Artaxo, P., Baltensperger, U., Coe, H., Facchini, M. C., Feingold, G., Fuzzi, S., Gysel, M., Laaksonen, A., Lohmann, U., Mentel, T. F., Murphy, D. M., O'Dowd, C. D., Snider, J. R., & Weingartner, E. (2006). The effect of physical and chemical aerosol properties on warm cloud droplet activation. *Atmospheric Chemistry and Physics*, *6*, 2593-2649.

Mertes, S., Verheggen, B., Walter, S., Ebert, M., Connolly, P., Weingartner, E., Schneider, J., Bower, K. N., Inerle-Hof, M., Cozic, J., Baltensperger, U., & Heintzenberg, J. (2007). Counterflow virtual impactor based collection of small ice particles in mixed-phase clouds for the physico-chemical characterisation of tropospheric ice nuclei: sampler description and first case study. *Aerosol Science and Technology*, *in press*.

Nyeki, S., Kalberer, M., Colbeck, I., De Wekker, S., Furger, M., Gaggeler, H. W., Kossmann, M., Lugauer, M., Steyn, D., Weingartner, E., Wirth, M., & Baltensperger, U. (2000). Convective boundary layer evolution to 4 km asl over high-alpine terrain: Airborne lidar observations in the Alps. *Geophysical Research Letters*, *27*, (5), 689-692.

Nyeki, S., Li, F., Weingartner, E., Streit, N., Colbeck, I., Gaggeler, H. W., & Baltensperger, U. (1998). The background aerosol size distribution in the free troposphere: An analysis of the annual cycle at a high-alpine site. *Journal of Geophysical Research Atmospheres*, *103*, (D24), 31749-31761.

Prenni, A. J., De Mott, P. J., & Kreidenweis, S. M. (2003). Water uptake of internally mixed particles containing ammonium sulfate and dicarboxylic acids. *Atmospheric Environment*, *37*, (30), 4243-4251.

Putaud, J. P., Raes, F., Van Dingenen, R., Bruggemann, E., Facchini, M. C., Decesari, S., Fuzzi, S., Gehrig, R., Huglin, C., Laj, P., Lorbeer, G., Maenhaut, W., Mihalopoulos, N., Mullller, K., Querol, X., Rodriguez, S., Schneider, J., Spindler, G., ten Brink, H., Torseth, K., & Wiedensohler, A. (2004). European aerosol phenomenology-2: chemical characteristics of particulate matter at kerbside, urban, rural and background sites in Europe. *Atmospheric Environment*, *38*, (16), 2579-2595.

Rader, D. J., & McMurry, P. H. (1986). Application of the Tandem Differential Mobility Analyzer to Studies of Droplet Growth or Evaporation. *Journal of Aerosol Science*, *17*, (5), 771-787.

Randall, D. A., Wood, R. A., Bony, S., Colman, R., Fichefet, T., Fyfe, J., Kattsov, V., Pitman, A., Shukla, J., Srinivasan, J., Stouffer, R. J., Sumi, A., & Taylor, K. E. (2007). *Contribution of Working Group I to the Fourth Assessment Report of the Intergovernmental Panel on Climate Change - Climate Models and their Evaluation*, Cambridge University Press, Cambridge, United Kingdom and New York.

Ray, J., & McDow, S. R. (2005). Dicarboxylic acid concentration trends and sampling artifacts. *Atmospheric Environment*, *39*, (40), 7906-7919.

Raymond, T. M., & Pandis, S. N. (2002). Cloud activation of single-component organic aerosol particles. *Journal of Geophysical Research-Atmospheres*, *107*, (D24), art. no.-4787.

Russell, L. M., & Ming, Y. (2002). Deliquescence of small particles. *Journal of Chemical Physics*, *116*, (1), 311-321.

Sjogren, S., Gysel, M., Weingartner, E., Baltensperger, U., Cubison, M. J., Coe, H., Zardini, A. A., Marcolli, C., Krieger, U. K., & Peter, T. (2007). Hygroscopic growth and water uptake kinetics of two-phase aerosol particles consisting of ammonium sulfate, adipic and humic acid mixtures. *Journal of Aerosol Science*, *38*, (2), 157-171.

Solomon, S., Qin, D., Manning, M., Alley, R. B., Berntsen, T., Bindoff, N. L., Chen, Z., Chidthaisong, A., Gregory, J. M., Hegerl, G. C., Heimann, M., Hewitson, B., Hoskins, B. J., Joos, F., Jouzel, J., Kattsov, V., Lohmann, U., Matsuno, T., Molina, M., Nicholls, N., Overpeck, J., Raga, G., Ramaswamy, V., Ren, J., Rusticucci, M., Somerville, R., Stocker, T. F., Whetton, P., Wood, R.

A., & Wratt, D. (2007). *Contribution of Working Group I to the Fourth Assessment Report of the Intergovernmental Panel on Climate Change - Technical Summary*, Cambridge University Press, Cambridge, United Kingdom and New York.

Stokes, R. H., & Robinson, R. A. (1966). Interactions in aqueous nonelectrolyte solutions. I. Solute-solvent equilibria. *J. Phys. Chem*, *70*, 2126-2130.

Swietlicki, E., Zhou, J. C., Covert, D. S., Hameri, K., Busch, B., Vakeva, M., Dusek, U., Berg, O. H., Wiedensohler, A., Aalto, P., Makela, J., Martinsson, B. G., Papaspiropoulos, G., Mentes, B., Frank, G., & Stratmann, F. (2000). Hygroscopic properties of aerosol particles in the northeastern Atlantic during ACE-2. *Tellus Series B Chemical and Physical Meteorology*, *52*, (2), 201-227.

Tang, I. N., & Munkelwitz, H. R. (1993). Composition and Temperature-Dependence of the Deliquescence Properties of Hygroscopic Aerosols. *Atmospheric Environment Part a-General Topics*, *27*, (4), 467-473.

Topping, D. O., McFiggans, G. B., & Coe, H. (2005a). A curved multi-component aerosol hygroscopicity model framework: Part 1 - Inorganic compounds. *Atmospheric Chemistry and Physics*, *5*, 1205-1222.

Topping, D. O., McFiggans, G. B., & Coe, H. (2005b). A curved multi-component aerosol hygroscopicity model framework: Part 2 - Including organic compounds. *Atmospheric Chemistry and Physics*, *5*, 1223-1242.

Verheggen, B., Cozic, J., Weingartner, E., Bower, K., Mertes, S., Connolly, P., Flynn, M., Gallagher, M., Choularton, T., & Baltensperger, U. (2007). Aerosol partitioning between the interstitial and the condensed phase in mixed-phase clouds. *Journal of Geophysical Research - Atmospheres*, *In press*.

Vlasenko, A., Sjogren, S., Weingartner, E., Stemmler, K., Gaggeler, H. W., & Ammann, M. (2006). Effect of humidity on nitric acid uptake to mineral dust aerosol particles. *Atmospheric Chemistry and Physics*, *6*, 2147-2160.

Weingartner, E., Gysel, M., & Baltensperger, U. (2002a). Hygroscopicity of aerosol particles at low temperatures. 1. New low-temperature H-TDMA instrument: Setup and first applications. *Environmental Science and Technology*, *36*, (1), 55-62.

Weingartner, E., Burtscher, H., & Baltensperger, U. (1997). Hygroscopic properties of carbon and diesel soot particles. *Atmospheric Environment*, *31*, (15), 2311-2327.

Weingartner, E., Nyeki, S., & Baltensperger, U. (1999). Seasonal and diurnal variation of aerosol size distributions (10 < D < 750 nm) at a high-alpine site (Jungfraujoch 3580 m asl). *Journal of Geophysical Research Atmospheres*, *104*, (D21), 26809-26820.

Weingartner, E., Saathoff, H., Schnaiter, M., Streit, N., Bitnar, B., & Baltensperger, U. (2003). Absorption of light by soot particles: determination of the absorption coefficient by means of aethalometers. *Journal of Aerosol Science*, *34*, (10), 1445-1463.

Weingartner, E., Gysel, M., & Baltensperger, U. (2002b). Hygroscopicity of aerosol particles at low temperatures. 1. New low-temperature H-TDMA instrument: Setup and first applications. *Environmental Science & Technology*, *36*, (1), 55-62.

Winklmayr, W., Reischl, G. P., Lindner, A. O., & Berner, A. (1991). New electromobility apectrometer for the measuremnt of aerosol size distributions in the size range from 1 to 1000 nm. *Journal of Aerosol Science*, *22*, 289-296.

Zelenyuk, A., Cai, Y., & Imre, D. (2006). From agglomerates of spheres to irregularly shaped particles: Determination of dynamic shape factors from measurements of mobility and vacuum aerodynamic diameters. *Aerosol Science and Technology*, *40*, (3), 197-217.

Zhang, Q., Jimenez, J. L., Canagaratna, M. R., & Allan, J. D. (2007). Ubiquity and dominance of oxygenated species in organic aerosols in anthropogenically-influenced Northern Hemisphere midlatitudes. *Geophysical Research Letters*.

7. Symbols

AA	Adipic acid
AS	Ammonium sulfate
ATD	Arizona test dust
CA	Citric acid
CCN	Cloud condensation nuclei
D	Particle diameter
D_0	Dry particle diameter
D_{Mob}	Mobility diameter
DMA1 or 2	Differential mobility analyzer (1^{st} or 2^{nd})
DRH	Deliquescence relative humidity
EC	Elemental carbon
EDB	Electrodynamic balance
ERH	Efflorescence relative humidity
FT	Free troposphere
RH	Relative humidity
GA	Glutaric acid
GF	Hygroscopic growth factor, D/D_0
GCM	Global climate model
HNO_3	Nitric acid, chemical formula
HTDMA	Hygroscopicity tandem differential mobility analyzer
IPCC	Intergovernmental Panel on Climate Change
JFJ	High-alpine research station Jungfraujoch
lpm	Liters per minute
$M(dry)$	Dry mass of the particle
NaHA	Humic acid
O_3	Ozone, chemical formula
OC	Organic carbon
RMSD intensity	Root mean square deviation from the intensity mean
τ_{res}	Residence time
ZSR	Zdanovskii-Stokes-Robinson
µm	Micrometer
nm	Nanometer

8. Acknowledgements - tack

Någonstans i hemmet med morsan och farsan så fick jag med mig en oerhörd optimism och säkerhet. Utan den skulle jag inte kunna ge av mig själv, utan att oroa mig för vad som blir kvar. Men det blir bara mer om man vågar verkligen ge. Sedan vill jag tacka syskonen och alla fran uppväxten, fran hemma i skogarna. Vännerna fran Alsterbro, som jag för länge sedan har förlorat adresserna till. Som fortfarande hänger kvar i hjärtat när sentimentaliteten slar till. Och de andra fran tjugoårsaldern, som jag faktiskt fortfarande har kontakt med. Tack vare er upplevde och lärde jag mig mycket därhemma, innan jag drog ut på denna resa som för tillfället slutar med detta arbete här nu, det absoluta slutet pa mina studier. Så; välkommen livet, och jag hoppas jag hittar hem nu.

The environment, and the atmosphere, is what this work is about. Four years ago, I was given the opportunity to study the uptake and release of water (hygroscopicity) of particles in the atmosphere (dust and exhaust pipe particles and similar things) at the Paul Scherrer Institute in Switzerland. I suppose you can say it has been a long journey, and that half the work performed is to develop oneself during these four years, the second half of the work was about science. About a half *of that* I have invested in atmospherical chemistry, and the last quarter I've chosen to study energy systems, more or less. So how does our everyday activities (i.e. a 300g steak per person imported from the southern hemisphere for the BBQ, or a married couple commuting with two cars >2h in total to work and back each day, or the purchase of a new Ipod© when the battery in the old one doesn't last) actually influence our resource and energy consumption, and thus our atmosphere and environment, and our climate? Not to mention specifically the cheap flights that brings us, in only hours, a thousand kilometers for a shopping spree (more *things*) for a weekend?

When I started this thesis I answered the question from Prof. Dr. Wokaun with "after a few years in the chemical industry, it would be nice to learn now what happens with the stuff that the industry [=society, yeah, *that's you and me*] puts out in the environment and atmosphere". This I have now to some extent learnt. And I am not pleased with the conclusions that I have made, for the medium-term future of the eco-system. Many species, and poor people, are in for suffering in the 21st century, as the industrialized society is slow to change direction and slow to dare to go in a new direction.

Mr O. asked "what do you actually learn, what do you especially develop, by doing a thesis?" I learnt that the conclusion above, and this thesis, *would not have been reached without the help of all involved.* A thesis is done in cooperation, and cannot (there are a few single exceptions throughout the history of science) be done without all of you. It is done *with* you, also you who read this.

Thanks goes to Tom, for his true existence, and teaching to have a smile about oneself, and his colleagues Claudia and Ueli of course (yeah, yeah, you think you know what I think, *but it isn't so*: I really have a high esteem about you and you have taught me so much). And -ale- of course many many thanks. There is the rest of the team at ETH Zurich as well to thank.

Urs, many many thanks for the effort you put in, to make it possible for us to study here!

I've much appreciated working with you Ernest; do you remember the first years when we measured and fiddled and fieldcampaigned? I believe you enjoyed, and still enjoy, these times as well. Thanks for having pulled me along on your aerosol research. For having selected me for this NF-project [n° 200021-100280 – I hope the goals stated in project description are ~satisfactory achieved for NF!], I am grateful to have been doing it, with you.

Many thanks go to HC Hansson for taking the time being an external referent for this thesis.

There are more players behind the curtains, without this wouldn't have been possible, Martin for inversion algorithms and thorough theoretical backup, Sasha, Olga, Thomas and Ammann for a step into gas uptake/reaction kinetics. Mike for my first 3000m, ehh, I mean when you where over for a month of lab measurements, and the gentlemen over at UMan, especially Coe and Topping and Crosier there. Axel & Silke (superb translation), Jonathan (for being yourself – thanks for giving good advice about what I can do as an individual), Julie (laisse la vie rouler dans la sense que ca prend), Rahel (I owe you a letter), Stefan, Christina, Rebecka, Rami (who also did AMS CLACE2 etc. – and thanks for the quality check of the shisha from Sinai), Nikolas (for that first field visit as a fresh PhD student at Zürich rangier yard), Bart, Long, René (für's technik), Doris, Bettina (for philosophy), yikes, I cannot put all names in – many thanks to the rest of you (LAC especially).

Other activities than science are also needed to balance so I appreciate divertissements from various friends (ranging from Spheres 2004 to chess games). It was good at times of desperation with this work, to find a way to proceed (whatever that really means). Thanks to you all and all bowshooters as well.

Due to some interesting changes in my personal life during these years, I suddenly found myself really prioritizing what to do with my time (a small thing can be a large help). So I express thanks to all that have done baby-sitting (a lot!) and helped with organization at home, especially Anne & Theo. My love to BIG BOY Lionel, and Mélanie.

Ps. If I've forgotten someone in this list above – it is only text. You know what I know. If anybody has any questions that I need to clear – just ask me to sit down with you for a cup of coffee. Magical things *do* happen.

Staffan Sjögren

Dammerkirchstrasse 76, 4056 Basel
Nationality Swedish
Born 1976, married, son Lionel ☺

Dolderhorn, 3640 m

Curriculum vitæ

Dr. sc. ETH Zürich (2007), M. sc. Chem. Eng, Univ. of Lund (1999)

Work experience

Oct 07 – Dec 07	BACCI PostDoc scholarship (http://nuclearphysics.pixe.lth.se), Univ. of Lund, S
Jul 03 – Aug 07	PhD at Paul Scherrer Institute (www.psi.ch), Villigen, CH
Jun 00 - Mar 03	Employment KÜHNI AG (www.kuhni.ch), project manager in Pilot Test Centre, Allschwil, Basel, CH
Sep 99 - Feb 00	Employment ProSim SA (www.prosim.net), sales engineer, Toulouse, F

Published papers

Feb 07	"*Hygroscopic growth and water uptake kinetics of two-phase aerosol particles consisting of ammonium sulfate, adipic and humic acid mixtures*", Sjogren S, Gysel M, Weingartner E, et al., JOURNAL OF AEROSOL SCIENCE 38 (2): 157-171
Jun 06	"*Effect of humidity on nitric acid uptake to mineral dust aerosol particles*", Vlasenko A, Sjogren S, Weingartner E, et al., ATMOSPHERIC CHEMISTRY AND PHYSICS 6: 2147-2160
May 05	"*Generation of submicron Arizona test dust aerosol: Chemical and hygroscopic properties*", Vlasenko A, Sjogren S, Weingartner E, et al., AEROSOL SCIENCE AND TECHNOLOGY 39 (5): 452-460
May 05	"*Secondary organic aerosols from anthropogenic and biogenic precursors*", Baltensperger U, Kalberer M, Dommen J, et al., FARADAY DISCUSSIONS 130: 265-278

Conference talks

Apr 07	"*Hygroscopic Growth and Water Uptake Kin. …*", EGU, Wien, AT
Aug 05	"*Hygroscopic Properties and Time of Equil. …*", EAC Gent, BE
Sep 04	"*Hygroscopic Growth and Phase Change. …*", EAC Budapest, HUN
Nov 01	"*Recovery of BuAc. …*", 1st DISTIL User Meeting, Frankfurt, DE
Oct 99	"*Identification Of Kin. Par. …*", Mettler-Toledo RC User Forum, Bern, CH

Education

95-99	Studies of chemical engineering at Lund Institute of Technology, Univ. of Lund, with finishing year at École Nationale Supérieure d'Ingénieurs de Génie Chimique, Toulouse, F (today www.ensiacet.fr)

Languages

Swedish:	mother tongue
English:	good level speaking and writing
French,German:	good level speaking, medium level writing
Spanish:	tourist level spoken

Interests Kyudo (japanese bowshooting, www.kyudo.ch/de/kyud.html)

Please ask for references